A Composite Study of the Madden-Julian Oscillation

by
Robert J. Falvey

Department of Atmospheric Science
Colorado State University
Fort Collins, Colorado

Colorado State University

Department of Atmospheric Science

Paper No. 494

A COMPOSITE STUDY OF THE MADDEN–JULIAN OSCILLATION

by

Robert J. Falvey

Department of Atmospheric Science
Colorado State University
Fort Collins, CO 80523

Spring 1992

Atmosperhic Science Paper No. 494

ABSTRACT

A COMPOSITE STUDY OF THE MADDEN-JULIAN OSCILLATION

A composite based on the phase of the 30-60 day oscillation (referred to here as the Madden-Julian Oscillation or MJO) is used to examine kinematic and thermodynamic fields over the equatorial western Pacific Ocean for three Northern Hemisphere winter seasons (1986-89). The composite is based on Outgoing Longwave Radiation (OLR) data from NOAA polar-orbiting satellites plotted in time versus longitude diagrams. Eastward propagation of low OLR (inferred deep convection) values associated with the trough of the MJO wave was clearly visible in these Hovmöller diagrams. These diagrams were used to construct a four convective phase composite. The composite is then applied to the OLR and model analysis data from the European Center for Medium Range Weather Forecasts (ECMWF) and the National Meteorological Center (NMC). Large scale heat and moisture budgets are calculated and compared to other tropical budget studies. Emphasis is placed on inter-phase variability and the role of El Niño-Southern Oscillation (ENSO) as a modulator of convective activity.

The OLR composite reveals that during the two warm years (1986-87 and 1987-88) the main convective activity was centered between the 2.5°S and 5.0°S. It shifted to between 10.0°S and 15.0°S during the cold year (1988-89). The OLR data also indicated that the convection was stronger in the warm years than in the cold year. The eastward propagation of the convection was also evident.

The composited low-level equatorial zonal winds were maximum westerly (associated with westerly wind bursts) during the decreasing convection phase, just west of the deep convection. This is consistent with the hypothesized structure of cloud clusters advanced

by Lau *et al.* (1989). Low-level convergence, however, is found to peak during the increasing convection phase, or just to the east of the deep convection.

The vertical motion composites from both the ECMWF and NMC models showed the maximum ascent during the maximum convection phase peaking near 300 mb in the warm years and near 500 mb in the cold year. However, both composite results exhibited marked differences in latitudinal distribution and magnitude of the vertical motion. The ECMWF composite showed the core of the vertical motion shifting from near 2.5°S during 1986-87 to near 15.0°S during 1988-89. The NMC composite maintained the main core of the vertical motion near 10.0°S during all three years. The NMC results are inconsistent with the OLR composite analysis which showed a southward shift of the convection during the cold year. Also, the magnitude of the vertical motion in the ECMWF composite was found to be stronger in the warm years than the cold year, while in the NMC composite the magnitudes remained nearly the same in all three years and were nearly 50% smaller than in the ECMWF composite.

The vertical profiles of Q_1 (the apparent heat source) appear very similar to the profiles of the vertical motion. The Q_1 heating peak is found to be at a higher level during the El Niño years (between 300-400 mb) than in the La Niña year (between 700-500 mb). The higher heating peak is suggestive of more vigorous convection and/or a greater fraction of upper-level stratiform precipitation in the warm years than in the cold year. The zonal distribution of heating during the cold year shows how the vertical profile of heating is strongly influenced by land masses. The heating peaks near 400 mb in the vicinity of Papua New Guinea and between 700 and 500 mb over the open ocean to the east.

The meridional profiles of Q_1 and Q_2 (the apparent moisture sink), showed a distinct cooling and moistening in the Northern Hemisphere north of 10.0°N throughout most of the troposphere. The low-level cooling and moistening peaks are most likely a result of the re-evaporation of trade-wind cumulus clouds and the secondary cooling peak in the upper troposphere is likely due to longwave radiation off the tops of the residual cirrus anvils. Within the minimum OLR regions south of the equator in both the warm and cold years, there was a clear separation of the Q_1 and Q_2 peaks, indicative of the prevalence of deep convection.

ACKNOWLEDGEMENTS

I would like to express my deepest appreciation to my advisor, Dr. Richard Johnson, for allowing me to pursue this research and for his unselfish dedication to the successful timely completion of this work. I would also like to thank my other committee members, Dr. William Gray and Dr. Jack Cermak.

I would also like to thank Jim Bresch and Bill Gallus, who were always available for questions and willing to share their knowledge and expertise and Bill Thorson and Scott Denning for their assistance in the operation of the many computer systems in the Department of Atmospheric Science.

Finally, thanks to Gail Cordova, who was instrumental in the completion of this manuscript and Judy Sorbie, who drafted some of the figures.

This research was supported by the National Oceanic and Atmospheric Administration Grant No. NA90RAH00077.

CONTENTS

LIST OF FIGURES

Chapter 1

INTRODUCTION

Since it was first detected in the surface pressure and zonal wind record of a single island in the tropical Pacific Ocean by Madden and Julian in 1971, the 30-60 day oscillation (later called the Madden-Julian Oscillation and hereafter referred to as the MJO) has been vigorously studied to document its characteristics, dynamics, and origin. The initial investigations were observational studies that aimed to confirm the existence and to examine the spatial and temporal scope of the oscillation. One inherent problem in studying any phenomenon located in the equatorial region of the globe is the lack of observational data with enough spatial and temporal resolution to accurately describe it in detail. However, investigators believed a more thorough understanding of this periodic feature could lead to more accurate mid- to long-range forecasts in the tropics.

A variety of data sets and analysis techniques have been employed to examine the characteristics of this atmospheric oscillation. Madden and Julian (1971) used nearly ten years of daily rawinsonde data in their initial investigation when they stumbled across the oscillation. Spectral and cross spectral analysis of data from Canton Island (3°S 172°W) revealed a long period oscillation in the station pressure and zonal winds. They found this oscillation had a lower frequency than any other wave phenomenon theorized before, but higher than the seasonal variation. The dominant period was on the order of 40-50 days. Their results showed the zonal winds at 850 mb were out of phase with those at 150 mb. They found low surface pressures were associated with strong 850 mb easterlies and high surface pressure associated with weak 850 mb easterlies or westerlies.

In their follow-on investigation, Madden and Julian (1972) employed the same spectral and cross spectral analysis technique to some twenty-five stations around the globe,

primarily located in the tropics. They found that stations within ten degrees of the equator in the Pacific and Indian Oceans between Caracao (12°N 68°W) and Singapore (1°N 103°E) showed spectral peaks in the surface pressure data with a period of 40-50 days. The equatorial Atlantic Ocean station data showed the 40-50 day peak was no more important than the 30 or 60 day peak. They then concluded the original 40-50 day oscillation was too restrictive and expanded it to the currently accepted 30-60 day oscillation. However, due to the large separation of these data points, there remained some question as to the continuous nature of the oscillation. Figure 1.1a is a schematic take from Madden and Julian (1972) which depicts the time and space evolution of a disturbance associated with the MJO. The letters A-H correspond to the dates associated with the oscillation Canton Island's pressure wave, shown in Fig. 1.1b. This schematic shows a disturbance developing in the eastern Indian Ocean (near 80°E), strengthening as it moves over Indonesia and into the western Pacific Ocean, and weakening and dissipating as it continues to propagate eastward over the central and eastern Pacific Ocean. The evolution of the disturbances that will be presented later in this study follows this schematic very well.

It is widely accepted that Outgoing Longwave Radiation (OLR) serves as a good proxy for convection in the tropical atmosphere (Heddinghaus and Krueger, 1981). The polar-orbiting meteorological satellite was a source of data that was of high enough spatial and temporal resolution to facilitate increased understanding of the large-scale oscillatory nature of this atmospheric phenomenon. Lau and Chan (1985) used Empirical Orthogonal Function (EOF) analysis of OLR data from NOAA polar-orbiting satellites and found, by first applying a 5-day running-mean filter and subtracting out the seasonal mean, that the OLR data also showed a spectral peak with a 30-60 day period. They found a dipole oscillation structure in the OLR data between the maritime continent of Borneo and Indonesia and the central Pacific Ocean on the two-to-three month and the inter-annual time scales. When there were low values of OLR over Borneo, there tended to be high values over the central Pacific and vice versa. They attribute the inter-annual dipole to the El Niño-Southern Oscillation (ENSO). In an earlier paper, Lau and Chan (1983) suggested the two-to-three month dipole may be linked to the MJO.

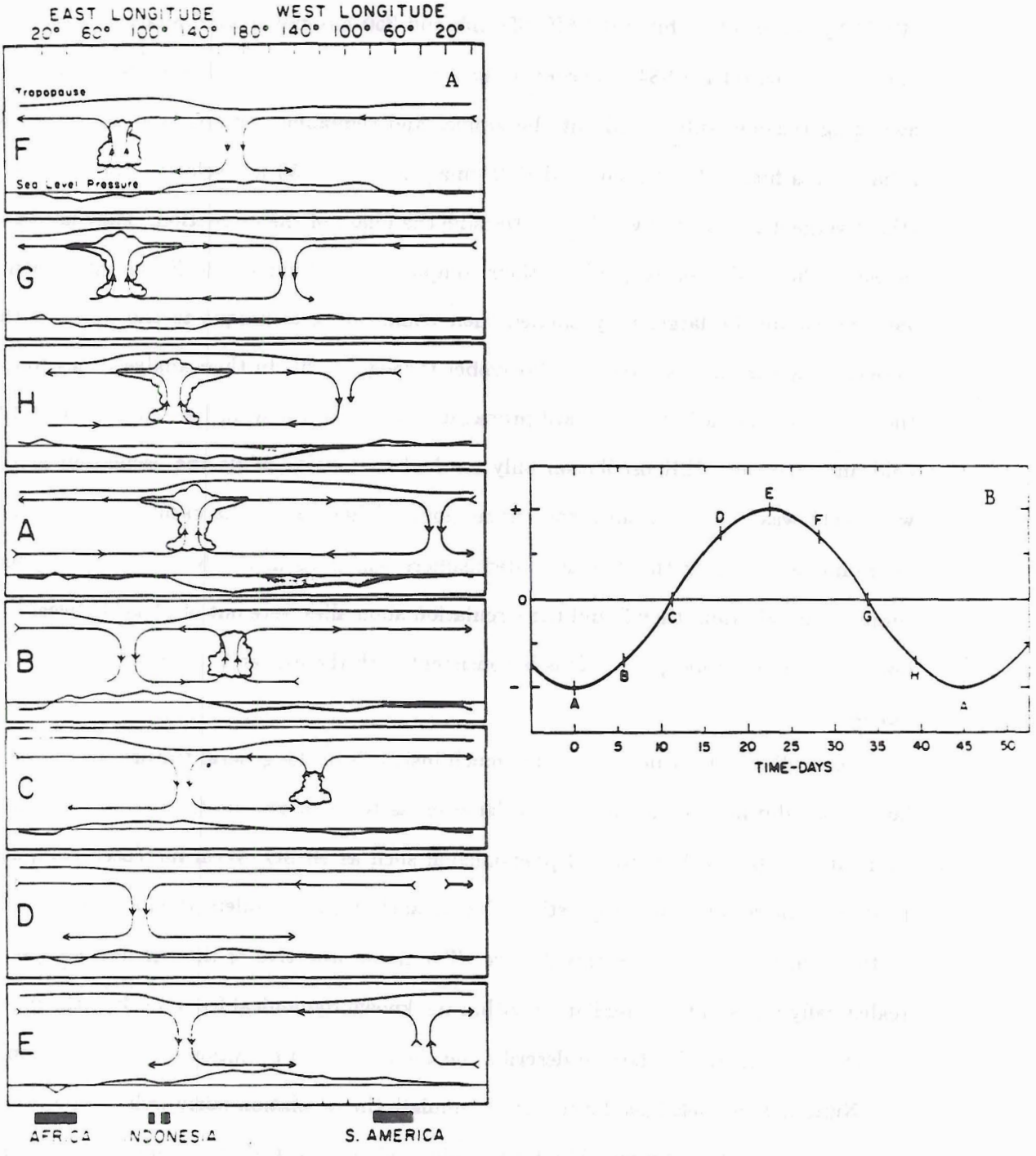

Figure 1.1: Schematic of the time and space evolution of a disturbance associated with the 30-60 day oscillation. Taken from Madden and Julian (1972). The letters at the left in Fig. 1.1a correspond to the dates associated with the oscillation in Canton Island's station pressure shown in Fig. 1.1b.

The life cycle of the 30-60 day oscillation was examined by Knutson and Weickmann (1987) by compositing filtered NMC 850 mb and 250 mb global wind analyses and OLR data for the period 1979-84. In order to isolate the desired period, they applied a five-day averaging scheme, subtracted out the annual and semiannual cycles, and then applied a band pass filter. They then used EOF analysis of the 250 mb velocity potential field (the divergent part of the wind) to determine the phase of the oscillation. They used the phase of the oscillation to perform their compositing technique. Realizing the seasonal variation would be large, they applied their compositing technique to the data for the periods May through October and November through April. In their analysis they found the oscillation had a faster eastward propagation speed in the wind field than in the OLR field and that the OLR oscillation only reached to 150°W, while the oscillation in the wind field was evident around the entire globe. They found the oscillations were not as pronounced during the Northern Hemisphere winter as in the Northern Hemisphere summer. In addition, they found the circulation anomalies were out of phase between the lower and upper troposphere. This is consistent with the earlier findings of Madden and Julian.

These diagnostic studies provided much insight into the general features of the oscillation, but did not provide a clear explanation as to its origin, its forcing mechanism or its relationship to other tropical phenomenon such as ENSO. With increased computer processing power and more sophisticated general circulation models, the focus was shifted to the accurate modeling of this feature. The main objective of the simulations was to realistically represent the oscillation within the known dynamical framework of the model and then use the model data to describe the the origin and evolution of the oscillation.

Numerical models have been able to simulate the oscillation fairly well. Lau and Lau (1986) used the Geophysical Fluid Dynamics Laboratory (GFDL) General Circulation Model (GCM) to examine the three dimensional structure and temporal evolution of the oscillation. They found a global scale oscillation in the form of eastward-propagating circulation cells oriented in the equatorial plane. In their 15 wavenumber model they found the 30-60 day signal was strongest in the velocity potential field (χ) and that the

oscillation occurs throughout the year. The velocity potential fields in the lower level of the model were out of phase with those in the upper levels. These findings are all consistent with the observations of Knutson and Weickmann (1987). However, one fault of the simulation was the speed of propagation. In their results the eastward propagation was approximately 15 m s^{-1} , while observations range from 4-10 m s^{-1} .

Lau and Peng (1987) and later Lau *et al.* (1989) used the five-layer model first introduced by Lau and Lim (1984) to test a theory of the origin of the intraseasonal oscillation in terms of 'mobile' wave-CISK (Conditional Instability of a Second Kind). Lau and Peng tested two scenarios, one with a local oscillating heat source and the other with an internally forced heat source. The first scenario, with maximum heating near 600 mb, resulted in atmospheric oscillations that propagated away from the source region in both directions. They determined the oscillations took the form of Rossby waves propagating to the west and Kelvin waves propagating to the east of the heat source. This is in disagreement with observations of eastward-only propagation, although Lau *et al.* (1989) showed some shorter period westward moving cloud clusters. Scenario two, which includes wave CISK-type internal heating maximized at 600 mb, resulted in circulation cells propagating eastward at approximately 19 m s^{-1} . The corresponding period of this oscillation is about 24 days. This speed is again faster than observations. The eastward-propagating Kelvin waves are divergent and the westward-propagating Rossby waves are rotational. They theorize that because the convergence associated with the Kelvin waves is greater than that associated with Rossby waves, the Kelvin waves will be enhanced more readily than the Rossby waves. The net result is that the Kelvin waves propagate eastward and enhance convergence and convection farther east via the CISK mechanism. The new heat source excites new Kelvin waves which propagate eastward, which in turn enhances convergence and convection to the east. They also suggest the Rossby waves do not grow because their response time is longer than Kelvin waves, so they do not have enough time to grow before the new heat source develops to the east.

However, the observations of Knutson and Weickmann (1987) indicate that the convective anomalies only propagate as far as 150°W, so how can the Kelvin wave be maintained around the globe? Lau and Peng theorize that if the Kelvin waves were strong

enough to make it around the globe one time they could be re-enhanced by the CISK mechanism once they got to the warm waters of the Indian and western Pacific Oceans again. Lau *et al.* (1989) tied the eastward propagation to Super Cloud Clusters (SCCs) that move discretely eastward due to successive formation of new westward-moving clusters to the east. This is similar to the propagation scenario described by Lau and Peng. In their model, they found that the speed of propagation is sensitive to the level of maximum heating. They found that maximum heating near 300 mb resulted in a propagation speed of 23 m s^{-1} while maximum heating between 700-500 mb resulted in speeds near 9 m s^{-1} . They argue that because Kelvin waves are non-dispersive and are unstable with respect to CISK, they are selectively amplified and Rossby waves are damped.

Figure 1.2 is a schematic taken from Lau *et al.* (1989) which gives a 3-dimensional illustration of their theory. It shows the largest disturbances associated with the Kelvin waves moving eastward and the smaller disturbances associated with the Rossby waves moving westward. It also shows westerly wind bursts to the west of the main convective disturbance. The results that will be presented in this study also show the strongest westerly winds to the west of the main convection.

Chang and Lim (1988) used a linear theoretical analysis of the equatorial β-plane wave-CISK and also found that the propagation speed of the CISK mode is sensitive to the level of maximum heating. They found speeds of 30 and 15 m s^{-1} for heating maximized at 400 and 600 mb respectively. If the maximum heating was in the lower troposphere, the CISK mode became nearly stationary. They also found that the 'moisture availability factor', which is directly related to the heating generated by the CISK mechanism through low level moisture convergence, has a large effect on the phase speed of the CISK mode. When they increased the moisture availability, the phase speed decreased rapidly. The results from Wang (1988) and Lau and Shen (1988) agree well with these findings. In his theoretical study of moist Kelvin waves, Wang found that if the mixing ratio within the planetary boundary layer increased, the phase speed of the Kelvin waves decreased. Lau and Shen used a shallow-water system of equations and found by increasing the sea surface temperature from 27 to 29°C, the phase speed could be reduced from 35 m s^{-1}

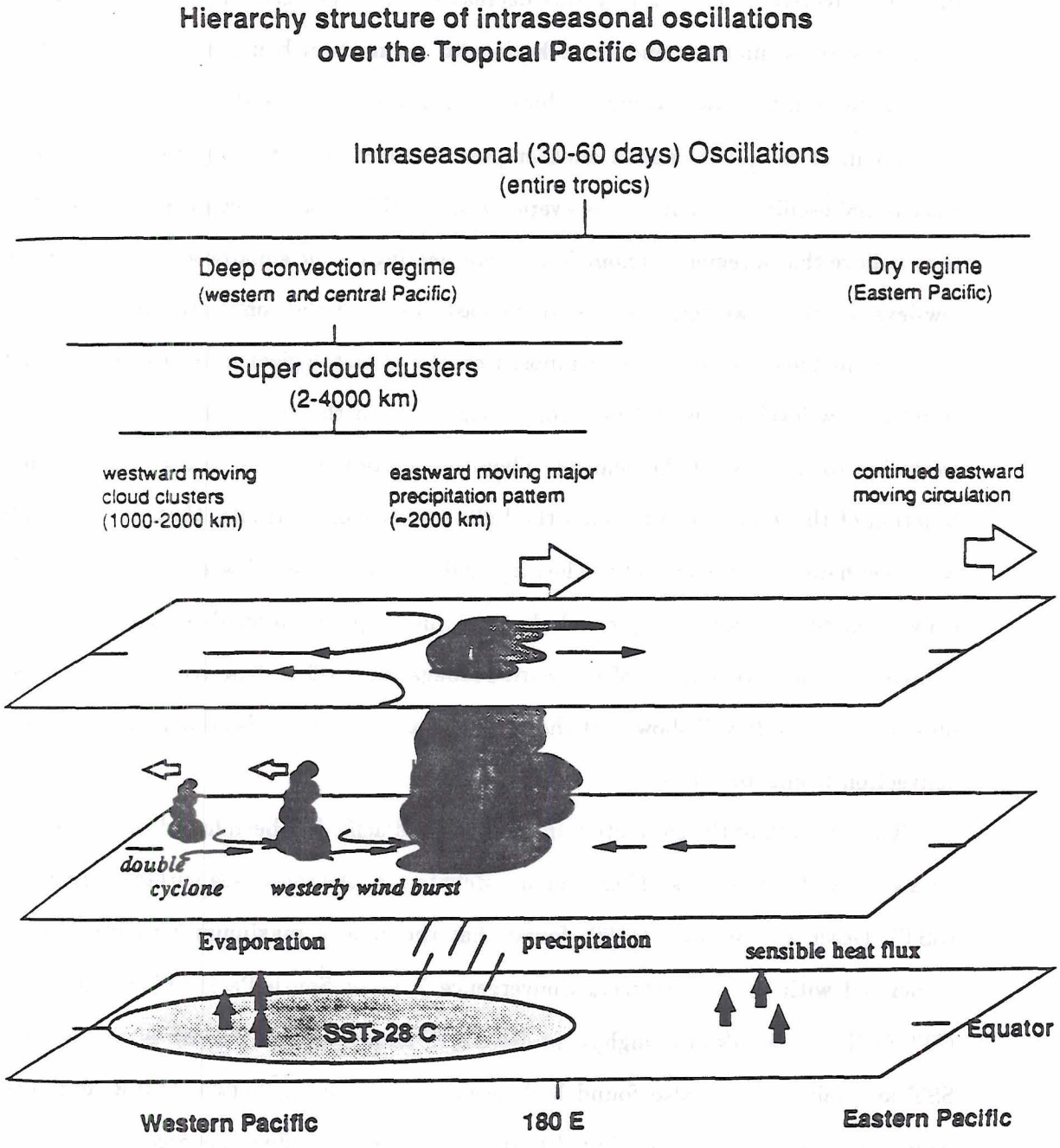

Figure 1.2: Schematic showing the 3-dimensional structure of the intraseasonal oscillation taken from Lau *et al.* (1989). Note the westerly wind bursts to the west of the major eastward moving precipitation pattern and the smaller westward moving cloud clusters. Also note the upper-level equatorial easterlies.

to less than 5 m s^{-1} . They attributed the slowing of the propagation to the increased latent heat from the ocean opposing the adiabatic cooling in the convective towers such that the effective static stability was decreased. This decrease in stability allowed for stronger vertical motions and more horizontal momentum being incorporated into the vertical motion, thereby slowing the horizontal propagation speed.

Neelin *et al.* (1987) added another possible mechanism for the existence of the intraseasonal oscillation, namely the evaporation-wind feedback mechanism. In this theory, they believe that a region of anomalous latent heating on the equator will force anomalous low-level easterly (westerly) winds to the east (west) of the convective anomaly. When these anomalous winds are superimposed on the climatological mean easterly flow, the resulting low-level winds will be stronger easterlies to the east and weaker easterlies or westerlies to the west of the heating. They then state that, because the evaporation is a function of the wind speed through the bulk aerodynamic formula, that the evaporation will be enhanced to the east of the heating and suppressed to the west, thereby enhancing convection to the east. They conclude that this evaporation-wind feedback mechanism is favorable for development of eastward-propagating modes. The results of the present observational study will show that the strongest anomalous winds actually occur after the convection begins to subside.

The strength of the convection in the tropical Pacific has been found to be modulated by a variety of parameters. There remains debate over the role of sea surface temperatures (SST). Deser and Wallace (1990) found that the area of maximum convection, usually associated with the Intertropical Convergence Zone or South Pacific Convergence Zone (ITCZ/SPCZ), follows the highest positive SST anomalies and intensifies with increased SST anomalies. They also found high negative correlations between OLR and surface wind convergence. They concluded that large scale vapor flux convergence rather than enhanced local evaporation is the main source for water vapor for enhanced precipitation. These results support the findings of Khalsa (1983). In his study of the 1972-73 El Niño data, he concluded that moisture convergence dominated over SST in determining the location of precipitation, despite the fact that monthly rainfall totals correlated equally

well with SST as with moisture convergence. By employing partial correlation analysis, he concluded that the correlations between SST and rainfall may be a result of the correlation between SST and surface winds and that the moisture convergence exerted the low-level control on rainfall.

Graham and Barnet (1987) analyzed SST, surface wind divergence and OLR and concluded that there is a critical temperature where convection is relatively unaffected by further increases in SST. Their results indicated that in regions with SST greater than 27°C, the convective activity is dominated by low level moisture convergence or some other remotely forced change in stability and/or vertical motion rather than SST. They also say that in a small range of temperatures either side of 27°C that the SST and OLR correlations were higher.

Zhang (1991) investigated the correlations between SST and OLR (as proxy for deep convection) in terms of the total fields rather than anomalies. By using monthly and climatological means, he concluded that oceanic regions not directly influenced by land masses or large scale circulation features show good correlations between persistently warm SST and OLR. He stressed the need for SST's to be sustained above a critical temperature for a time scale of months in order for deep convection to occur.

From these results one could infer that the MJO, which is believed to be convectively driven, is also modulated by SST in some manner. Or at least that the convection associated with it is modulated by SST.

Many studies have strived to describe the nature of convection, both in the tropics and the midlatitudes. If convection is an essential part of the MJO, then it is important to understand its characteristics. The problem again returns to data resolution. Our current observation network is unable to resolve the small-scale features within active convective towers. Even special observing programs, like GATE, have not allowed fine detailed analysis of individual convective elements whose lifespan is on the order of an hour.

Thus, investigators have used the data from the large-scale environment to infer properties of the small-scale cumulus regime. Large-scale heat and moisture budgets are

one way of characterizing the convective activity. The location of maximum heating often will shed light on the intensity of the convective activity. Deep intense tropical convective towers will have a peak in heating at higher levels than shallow trade wind cumulus. Johnson (1984) gives a good summary of the tropical budget studies (his Table 1). As mentioned earlier, several authors have shown that the propagation speed of the modeled MJO is sensitive to the level of the peak in heating.

Reed and Recker (1971) and Yanai *et al.* (1973) are among the first to investigate heat and moisture budgets over the tropical Pacific Ocean. Their results were very similar in that the maximum heating was found to be in the upper troposphere between 300-500 mb. In both these studies convective disturbances in the Marshall Islands were analyzed. The former utilized composited data associated with 18 synoptic-scale disturbances during July-September 1967, while the latter used data from cloud clusters during the period 15 April to 22 July 1956.

More recently and more in line with the present study, Chen and Yen (1991) completed a study of the diabatic heating associated with the MJO using data from the National Meteorological Centers (NMC) Global Data Assimilation System (GDAS). Because the MJO is evident in the velocity potential field (χ), they formulated a diagnostic relation between χ and the diabatic heating. They used this relationship to examine the diabatic versus adiabatic heating contributions to the total χ field. They found the first two eigenfunctions were in quadrature ($\frac{1}{4}$ wavelength out of phase), which has been found to be a characteristic of the MJO. They then concluded that the diabatic heating is the dominant forcing mechanism of the MJO.

Vincent *et al.* (1991) used a ECMWF global analysis data set to compute precipitation rates in the tropics using the Q_1 budget method of Yanai *et al.* (1973). They were able to produce monthly precipitation maps that were in good agreement with observations, despite using estimates of the sensible heating and radiation terms.

In this study a compositing scheme based OLR analysis during the Northern Hemisphere winter season (to be discussed in chapter 3) is applied to allow partitioning of the MJO into four phases: a convectively active phase, a convectively inactive phase and two

transition phases. Data from ECMWF and NMC (obtained from NCAR) are folded into this composite and analyzed.

The first objective of this study is to document the kinematic and thermodynamic characteristics of the MJO over the equatorial western Pacific Ocean and to show the evolution of these fields with the approach and passage of the active phase.

The second objective is to analyze the large-scale heat and moisture budgets associated with the MJO. Observational studies are important in light of the sensitivity of models of the oscillation to the vertical distribution of heating. As with the first objective, emphasis will be placed on the changes that occur within the four phases of the oscillation and the differences between the warm SST years and the cold SST year.

In both cases, horizontal and vertical cross-sections will be presented and compared to applicable previous studies. Also, a comparison between the results using the NMC and ECMWF data is done to allow some reliability estimates to be drawn. It is well known, however, that the analysis fields from the operational centers do not properly represent the tropical divergence fields (Kashahara *et al.* 1987). Results will be interpreted in light of the model differences in the tropics.

Chapter 2

BUDGET EQUATIONS AND COMPUTATIONAL METHODS

2.1 Budget Equations

It is widely accepted that organized cumulus convection has a great impact on the large scale circulation features within the atmosphere, both in the tropics and the mid-latitudes. In a study using composited soundings from Darwin, Australia, and OLR data, Hendon and Liebmann (1990) showed that the onset of the Australian summer monsoon and the associated changes in the large scale circulation patterns could be attributed to the passage of the first convectively active MJO across northern Australia. However, due to the lack of sufficient conventional observations on a scale comparable to the scale of the convection, the detailed characteristics of the convection could not be obtained directly. This is especially true in the region of this study, namely the equatorial western Pacific Ocean, where observations are typically separated by several thousand kilometers.

In order to gain insight into the effects of cumulus convection, researchers have typically resorted to an area-averaging scheme when computing heat and moisture budgets (e.g., Yanai *et al.* 1973). In this study time averaging is also used. By computing Q_1 (the apparent heat source) and Q_2 (the apparent moisture sink) at each grid point in the domain and then applying the compositing scheme (to be discussed later), we hope to determine the large scale character of the heat and moisture budgets within the MJO. After the compositing scheme is accomplished, some additional area averaging over latitudinal and longitudinal belts is done to determine the large-scale spatial variability of the oscillation.

The equations for Q_1 and Q_2, as derived by Yanai *et al.* (1973), are

$$Q_1 \equiv \frac{\partial \bar{s}}{\partial t} + \nabla \cdot \bar{s}\bar{\mathbf{V}} + \frac{\partial \bar{s}\bar{\omega}}{\partial p} = Q_R + L_v(\bar{c} - \bar{e}) - \frac{\partial \overline{s'\omega'}}{\partial p} \tag{2.1}$$

$$Q_2 \equiv -L_v \left(\frac{\partial \bar{q}}{\partial t} + \nabla \cdot \bar{q}\bar{\mathbf{V}} + \overline{\frac{\partial \bar{q}\bar{\omega}}{\partial p}} \right) = L_v(\bar{c} - \bar{e}) + L_v \frac{\partial \overline{q'\omega'}}{\partial p} \tag{2.2}$$

where

$$s \equiv c_p T + gz \tag{2.3}$$

is the dry static energy, q is the specific humidity, c is the rate of condensation, e is the rate of evaporation of cloud droplets and rain droplets, and Q_R is the radiative heating rate. The primes indicate perturbations from the mean and the overbar is an area average over a $5° \times 5°$ region.

From Eq. (2.1) it can be seen that Q_1 is the sum of the radiative heating/cooling, the net condensational latent heating, and the vertical convergence of the eddy transport of sensible heat. From Eq. (2.2), it can be seen that Q_2 is the sum of the net condensational heating and the vertical divergence of the eddy moisture transport.

2.2 Computational Methods

In all the calculations, finite differences are used to calculate the horizontal and vertical derivatives. This means, because the grid spacing is 2.5°, the averages were calculated centered on each grid over a horizontal area of approximately 555 × 555 km.

Vertical velocity was available in ECMWF data set as provided at NCAR, but had to be calculated for the NMC data set. The kinematic method was used to calculate ω with the method of adjustment described by Takayabu and Murakami (1991) applied in order to fix ω at 100 mb to zero.

Their equation is

$$\omega(p) = \omega_s + \int_p^{p_s} D dp - \omega(100mb) \times \frac{(p - p_s)}{(100 - p_s)} \tag{2.4}$$

where D is the horizontal divergence and ω_s is at the vertical velocity at the surface (set equal to zero). The last term on the right hand side of Eq. (2.4) results in a linear correction to ω.

The choice of 100 mb for the tropopause was made after examining the mean height of the tropopause from the study by Johnson (1986). In his analysis of the variation of the height of the tropopause over the MONEX area during December, he found the tropopause height varied from 80 to 100 mb. This was determined from sounding data launched from the *AK. Korolov* which was located near 4°N 111°E. This location is just west of the domain of this study, but is representative of the typical tropopause height in the equatorial western Pacific Ocean region.

In the budget equation for Q_2, Eq. (2.2), the mean specific humidity is used. Both data sets contained relative humidity rather than specific humidity and therefore q was calculated. The NMC data set contained virtual temperature instead of temperature (Jenne 1991) and because of the difficulty in reconstructing the temperature field, budget calculations were not done using the NMC data set. The saturation vapor pressure was calculated using the method described by Lowe and Ficke (1974). This method uses a polynomial formula involving temperature (°C) and seven constants. Their equation is

$$e_s = a_0 + T(a_1 + T(a_2 + T(a_3 + T(a_4 + T(a_5 + a_6 T))))) \tag{2.5}$$

where the constants (a_{0-6}) were calculated using a least-squared fitting procedure to the saturation vapor pressure versus temperature curves. The original intent of the procedure of Lowe and Ficke was to reduce the amount of computer time needed to calculate e_s by using a polynomial expression rather than the typical exponential function in Tetëns formula. The sixth order polynomial (2.5) yielded maximum percent errors of less than one percent for both ice and water phases. This procedure may have been more robust than was necessary given the data resolution, but the speed of the computations kept costs down. A -40°C threshold was used to differentiate between calculating with respect to water versus ice.

Mixing ratio was then calculated using

$$w = \frac{RH}{100} \times (0.62197) \times \left(\frac{e_s}{p - e_s}\right) \tag{2.6}$$

where e_s, p and RH are saturation vapor pressure, atmospheric pressure and relative humidity, respectively. Finally the specific humidity is arrived at by

$$q = \frac{w}{w+1} \tag{2.7}$$

It is often useful to examine anomaly fields rather than the total fields, especially those fields that show only small variations (eg., temperature and moisture). Typically anomalies are calculated by subtracting some long term annual mean. However, in this study we chose to calculate averages using only the data within the time of our analysis. We calculated means for the four month period (Nov-Feb) for each year and used these averages in computing anomalies of surface pressure, temperature and relative humidity.

Chapter 3

DATA AND COMPOSITING TECHNIQUE

The purpose of this chapter is to describe the data sets used in this study and to explain the method used in compositing the data.

3.1 Data Description

3.1.1 Outgoing Longwave Radiation (OLR)

The OLR data used in this study consists of daily-averaged radiation values in W m^{-2} from NOAA polar-orbiting satellites on a 2.5°×2.5° latitude-longitude grid. The time period used was September to April for 1986-87 and 1987-88 and October to April for 1988-89. The former were obtained from the Climate Applications Center (CAC) and consisted of a daily-average value for each grid point. The latter were retrieved from the National Center for Atmospheric Research (NCAR) Mass Storage System (MSS). The data from NCAR consisted of separate day and night values that were averaged together to yield a daily average. Missing data were not used in the averaging.

3.1.2 European Center For Medium Range Weather Forecasts (ECMWF)

A special ECMWF/TOGA global analysis data set was used in this study to describe the large scale environmental features in the tropical Pacific Ocean. This data set consists of uninitialized twice-daily surface and upper-air grid-point fields. The surface fields include pressure, temperature, horizontal component winds at 10 m and temperature at 2 m. The upper-air fields include geopotential, temperature, three-dimensional component winds and relative humidity at eleven standard pressure levels (1000, 850, 700, 500, 400, 300, 250, 200, 150, 100 and 70 mb). The data was retrieved from the MSS at NCAR and was stored on a 2.5°×2.5° latitude-longitude grid like the OLR data. Trenberth and

Olson (1988) give a full description of the ECMWF global analysis process and a list of major changes that have occurred between 1980 and 1988. Some of the most significant changes occurred during and after 1985. They include additional satellite winds (Feb 1985), substantial changes to physical parameterizations including clouds, convection and condensation (May 1985) and divergent structure functions in the mass and wind fields (Jan 1988). They also noted that the changes affected the divergent wind fields and associated vertical motion and moisture fields the most. The last change will need to be kept in mind when referring to the results of this study.

3.1.3 National Meteorological Center (NMC)

In order to determine the reliability of the ECMWF composited data analysis and to document differences between the two centers, we have used a similar data set from the NMC global analysis. The hope is that if the results using data from the two centers are similar, they will be more believable. The NMC data set, like the ECMWF set, consists of surface and upper-air fields on a $2.5° \times 2.5°$ latitude-longitude grid. The surface fields include virtual temperature, pressure and horizontal wind components and the upper-air fields used include geopotential height, virtual temperature, horizontal wind components, and relative humidity at 12 standard pressure levels (same as ECMWF with the addition of 50 mb). The NMC data does not include vertical motion, therefore, it is computed from the derived divergence.

3.2 Compositing Technique

It has been common practice to use compositing techniques to ascertain the structure of various tropical phenomena, including the MJO. Knutson and Weickmann (1987) used composited OLR and NMC data to describe the life cycle of the 30-60 day oscillation and Deser and Wallace (1990) used composited sea surface temperatures (SST), sea-level pressure, surface winds and OLR to examine the large scale atmospheric circulation features of warm and cold episodes in the tropical Pacific, just to name a few.

In this study, a composite based on the amount or phase of convective activity associated with the MJO is used. The intent is to try to isolate the large-scale characteristics

of the atmosphere associated with this global-scale phenomenon. Figure 3.1 shows the equatorial Pacific Ocean SST anomalies for Niños 1-4 (four regional descriptions of the El Niño, as defined by the Climate Analysis Center). From this figure it is clear that for Niño-4 (top curve), which includes the area between 5°N-5°S and 160°E-140°W, the SST anomalies are positive from mid 1986 to the beginning of 1988. The peak anomaly occurs during the 1987-88 Northern Hemisphere winter season at a maximum of 1.4°C.

However, by the classical definition of the El Niño, which refers to regions Niño-1 and Niño-2, the winter of 1987-88 would have to be considered a transition between a warm and a cold event. We have decided not to use the classical definition of El Niño and have categorized 1986-87 and 1987-88 as warm years and 1988-89 as a cold year in order to examine how the SST's modulate the oscillation. We feel this is acceptable because, as will be seen later, the results from 1986-87 and 1987-88 are very similar, presumably due to the similar SST's.

Figure 3.2 shows the main area of interest for this study in the tropical Pacific Ocean, specifically the area bounded by 20°N to 20°S and 140°E to 180°. Special attention will be given to the area near and south of the equator due to seasonal considerations and in light of the upcoming TOGA COARE (WMO 1990) field experiment that will be taking place during the same months as in this study in the region indicated on the figure.

A 1-2-3-2-1 filter was applied to the OLR data set in order to eliminate the shortest time period fluctuations and allow a smoother time-longitude (Hovmöller) analysis. The seasonal and annual cycles were not removed from the data prior to the analysis because the time period is only four months. Again, missing data were not used in the averaging. The data between 5.0°N and 5.0°S were averaged together and then plotted in time-longitude sections as shown in Figs. 3.3-3.5. The contour interval is 20 W m^{-2} and areas less than 200 W m^{-2} are cross-hatched. Migratory convection can easily be seen moving from west to east in all three figures. The areas of minimum (maximum) OLR are interpreted as the active (inactive) phase of the MJO and will become the basis for the compositing scheme.

The compositing method consists of both subjective and objective analysis of the Hovmöller diagrams. The axes of maximum and minimum OLR were first determined

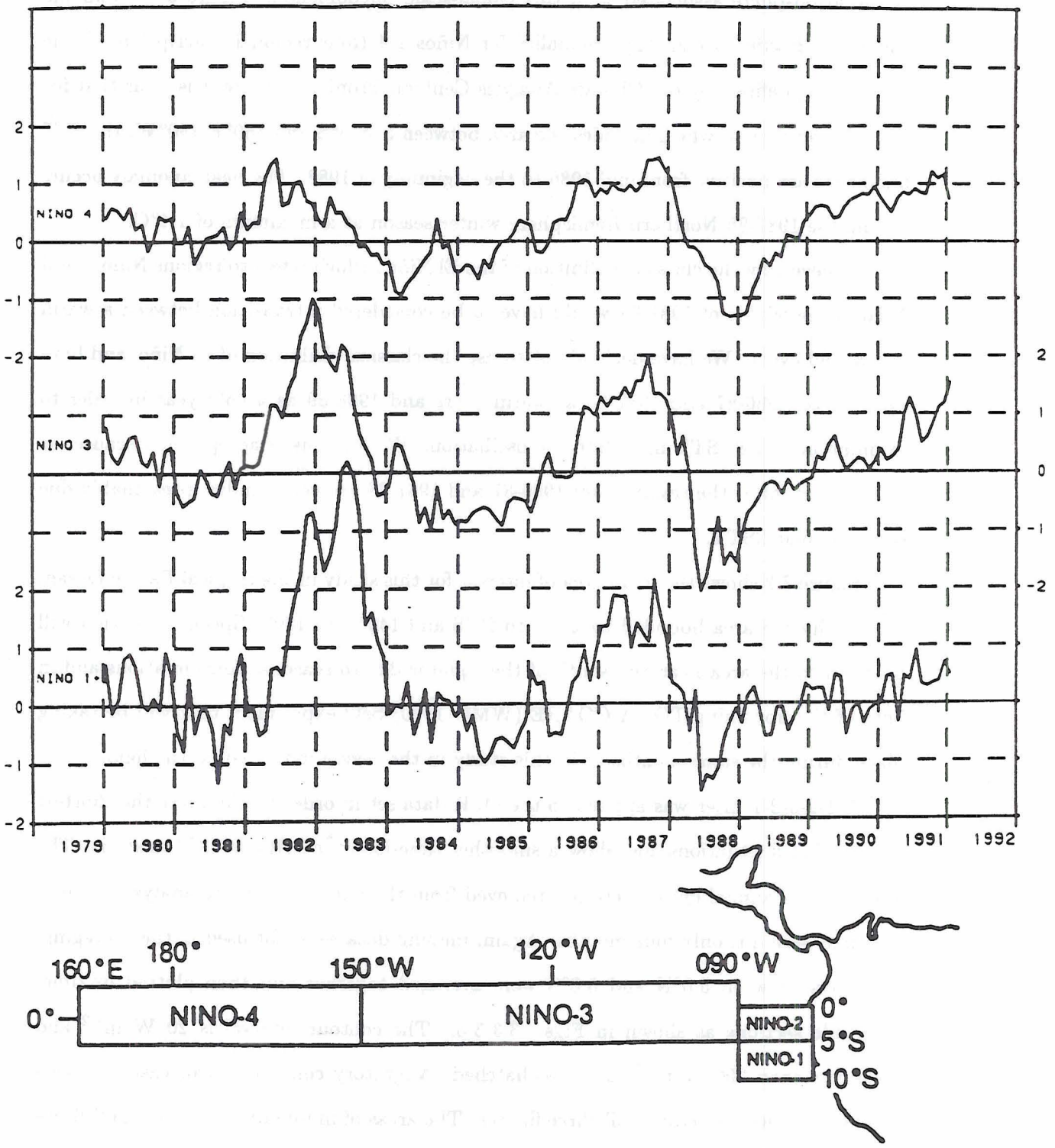

Figure 3.1: Equatorial Pacific Ocean sea surface temperature anomalies (°C) for the areas indicated at the bottom of the figure. Taken from Climate Diagnostics Bulletin, July 1991. Note for Niño-4, November through February of 1986-87 and 1987-88 have positive SST anomalies and 1988-89 have negative anomalies.

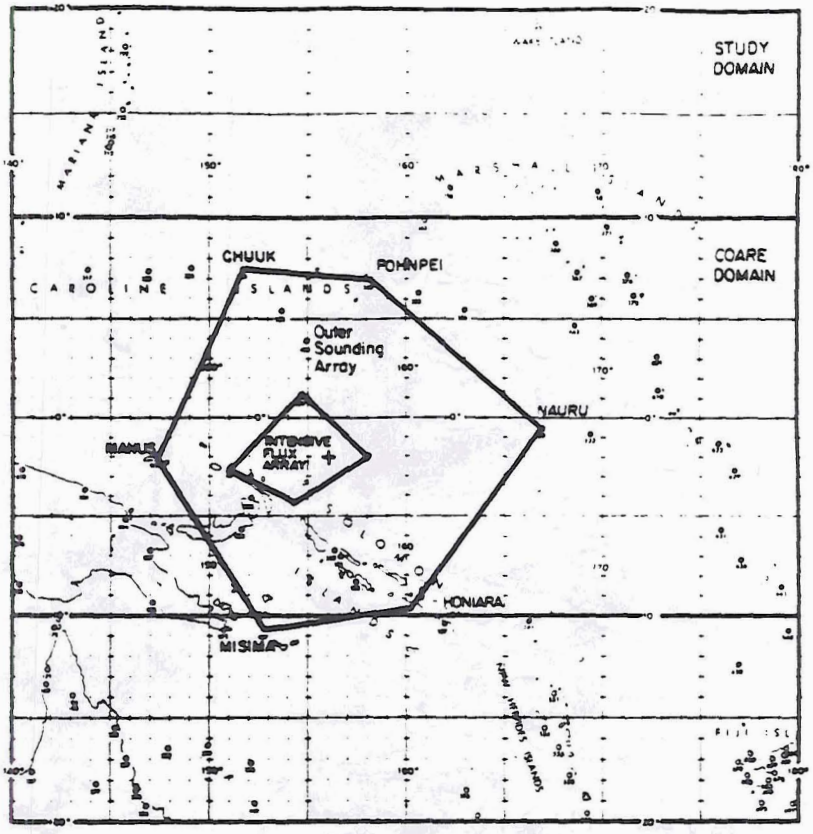

Figure 3.2: Map of the western Pacific Ocean showing the domain of this study and the domain of the 1992-93 TOGA/COARE experiment (from the TOGA/COARE Operations Plan 1992). The outer region represents the domain of this study. The rectangular box indicates the COARE large-scale domain. The larger trapezoid is the outer sounding array (OSA) and the interior region is the intensive flux array (IFA).

subjectively, taking care to use the entire 170 degree longitudinal extent of the data. As is quite evident, the exact determination of these axes was difficult in some instances. This was especially true of the OLR maximum axes. Once this procedure was completed, the remaining areas between the axes were objectively partitioned into four equal divisions. These divisions were then paired into four OLR phases, increasing, maximum, decreasing, and minimum which correspond to the opposite convective phases. That is, maximum OLR corresponds to minimum convection, etc. Figure 3.6 is a schematic describing the compositing technique. The solid line represents the amount of OLR and the dashed line is the corresponding convective activity.

With the diagram divided into phases, the days that fit each phase for each longitude belt from 1 November to 28 February (29 in 1988) were determined. Using these dates, two to three complete cycles of the wave were captured. Because the data consists of twice-

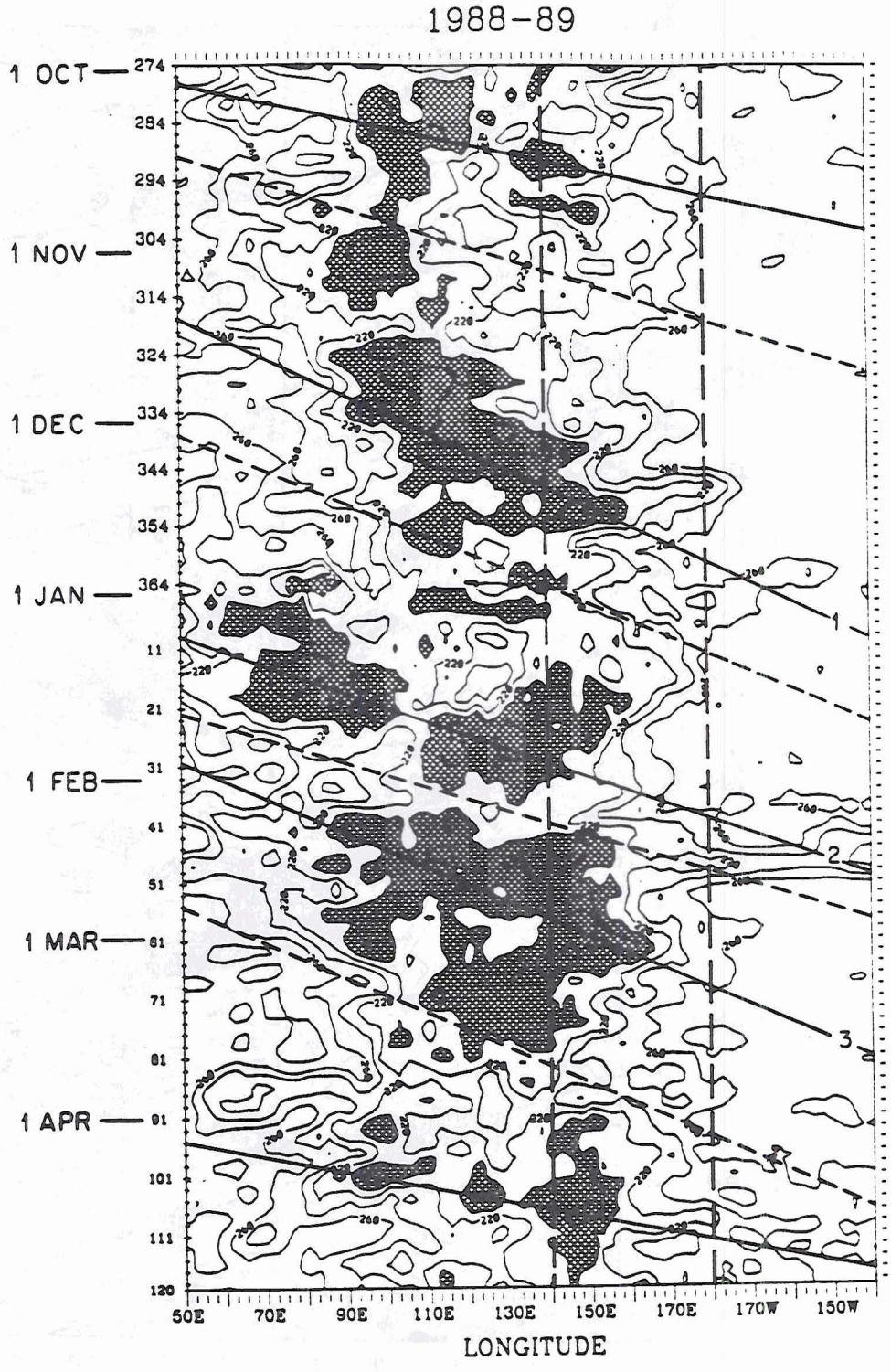

Figure 3.5: Same as Fig. 3.3, except October 1988 through April 1989.

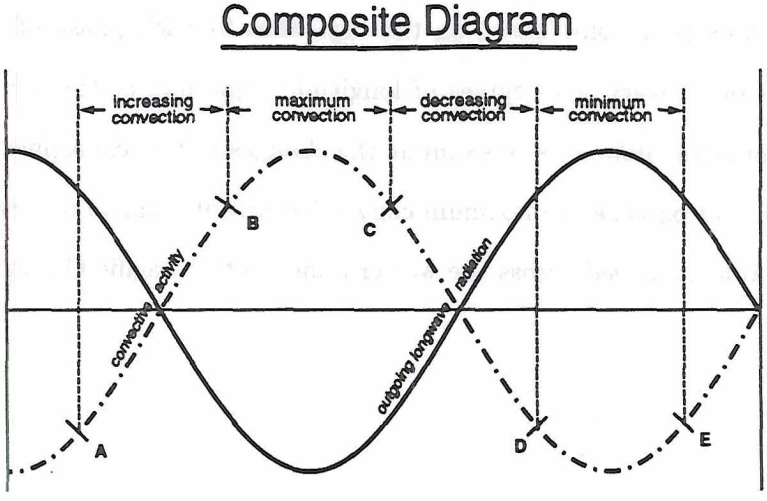

Figure 3.6: Schematic describing the compositing technique. The solid curve represents the idealized outgoing longwave radiation and the dashed curve represents the corresponding convective activity. The regions between the dashed vertical lines represent the four phases of the composite.

daily values, the number of days (Nov-Feb) is essentially half the number of observations for each phase of the composite. Thus the total number of observations ranged from 228 to 242. The period between November 2 and November 8 1986 was not used in the composite for the NMC data due to erroneous data during those days. A complete list of days used in each phase category for each year is presented in Tables A.1-A.3 in the appendix.

The next step was to apply the composite days to each data field by averaging together all the data that fit a particular category for a specific grid point. Hence, for example, at a given grid point, say 5.0°S and 155.0°E, all the data for days fitting the maximum convection phase are averaged together. This process is repeated for the entire grid at each level. This compositing method enabled us to examine the north-south structure at a given longitude or, by combining the data at all longitudes, to examine the average meridional characteristics.

In order to better examine the east-west structure of the atmosphere as the convection propagated across the western and central Pacific Ocean, a slightly different compositing procedure was used. The convective phases at five longitudinal points were used as the basis for five separate composites. For example, the composite based on the phase of convection at 160°E was constructed by averaging data at each grid point with other data

at that same grid point based on the days that fit each phase of convection at 160°E. This was done every ten degrees of longitude beginning at the left edge of the domain. This composite allowed us to examine the changes in the atmosphere associated with the approach and passage of maximum convective activity and to observe changes within the oscillation as it moved across the western and central Pacific Ocean.

Chapter 4

OUTGOING LONGWAVE RADIATION (OLR) ANALYSIS

4.1 Time-Longitude Diagrams

As discussed in chapter 3, the daily OLR data were subjected to a 1-2-3-2-1 filter, averaged between 5.0°N and 5.0°S and then displayed in time-longitude diagrams in order to determine the four convective phases of the MJO (Figs. 3.3-3.5). These phases were then used in the compositing technique. The contour interval is 20 W m^{-2} and values less than or equal to 200 W m^{-2} are cross-hatched. The eastward propagation of convection (low OLR values) can easily be seen following the cross hatched regions.

Some interannual similarities can be seen in Figs. 3.3-3.5. There appears to be a fairly consistent longitude where deep convection initiates. In each of the three years the minimum in OLR begins near 90°E and propagates eastward. This location is similar to what was presented in the original schematic of the MJO by Madden and Julian (1972). The reason for this preferred location is not clear from our analysis, yet SST analysis yields a possible explanation. Close inspection of SST's in the region near 90°E (Figs. 4.1a-c) indicates a tongue of SST $\geq$ 29°C extending west of the Sumatra during two of the three analysis periods. In Figs. 4.1a and 4.1b, which are December-January-February averages for 1986-87 and 1987-88 respectively, the dashed line shows that the 29°C contour extends to near the point where the convection initiates. A similar 3-month average was unavailable for 1988-89, so Fig. 4.1c is the analysis for January 1989. This figure does not show this tongue of warm water, but December 1988 (not shown) does. This is, in all likelihood, not the only explanation, but it is no doubt a possible contributing factor.

It is interesting to note that the propagation signal in OLR is most evident in the El Niño years. However, recall from Fig. 3.1 that the sea surface temperature anomalies

of 4-6 m s^{-1} and velocity potential speeds of nearly 10 m s^{-1} . The corresponding period for these 4-6 m s^{-1} phase speeds are 116-77 days, while that for the velocity potential is 46 days. We calculated phase speeds from the time-longitude diagrams in two ways. First the number of days between the axes of minimum OLR was extracted from Figs. 3.3-3.5 for every ten degrees of longitude between 140°E to the International Dateline. This was interpreted as the time it took the wave to complete on revolution around the globe at equator. The speed was determined using a mean equatorial radius of 6378 km. The second method again used the axis of minimum OLR, but only the cross hatched region was used. The slope of the axis was used to determine the speed by using the number of days divided by the corresponding longitudinal distance traveled. Table 4.1 shows the phase speed computed using the second method for each of the waves used in the composite analysis. Note the broad range of values, even within the same year. Note also that the average speed in the two years with positive SST anomalies are slightly faster than the year with negative anomalies. However, it should be kept in mind that the sample size used to calculate these averages is very small and therefore, the results are not statistically significant. Nonetheless, these results are consistent with the results of numerical simulations of the MJO (e.g., Chang and Lim 1988; Lau *et al.* 1989; Sui and Lau 1989) in that when the maximum heating is in the upper troposphere (above 500 mb), as it would be expected in the warm SST years and is confirmed later in this study, the phase speed is faster.

Table 4.1: Translation Speed (m s^{-1})

Year	Wave 1	Wave 2	Wave 3	Average
1986-87	5.6	5.7	5.1	5.5
1987-88	8.3	4.4	4.1	5.6
1988-89	4.1	5.7	4.3	4.7

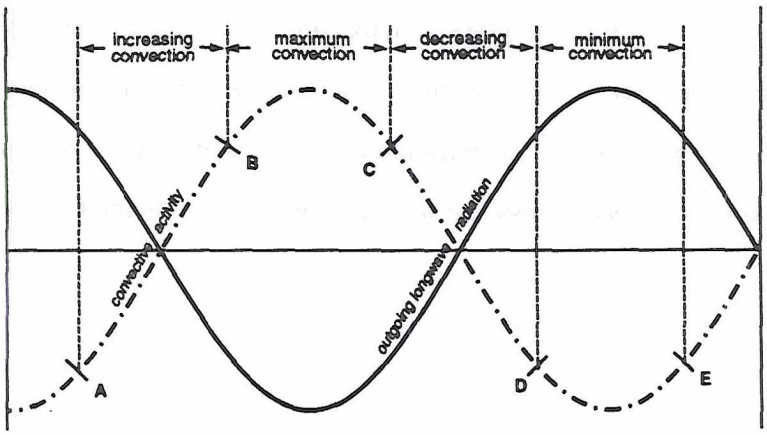

Figure 3.6: Schematic describing the compositing technique. The solid curve represents the idealized outgoing longwave radiation and the dashed curve represents the corresponding convective activity. The regions between the dashed vertical lines represent the four phases of the composite.

daily values, the number of days (Nov-Feb) is essentially half the number of observations for each phase of the composite. Thus the total number of observations ranged from 228 to 242. The period between November 2 and November 8 1986 was not used in the composite for the NMC data due to erroneous data during those days. A complete list of days used in each phase category for each year is presented in Tables A.1-A.3 in the appendix.

The next step was to apply the composite days to each data field by averaging together all the data that fit a particular category for a specific grid point. Hence, for example, at a given grid point, say 5.0°S and 155.0°E, all the data for days fitting the maximum convection phase are averaged together. This process is repeated for the entire grid at each level. This compositing method enabled us to examine the north-south structure at a given longitude or, by combining the data at all longitudes, to examine the average meridional characteristics.

In order to better examine the east-west structure of the atmosphere as the convection propagated across the western and central Pacific Ocean, a slightly different compositing procedure was used. The convective phases at five longitudinal points were used as the basis for five separate composites. For example, the composite based on the phase of convection at 160°E was constructed by averaging data at each grid point with other data

at that same grid point based on the days that fit each phase of convection at 160°E. This was done every ten degrees of longitude beginning at the left edge of the domain. This composite allowed us to examine the changes in the atmosphere associated with the approach and passage of maximum convective activity and to observe changes within the oscillation as it moved across the western and central Pacific Ocean.

Chapter 4

OUTGOING LONGWAVE RADIATION (OLR) ANALYSIS

4.1 Time-Longitude Diagrams

As discussed in chapter 3, the daily OLR data were subjected to a 1-2-3-2-1 filter, averaged between 5.0°N and 5.0°S and then displayed in time-longitude diagrams in order to determine the four convective phases of the MJO (Figs. 3.3-3.5). These phases were then used in the compositing technique. The contour interval is 20 W m^{-2} and values less than or equal to 200 W m^{-2} are cross-hatched. The eastward propagation of convection (low OLR values) can easily be seen following the cross hatched regions.

Some interannual similarities can be seen in Figs. 3.3-3.5. There appears to be a fairly consistent longitude where deep convection initiates. In each of the three years the minimum in OLR begins near 90°E and propagates eastward. This location is similar to what was presented in the original schematic of the MJO by Madden and Julian (1972). The reason for this preferred location is not clear from our analysis, yet SST analysis yields a possible explanation. Close inspection of SST's in the region near 90°E (Figs. 4.1a-c) indicates a tongue of SST $\geq$ 29°C extending west of the Sumatra during two of the three analysis periods. In Figs. 4.1a and 4.1b, which are December-January-February averages for 1986-87 and 1987-88 respectively, the dashed line shows that the 29°C contour extends to near the point where the convection initiates. A similar 3-month average was unavailable for 1988-89, so Fig. 4.1c is the analysis for January 1989. This figure does not show this tongue of warm water, but December 1988 (not shown) does. This is, in all likelihood, not the only explanation, but it is no doubt a possible contributing factor.

It is interesting to note that the propagation signal in OLR is most evident in the El Niño years. However, recall from Fig. 3.1 that the sea surface temperature anomalies

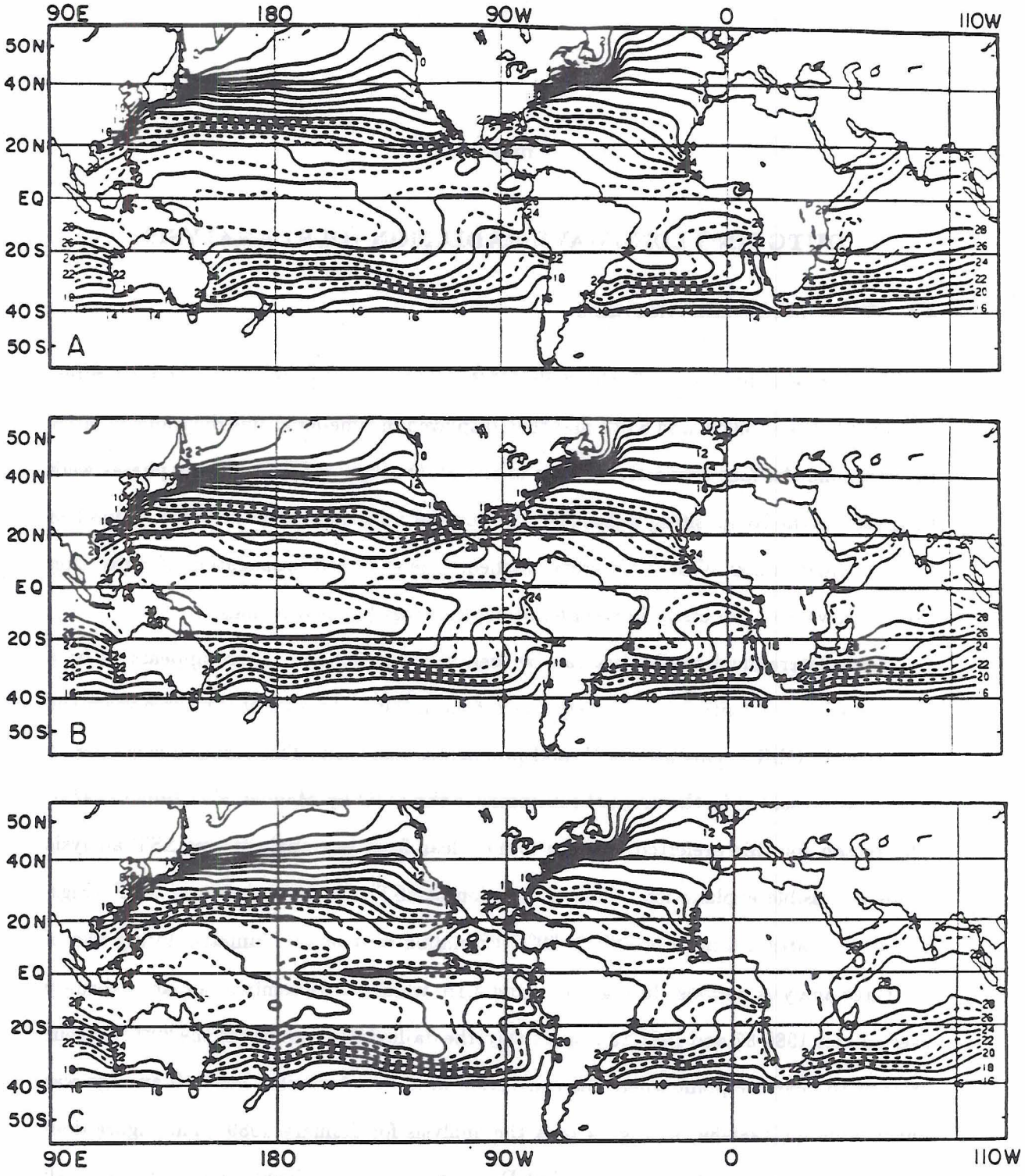

Figure 4.1: Mean sea surface temperatures (°C) around the globe for a.) DJF 1986-87, b.) DJF 1987-88, and c.) January 1989 (from Climate Diagnostics Bulletins). Note the region of 29°C water extending to 90°E in a and b.

in the Niño-4 region (between 160°E and 150°W) are positive during the years that the OLR propagation can most readily be seen. Also noteworthy is that the propagation is most coherent during the warm events. The warm sea surface temperatures are believed to be instrumental in maintaining the convection. Close inspection of the regions of minimum OLR indicates the convection is most intense during these same years. This is seen by the number of contours within the shaded regions. Values of OLR are typically between 180-200 W m^{-2}. During 1986-87 and 1987-88 there are more areas that have OLR values less than 180 W m^{-2} than in 1988-89. This is consistent with the findings of Liebmann and Hartmann (1982). Deser and Wallace (1990) also showed the convection within the Intertropical Convergence Zone (ITCZ) is more intense during an El Niño event than during a La Niña event. However, it should be kept in mind that these Hovmöller diagrams were constructed using OLR values averaged between 5.0°N and 5.0°S, so that convection outside this equatorial belt was not sampled.

Some obvious inter-annual differences can also be seen. The most distinct difference is the distance the deep convection travels. Low OLR values extend to 150°W during 1986-87, to 170°W in 1987-88 and only to 160°E in 1988-89. However, because these Hovmöller diagrams were created using OLR data averaged between 5.0°N and 5.0°S, it is possible that the propagation during 1988-89 shifted south of this latitude belt. Knutson and Weickmann (1987) used a six year record of OLR to examine the composite life cycles of convection and found that during the Northern Hemisphere winter (defined by them as November to April) the convection did not penetrate east of 150°W. This is consistent with the eastern extent of convection in our study for the years when SST anomalies are positive in Niño-4.

It has been well documented that the OLR signal propagates at a somewhat slower speed than that of other parameters, like zonal winds. Lau and Chan (1985) found the OLR phase speed to be approximately 4-5 m s^{-1} in their 1974-83 analysis, while Knutson and Weickmann (1987) found a characteristic speed of 3-6 m s^{-1} for the years 1979-84. In a 1981-82 case study of the shift of convection from the Indian Ocean to the western Pacific Ocean, Weickmann and Khalsa (1990) documented convective propagation speeds

of 4-6 m s^{-1} and velocity potential speeds of nearly 10 m s^{-1} . The corresponding period for these 4-6 m s^{-1} phase speeds are 116-77 days, while that for the velocity potential is 46 days. We calculated phase speeds from the time-longitude diagrams in two ways. First the number of days between the axes of minimum OLR was extracted from Figs. 3.3-3.5 for every ten degrees of longitude between 140°E to the International Dateline. This was interpreted as the time it took the wave to complete on revolution around the globe at equator. The speed was determined using a mean equatorial radius of 6378 km. The second method again used the axis of minimum OLR, but only the cross hatched region was used. The slope of the axis was used to determine the speed by using the number of days divided by the corresponding longitudinal distance traveled. Table 4.1 shows the phase speed computed using the second method for each of the waves used in the composite analysis. Note the broad range of values, even within the same year. Note also that the average speed in the two years with positive SST anomalies are slightly faster than the year with negative anomalies. However, it should be kept in mind that the sample size used to calculate these averages is very small and therefore, the results are not statistically significant. Nonetheless, these results are consistent with the results of numerical simulations of the MJO (e.g., Chang and Lim 1988; Lau *et al.* 1989; Sui and Lau 1989) in that when the maximum heating is in the upper troposphere (above 500 mb), as it would be expected in the warm SST years and is confirmed later in this study, the phase speed is faster.

Table 4.1: Translation Speed (m s^{-1})

Year	Wave 1	Wave 2	Wave 3	Average
1986-87	5.6	5.7	5.1	5.5
1987-88	8.3	4.4	4.1	5.6
1988-89	4.1	5.7	4.3	4.7

4.2 Composited OLR

The variation in convective activity from year to year can also be seen in the composited OLR data. Figures 4.2-4.4 show the latitudinal and longitudinal changes of the OLR for each phase of the oscillation after applying the composite based on the phase at 160°E. It is clearly evident that the distribution of convection is very different during the El Niño years verses the La Niña year. However, the eastward propagation that was seen in the Hovmöller diagrams (Figs. 3.3-3.5) is evident in the composited OLR in all three years.

The two warm anomaly years are quite similar with convection centered near the equator and extending to the dateline with very little slope indicated. In contrast, in 1988-89 the convection has moved nearly ten degrees to the south, especially during the minimum (maximum) OLR (convection) phase. Also, there is a very distinct slope from the northwest to the southeast corresponding to the location of the South Pacific Convergence Zone (SPCZ). This is consistent with the findings of Deser and Wallace (1990) who showed that during El Niño events the convection shifts eastward and moves closer to the equator following the warm SSTs and the equatorial dry zone shrinks in size and during La Niña events the convection moves off the equator and the equatorial dry zone expands.

Another feature seen in the composited OLR is the location of the Northern Hemisphere subtropical ridge. During the warm years the convection is closer to the equator and the subtropical ridge, indicated by the highest values of OLR, is located north of 20.0°N. In contrast, the ridge axis is clearly located between 15.0°N and 20.0°N during the cold year of 1988-89. The convection is believed to have changed the location of the Hadley circulation and the position of the subtropical high.

Also evident in the warm year of 1987-88 is a meridional shift of the subtropical ridge with the change of the phase of the MJO. The highest OLR values reach their most southern extent during the minimum convection phase and then retreats northward as the convective activity increases. A similar trend is apparent in 1986-87, but not nearly as obvious. The difference in the latter year may be due to the fact that there is more convection north of the equator during this year, thereby causing the subtropical ridge

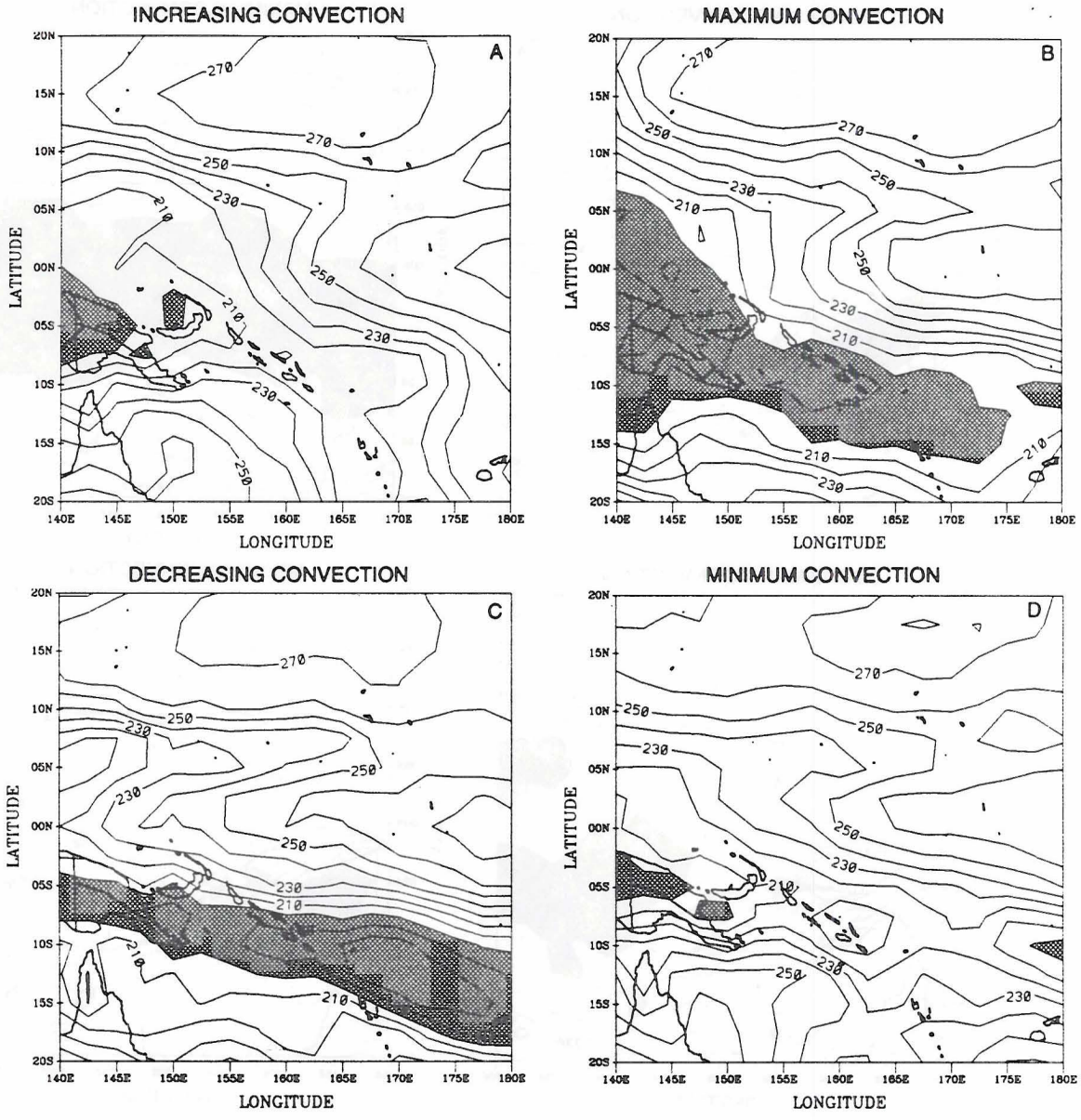

Figure 4.4: Same as Fig. 4.2, except 1988-89.

to be slightly farther north. Thus, a shift in the position may be occurring north of the analysis domain.

Examination of the maximum convection phase (minimum OLR) analyses shown in Figs. 4.2b, 4.3b and 4.4b, indicate there is generally good agreement with the intensity results of Liebmann and Hartmann (1982) and Deser and Wallace (1990) discussed earlier. The convection appears more intense during the warm years. It is also evident that the areal coverage of convection appears to be largest during the warm years, as evident in a comparison of the amount of cross hatched area for the three years.

Chapter 5

COMPOSITE KINEMATIC AND THERMODYNAMIC FIELDS

The purpose of this chapter is to show the variations of kinematic and thermodynamic fields with respect to the phase of the MJO. The primary flow features of the MJO are best seen in the zonal wind component, but the meridional component is also presented. In addition, the divergence and vertical motion fields are also examined. The kinematic fields will be presented as total fields and surface pressure, temperature and relative humidity will be presented in the form of anomalies.

5.1 Kinematic Fields

5.1.1 Zonal Winds

In order to describe the character of the zonal winds associated with the MJO, a vertical profile of the u-component is presented in a pressure versus convective phase diagram. In this diagram, the phases are positioned in such a way that the true west-to-east structure of the MJO can be visualized. An average of all longitudes (140°E-180°) was computed for each latitude. The results between the equator and 10.0°S are very similar, so only those at 5.0°S are presented in Fig. 5.1.

Some interesting similarities exist in all three years of the analysis. In each year there are low-level westerly wind maxima to the west of the maximum deep convection (during the decreasing convection phase). This result is consistent with the hierarchy structure of intraseasonal oscillations described by Lau *et al.* (1989) (see Fig. 1.2). However, the character of the westerly wind maximum during the cold year, 1988-89, is strikingly different from that in the two warm years.

In 1988-89, the westerly winds never quite reach the surface during any of the four convective phases. This does not mean that there are never westerly winds at the surface

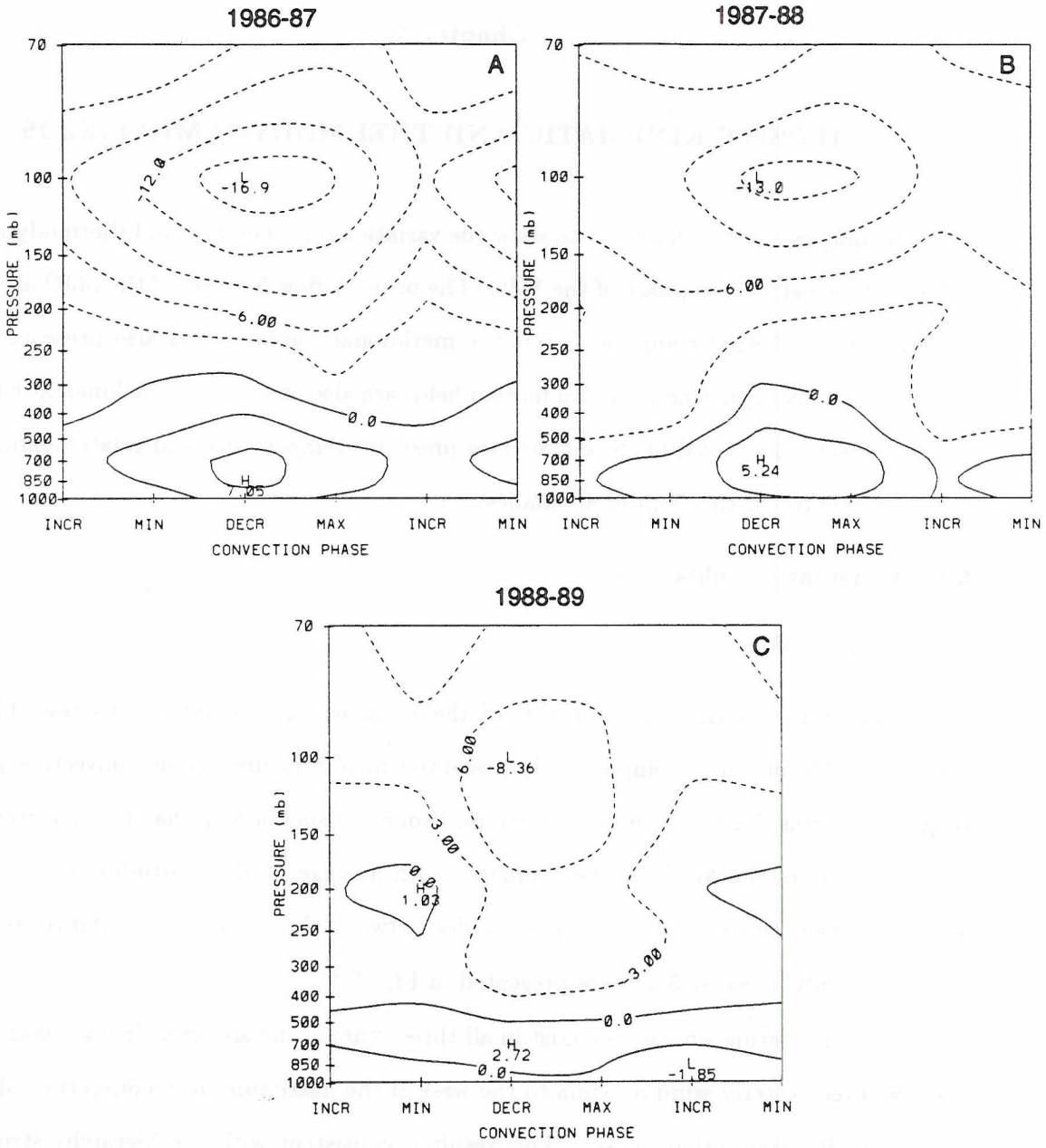

Figure 5.1: Pressure-phase diagrams of ECMWF composited zonal wind (m s^{-1}) averaged from 140°E to 180° at 5.0°S for a.) 1986-87, b.) 1987-88 and c.) 1988-89. Solid contours represent westerly winds and dashed represent easterlies. The contour interval is 3.0 m s^{-1}

.

during this La Niña year, but that in the average over the region between 140°E and 180°, surface easterlies dominate. It also appears that the peak in the westerlies is at a higher level during the cold year. The maximum for the two warm years is between 850 mb and 700 mb and it is closer to 650 mb for the cold year. This is evident in the composites done with both the ECMWF and NMC data (Fig. 5.2). For the most part there is good agreement between the two data sets, the only exception being the magnitudes of the winds are larger in the ECMWF composite. The overall patterns are very similar.

The fact that the maximum westerlies lag the maximum convective activity is an interesting finding. Numaguti and Hayashi (1991) discuss three theoretical concepts of interaction of cumulus convection and the large-scale circulations. One theory of the mechanism for the MJO is frictional Convective Instability of the Second Kind (frictional CISK). In this theory a disturbance is maintained by the intensification of convection caused by frictionally induced moisture convergence in the planetary boundary layer. Wang (1988) argued that friction in the planetary boundary layer dissipates kinetic energy, but also generates eddy potential energy through moisture convergence. It is theorized that when the moisture convergence becomes larger than the frictional dissipation, the longest waves will become unstable and amplify which would lead to atmospheric oscillations with a period near the MJO. A second theory is the wave-CISK theory, which states that a disturbance is maintained through intensification of convection enhanced by the vertical motions associated with the wave. Lau *et al.* (1989) argue in favor of this theory. A third theory is the evaporation-wind feedback mechanism. In this theory the disturbance is maintained by the evaporation of moisture from the surface which is a function of wind speed by the bulk aerodynamic formula. Neelin *et al.* (1987) argue in favor of this theory. The phase results presented here could support both the frictional-CISK and the wave-CISK theories. These results do not support the third theory because the evaporation-wind feedback mechanism would require enhanced low-level flow prior to the enhancement of the convective activity. It should be mentioned that the maximum low-level convergence does in fact occur during the increasing convective phase, as will be shown later in this chapter.

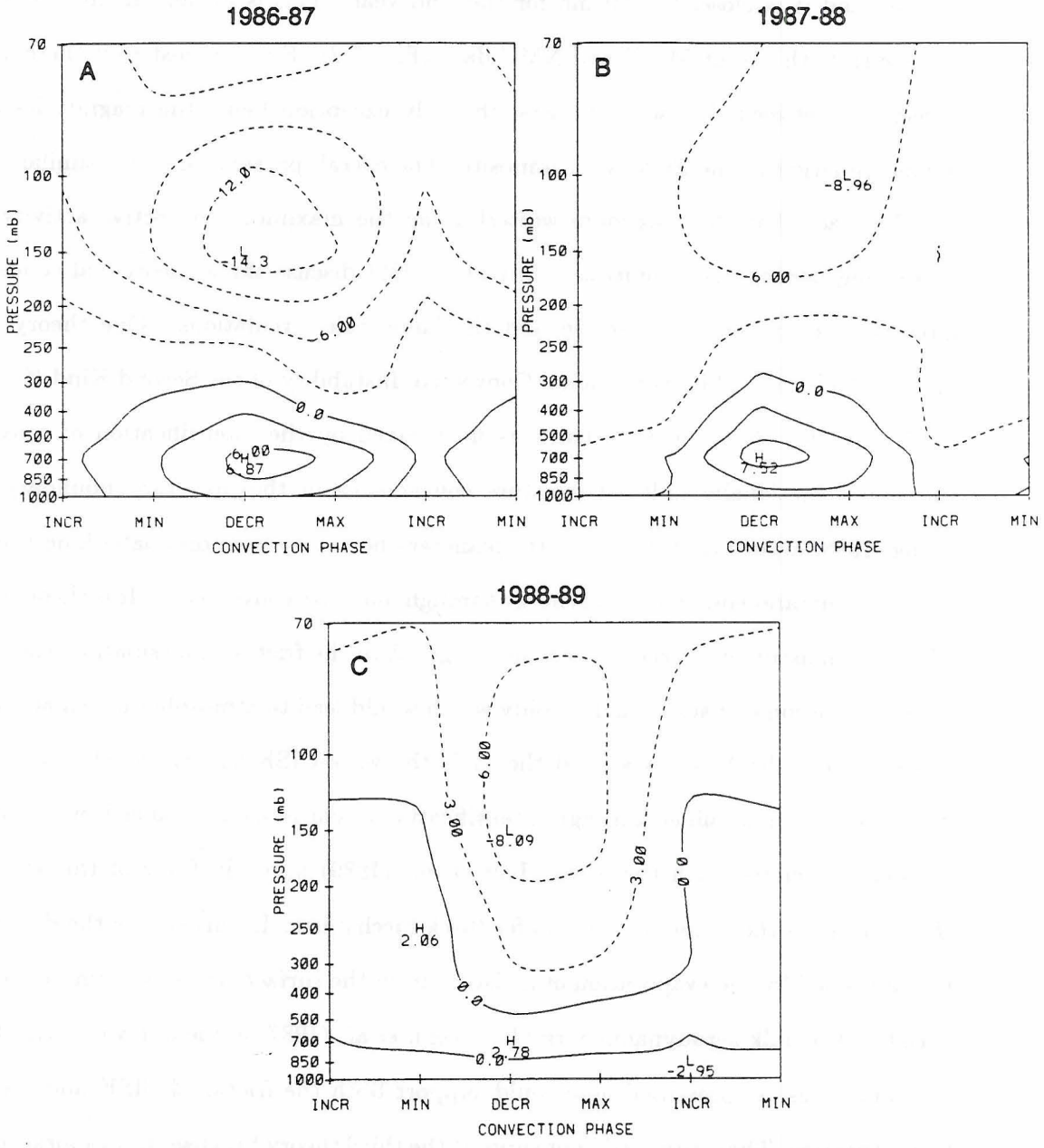

Figure 5.2: Same as Fig. 5.1, except for NMC composite.

Another obvious similarity between the three years is the phase reversal of the wind with height. In all years there are westerlies in the low-levels with easterlies in the upper-levels. This is consistent with the observational studies by Madden and Julian (1971) and later by Madden (1986). However, the results of Madden and Julian (1971), using sounding data from Canton Island (3°S 172°W), indicated there is an abrupt reversal in the winds between 500 mb and 600 mb. Figure 5.1 indicates the transition from westerlies to easterlies during the decreasing convective phase when the westerlies are maximum, occurs between 300-400 mb during the warm years and between 400-500 mb for the cold year. Also, the transition does not appear to be abrupt. The difference in the abruptness of the phase reversal could be due to the fact that Canton Island is located to the east of the domain of this study or it could be a result of the averaging over many longitudes that has been done in this study. Again these results are consistent in the two data sets.

While easterlies are present at upper-levels in each of the three years, the structure is different during the La Niña year. The first difference that is evident is the narrow easterly core in the upper-levels and the double jet pattern apparent during 1988-89. Both data sets show a weaker easterly jet core (8 m s^{-1} versus 12-15 m s^{-1} in the El Niño years) that is restricted between the maximum and decreasing convective phases during this cold year. This narrow core of easterlies is in contrast to the rather broad area of easterlies in the El Niño years. In fact, there are weak westerlies between 200-250 mb during the minimum convective phase in the La Niña year.

The regional variation of zonal winds are best seen using latitude versus longitude diagrams at a specific pressure level. The composite based on the convective activity at 160°E was used to construct Figs. 5.3-5.5 and applies to all of the following discussions of regional variability.

At the low-levels, the most striking feature is the existence of westerly winds in the regions of greatest convective activity. The location of the westerlies is coincident with the regions of the lowest OLR values (strongest convective activity) shown in Figs. 4.2-4.4 and the orientation of the axes of the westerlies are also very similar to the orientation of the axes of OLR. Also, as with the OLR analysis, the westerly winds, centered on and

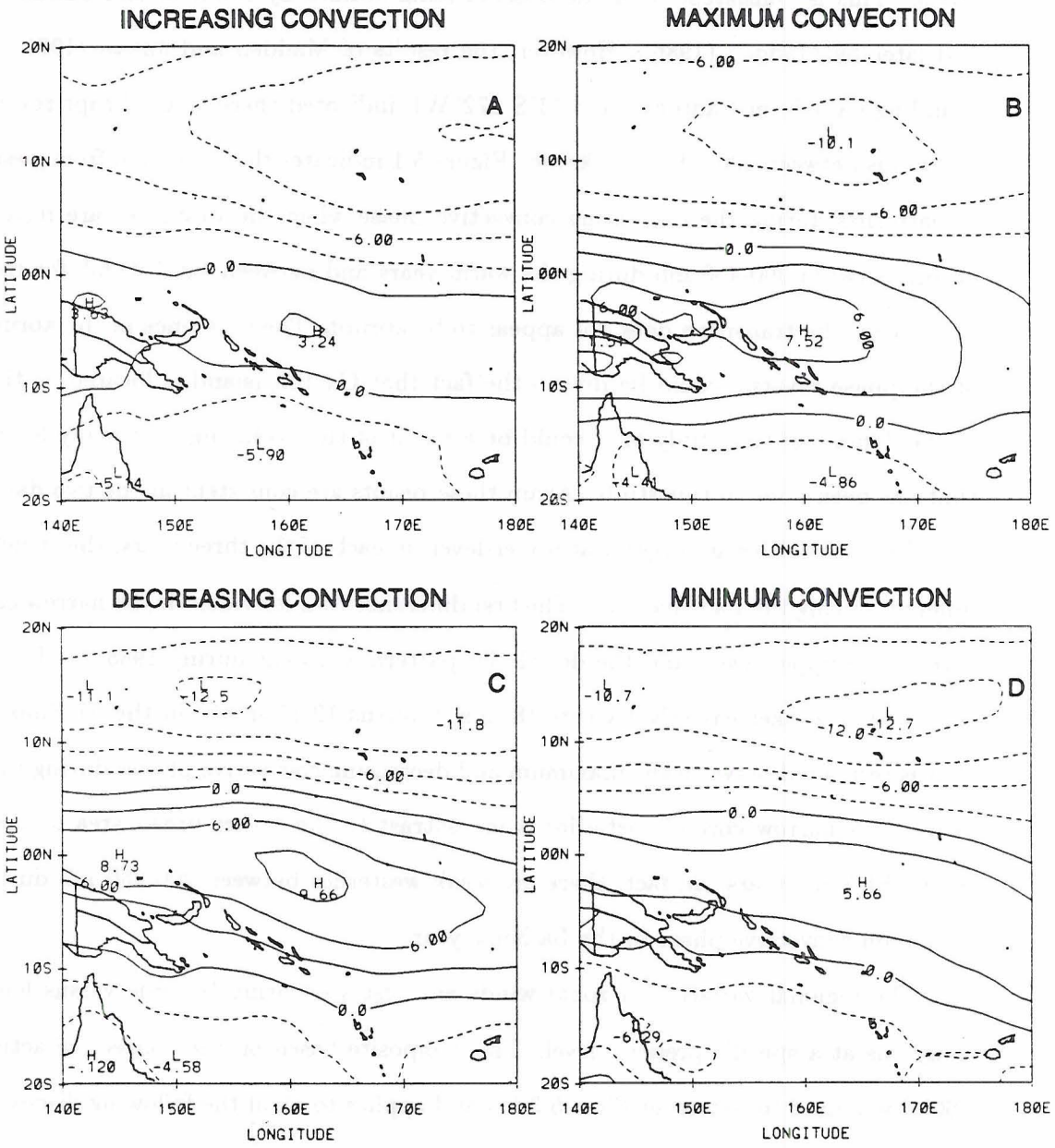

Figure 5.3: 1986-87 latitude-longitude diagrams of ECMWF composited zonal wind (m s^{-1}) at 850 mb for the a.) increasing, b.) maximum, c.) decreasing and d.) minimum convection phases of the MJO. Solid contours represent westerly winds and dashed represent easterlies. The contour interval is 3.0 m s^{-1} .

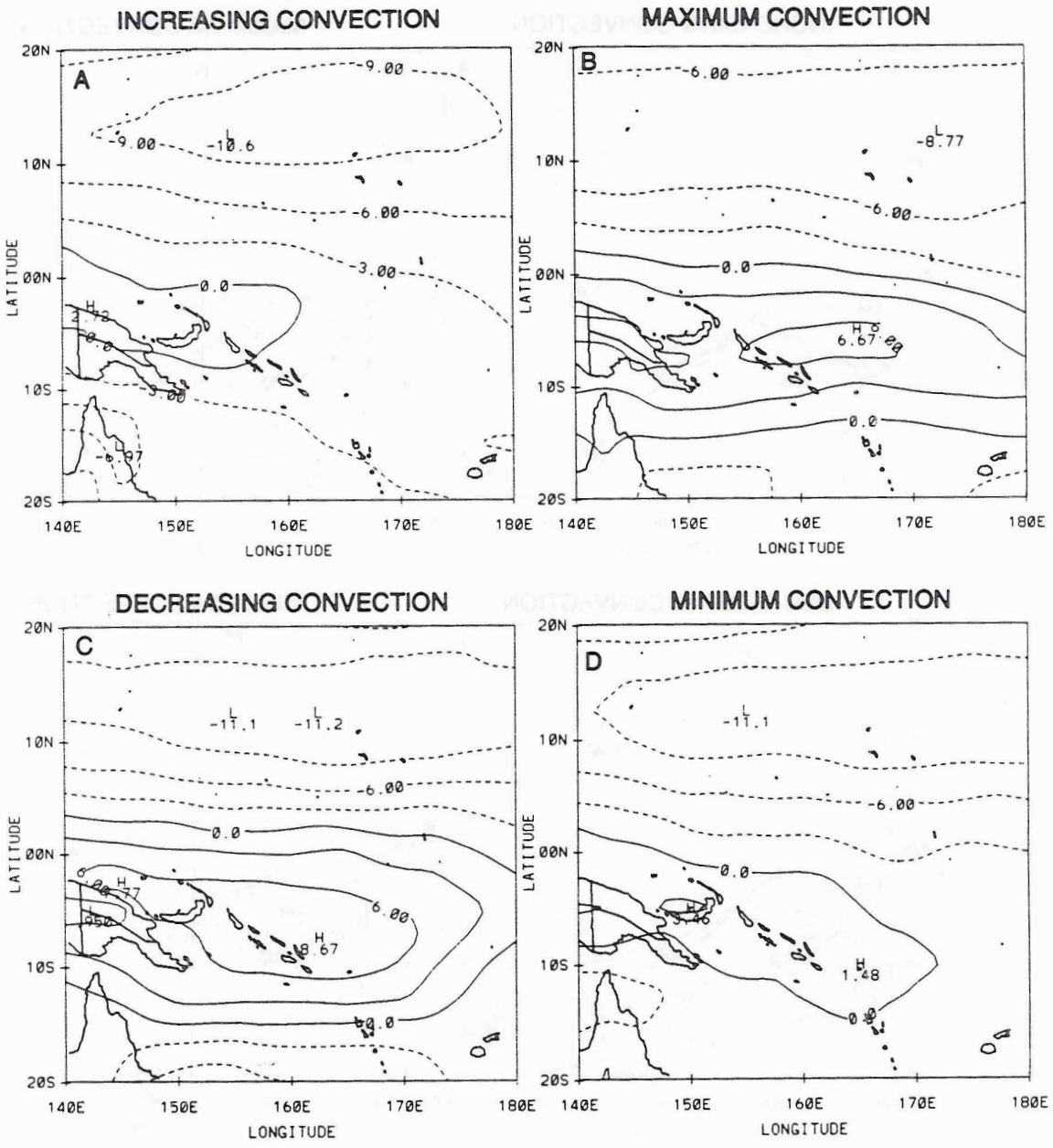

Figure 5.4: Same as Fig. 5.3, except for 1987-88.

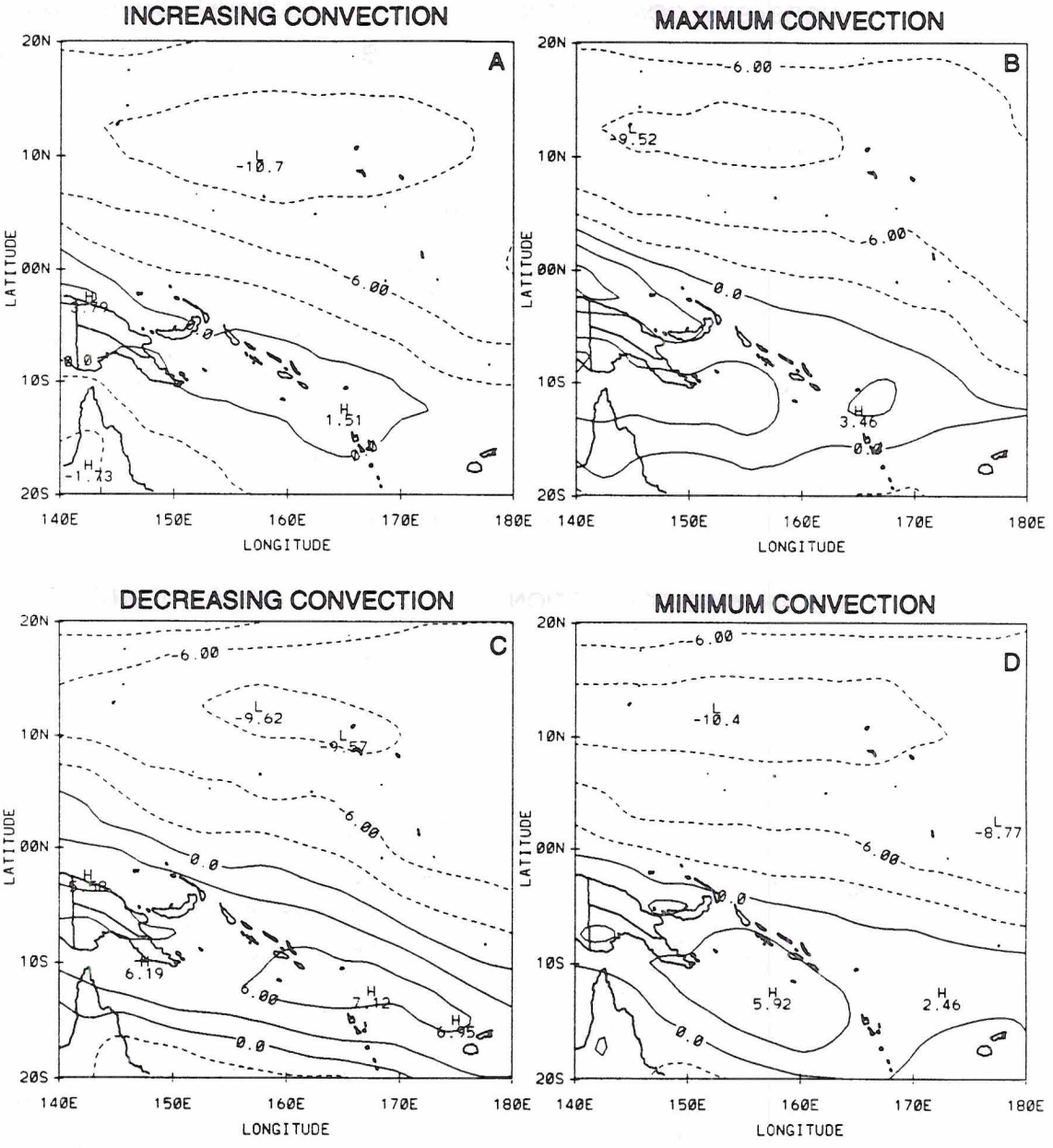

Figure 5.5: Same as Fig. 5.3, except for 1988-89.

just south of the equator during the warm years, shift more than 10° south in the cold year. These features are evident at both 1000 mb and 850 mb. The strongest westerly winds occur at 850 mb and are evident during all three years of the analysis and in each of the two data sets.

In comparing the four different phases of the oscillation, one can see again that in the low-levels the maximum westerlies occur during the decreasing convective phase (just west of the peak in convection in the MJO) and the minimum westerlies or maximum easterlies winds occur during the increasing convective phase. Thus it appears that the peak westerly winds lag the convection. This lag is apparent in each of the three years and also occurs in each of the data sets. As with the maximum westerlies, the time lag is most evident at 850 mb (shown in Figs. 5.3-5.5). As was mentioned earlier, the convergence is found to lead the maximum convective phase (to be discussed later).

Farther to the north, the main core of the low-level easterlies remains in the typical climatological location between 10.0°-20.0°N during all phases and during all three years. One noticeable difference between the warm years and the cold year is that the easterly trades expand southward to the equator during the cold year, especially in the eastern portion of the domain near the International Dateline, where they reach as far as 10.0°S. This occurs during all four phases of the oscillation. During the warm years the equatorial region is dominated by westerlies for all phases except the increasing convection phase during 1987-88. Even in this case, the equatorial easterlies only reach to about 160°E and are very weak ($\leq$ 2m s^{-1}).

At the upper-levels (Figs. 5.6-5.8), the gross features of the flow during the two El Niño years have a similar pattern. The main easterly jet core is centered at the equator and extends across the entire domain. This jet is due to the convergence of the equatorial edges of the Northern and Southern Hemisphere subtropical ridges. The axes of these anticyclonic circulations are indicated by the zero contour line, where there is a shift from easterlies to westerlies.

However, there are two differences apparent between the El Niño years of 1986-87 and 1987-88 (see Figs. 5.6-5.7) First, the maximum easterlies extend farther east during

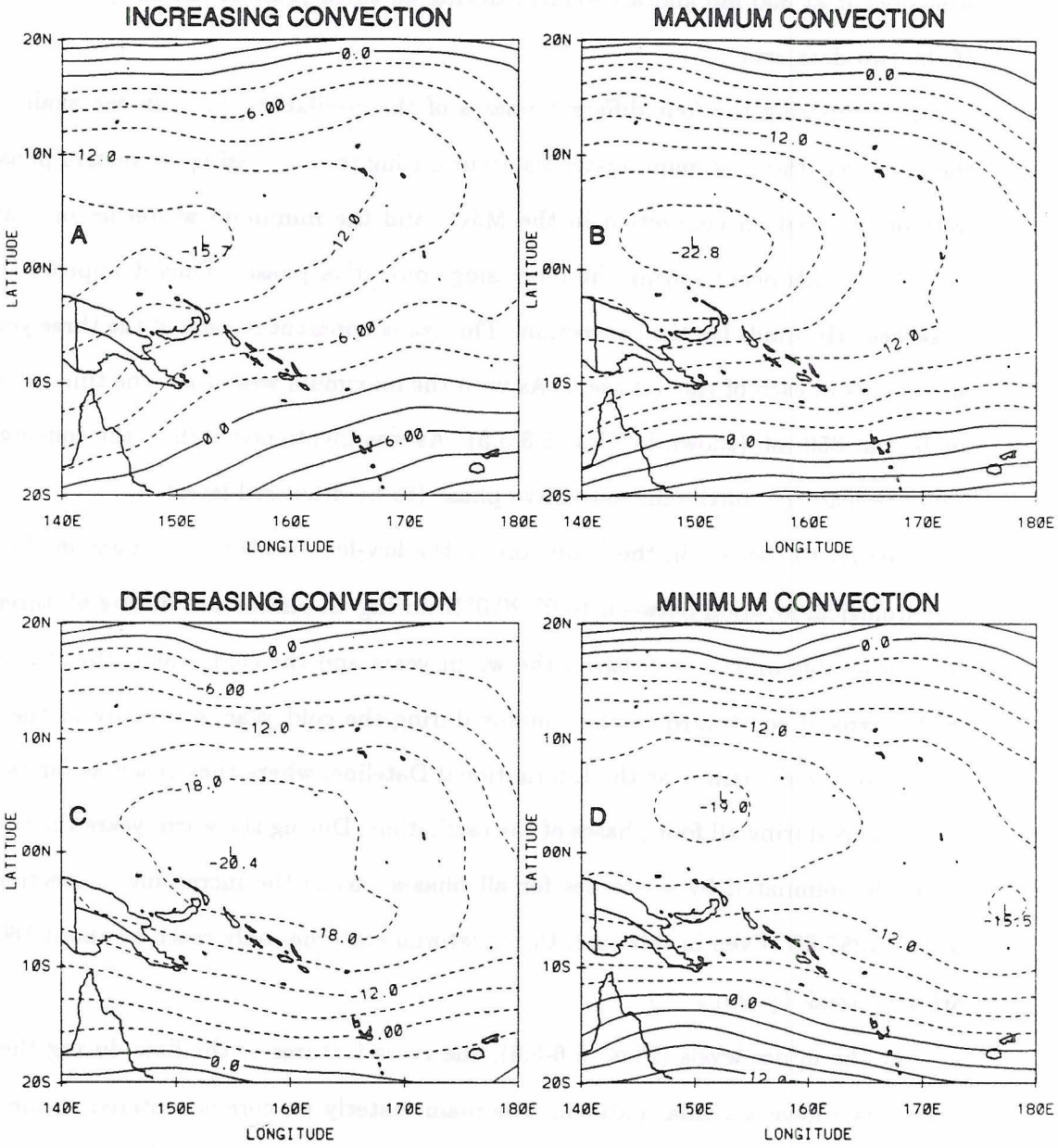

Figure 5.6: 1986-87 latitude-longitude diagrams of ECMWF composited zonal wind (m s^{-1}) at 100 mb for the a.) increasing, b.) maximum, c.) increasing and d.) minimum convection phases of the MJO. Solid contours represent westerly winds and dashed represent easterlies. The contour interval is 3.0 m s^{-1} .

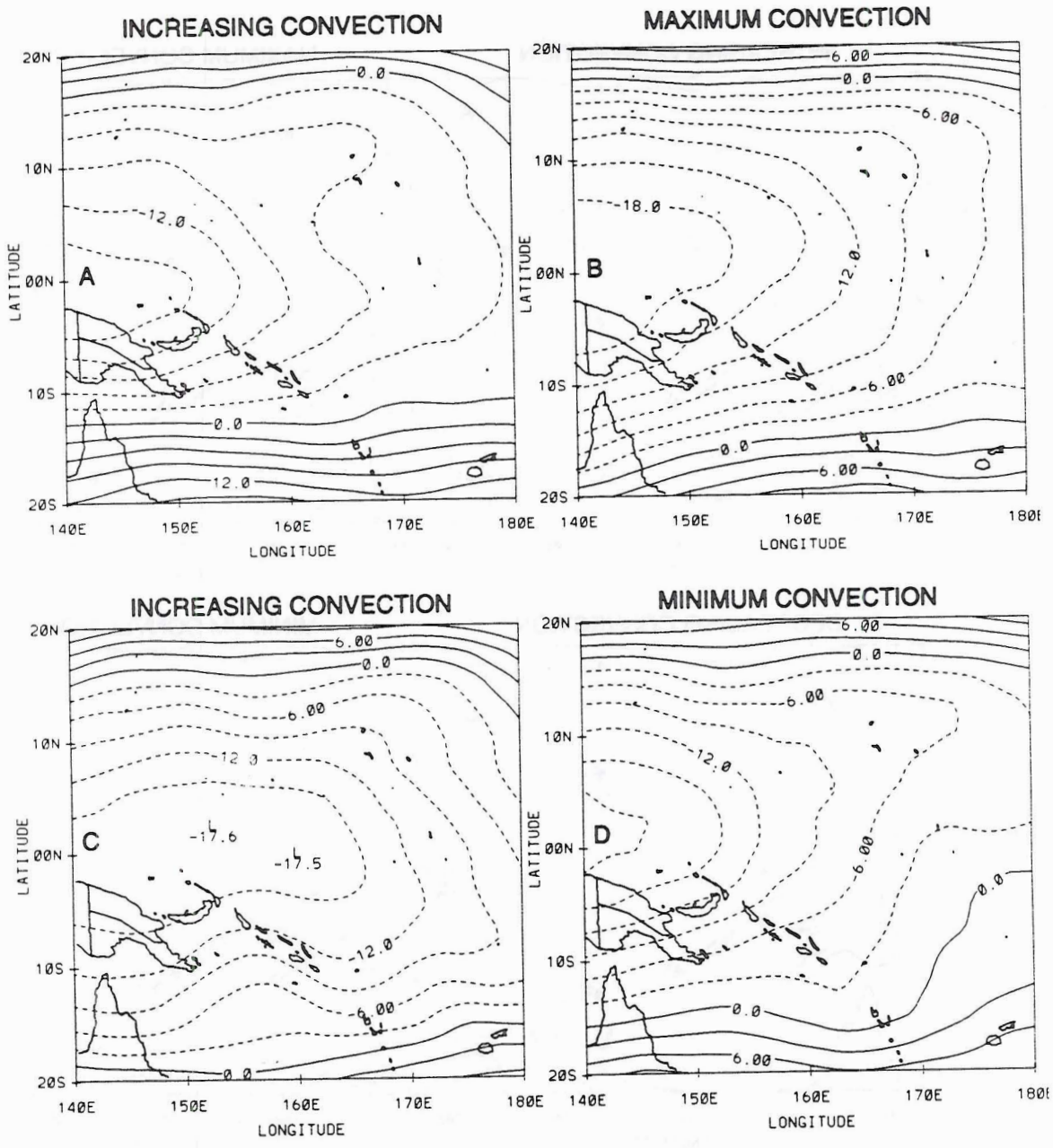

Figure 5.7: Same as Fig. 5.6, except for 1987-88.

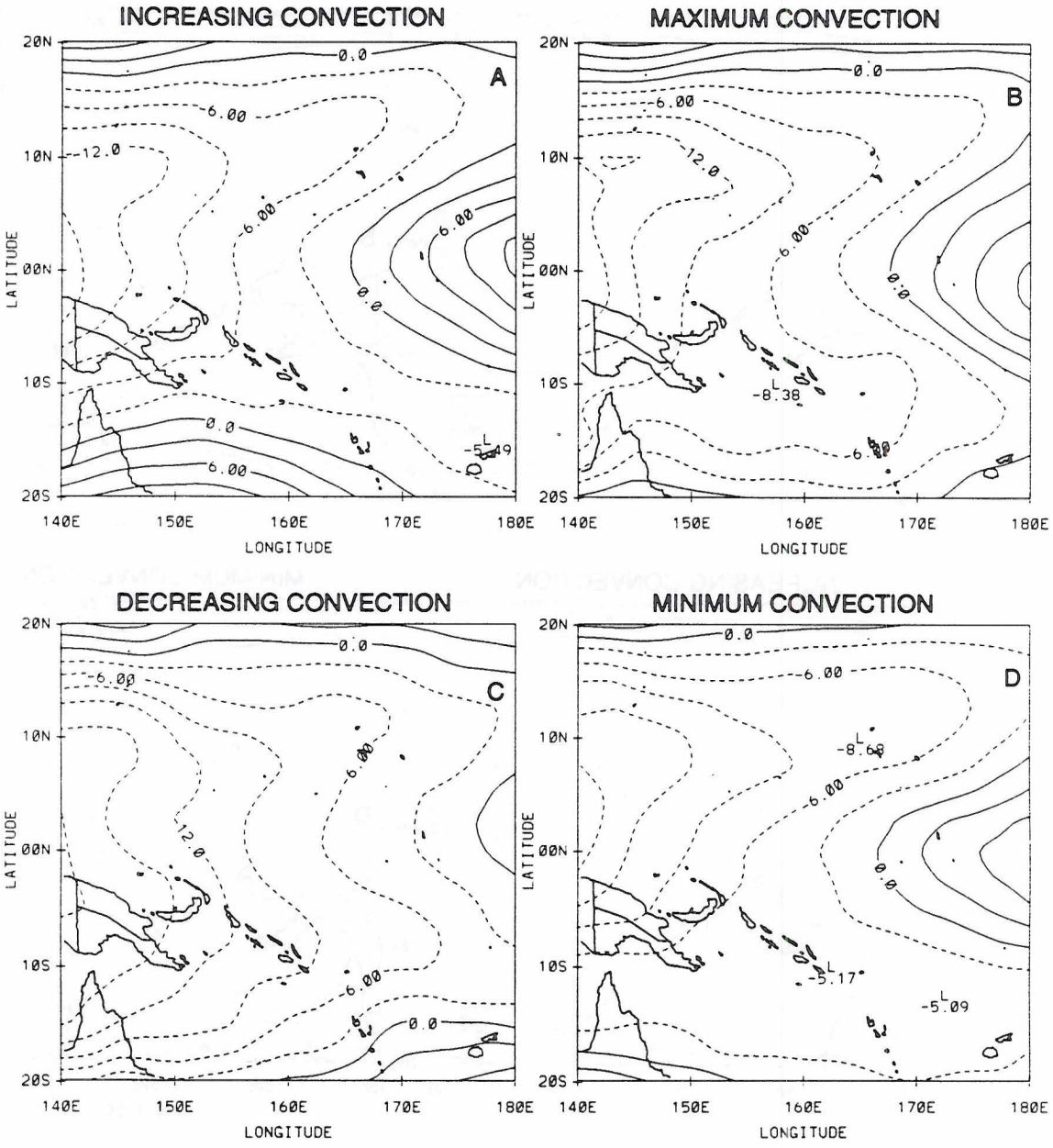

Figure 5.8: Same as Fig. 5.6, except for 1988-89.

1986-87. Second, the speeds within the core of the easterlies are higher during the same year. This trend is also apparent in the NMC composite (not shown). This would suggest that the subtropical ridges were somewhat weaker and displaced westward during 1987-88. Inspection of the 1988-89 composite (Fig. 5.8) indicates that this trend continued in the La Niña year, where it is seen that the equatorial easterlies do not extend as far eastward. During all but the decreasing convective phase there are westerlies east of 170°E.

Again, the patterns at 100 mb are very similar in the ECMWF and NMC data sets. However, the differences in the magnitude of the winds that were noticed at 850 mb are larger at 100 mb. The ECMWF composite shows easterlies 4-8 m s^{-1} stronger than the NMC composite at 100 mb, but a comparison of the ECMWF composite at 100 mb and the NMC composite at 150 mb reveals that the easterlies are within 1-2 m s^{-1} of each other. Thus, it appears that NMC has the core of the easterlies at a slightly lower altitude than the ECMWF. This might be related to the level that upper-level cloud-drift winds are assigned in each model analysis routine.

In order to examine latitudinal variations of the MJO, north-south vertical cross-sections are presented. Figures 5.9-5.11 were constructed using values at all longitudes from 140°E to 180° averaged together. Similar results are obtained with the NMC data set and therefore are not shown.

During the warm years, there are low-level westerlies centered between the equator and 10.0°S for all convective phases, except the increasing convection phase during 1987-88. These low-level westerlies underlay upper-level easterlies which are centered mainly between the equator and 5.0°N. Thus, there appears to be a south to north tilt with height as well as a phase reversal. There is one main core of upper-level easterlies at about 100 mb near the equator and a weaker center of easterlies between 1000-500 mb located between 5.0-15.0°N. These low-level easterlies are commonly referred to the easterly trade winds. There are no obvious MJO modulation on the trade winds. The magnitude and orientation remains fairly consistent throughout all phases.

During the cold year (Fig. 5.11), there are significant differences. The most obvious at first glance is the chaotic nature of the diagram. In the warm years the pattern is very

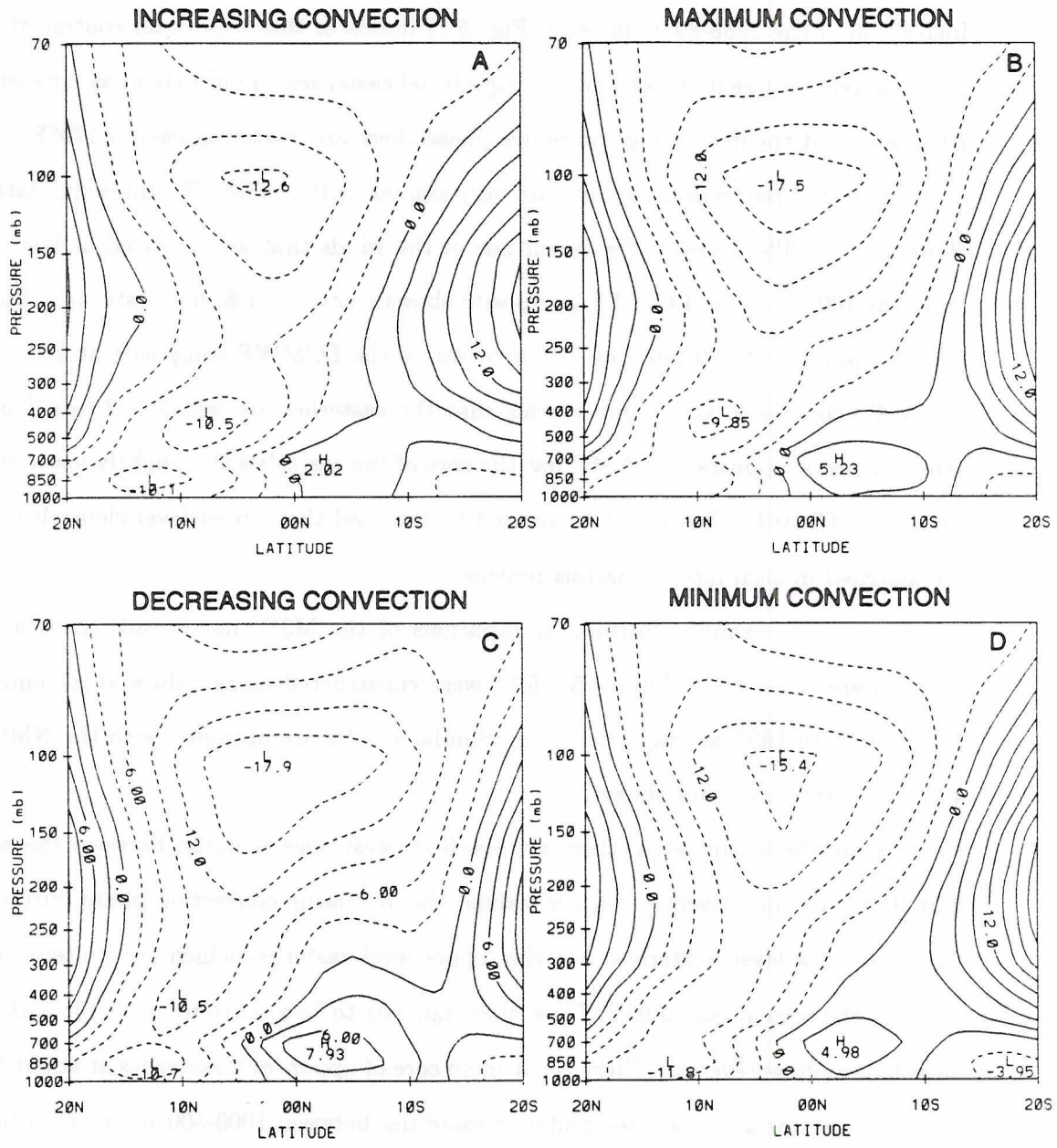

Figure 5.9: 1986-87 pressure-latitude diagrams of ECMWF composited zonal wind (m s^{-1}) at 100 mb averaged form 140°E to 180° for the a.) increasing, b.) maximum, c.) increasing and d.) minimum convection phases of the MJO. Solid contours represent westerly winds and dashed represent easterlies. The contour interval is 3.0 m s^{-1} .

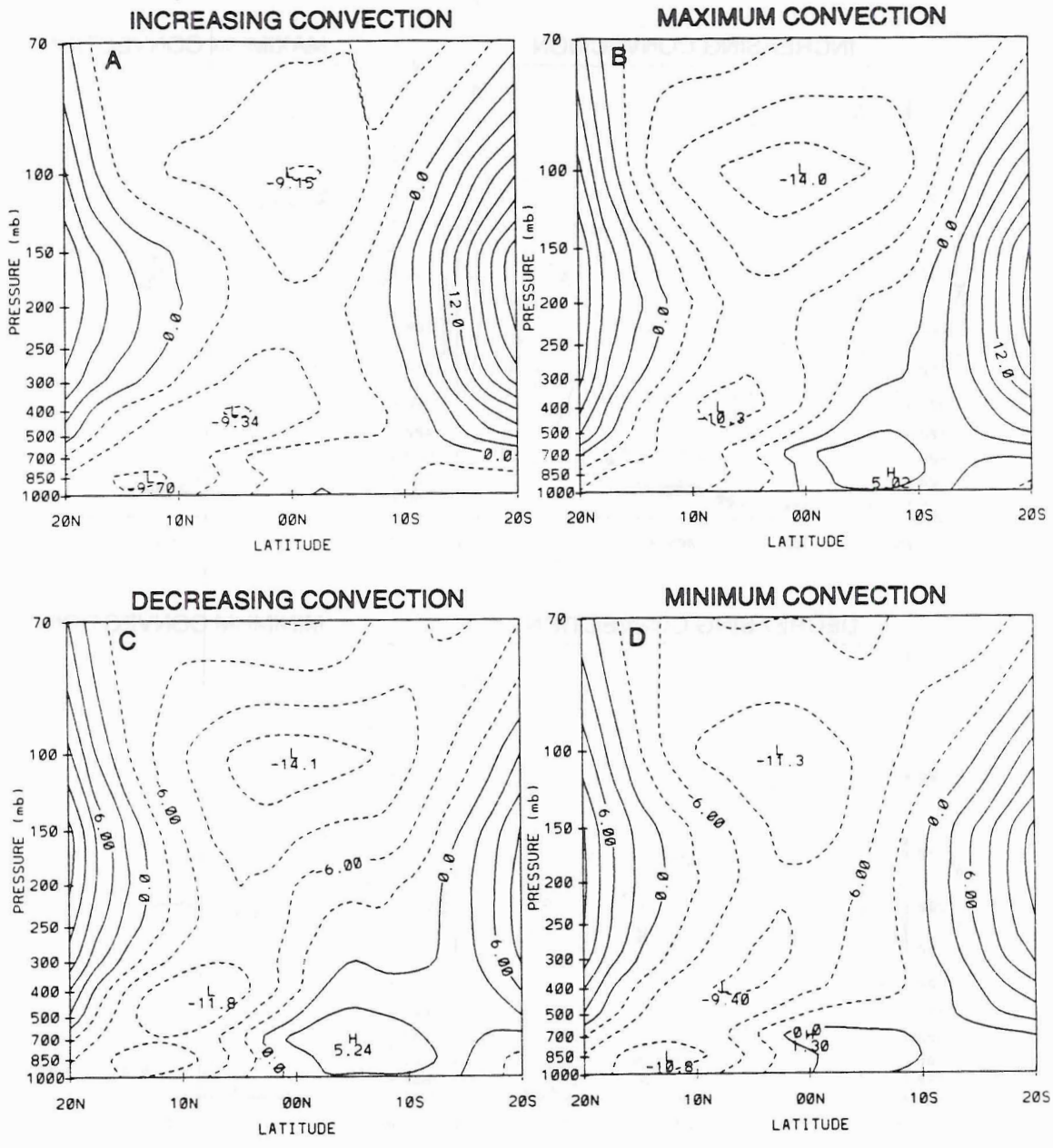

Figure 5.10: Same as Fig. 5.9, except for 1987-88.

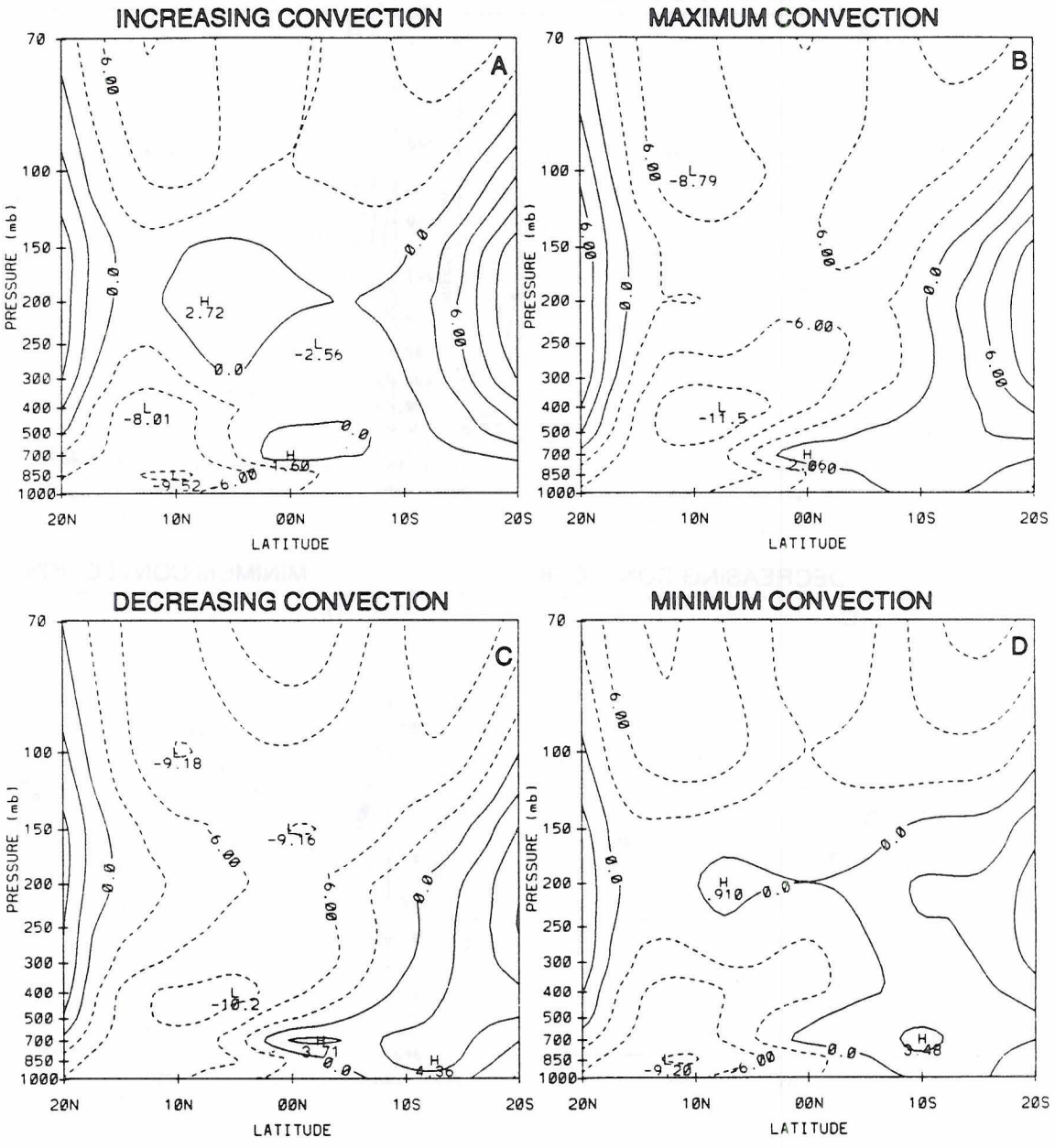

Figure 5.11: Same as Fig. 5.9, except for 1988-89.

smooth and ordered, but in 1988-89, the pattern becomes much more disorganized. This is especially true during the minimum convective phase. The main core of upper-level easterlies that was centered over the equator during the two warm years appears to have split into two separate weaker cells and moved away from the equator. One of the cells is located near 10.0°N and the other near 15.0°S.

The phase reversal, that is upper tropospheric easterlies over lower tropospheric westerlies, is still evident, but the slope that was noted during the warm years is not obvious. The low-level westerlies have shifted poleward to beyond 10.0°S and have weakened. The westerlies at 700 mb continue to extend from the equator to the southern extreme of the domain, but from the surface to 850 mb the easterlies have penetrated across the equator to about 5.0°S.

In all four phases, the core of the low-level westerly winds can be seen to shift away from the equator from the warm years to the cold year. In 1986-87 during the decreasing convective phase the core of westerlies is centered near 2.5°S, during 1987-88 it shifts to 5.0°S and by 1988-89 it has shifted to 12.5°S. This is consistent with the shifting of convection away from the equator during the La Niña year seen in Figs. 4.2-4.4.

Some interesting variations in the MJO composite are apparent in the zonal direction also. Figures 5.12-5.14 are east-west vertical cross-sections using the ECMWF composited data based on the phase of convective activity at 160°E. These figures are were constructed using average values between the equator and 10.0°S.

The low-level westerlies discussed earlier reach maximum strength during the decreasing convection phase of the MJO and reach minimum strength during the increasing convection phase (Figs. 5.12-5.14). The westerlies also have a larger areal extent during the warm El Niño years versus the cold La Niña year. It is interesting to note that the magnitude of the maximum westerly winds during the decreasing convection phase are within 2.0 m s^{-1} of each other in all three years.

During 1986-87, low-level westerlies occur over the entire domain during all four phases of convective activity. It appears that the core of the westerlies begins to develop at 160°E during the maximum convection phase, shift eastward and reach maximum intensity

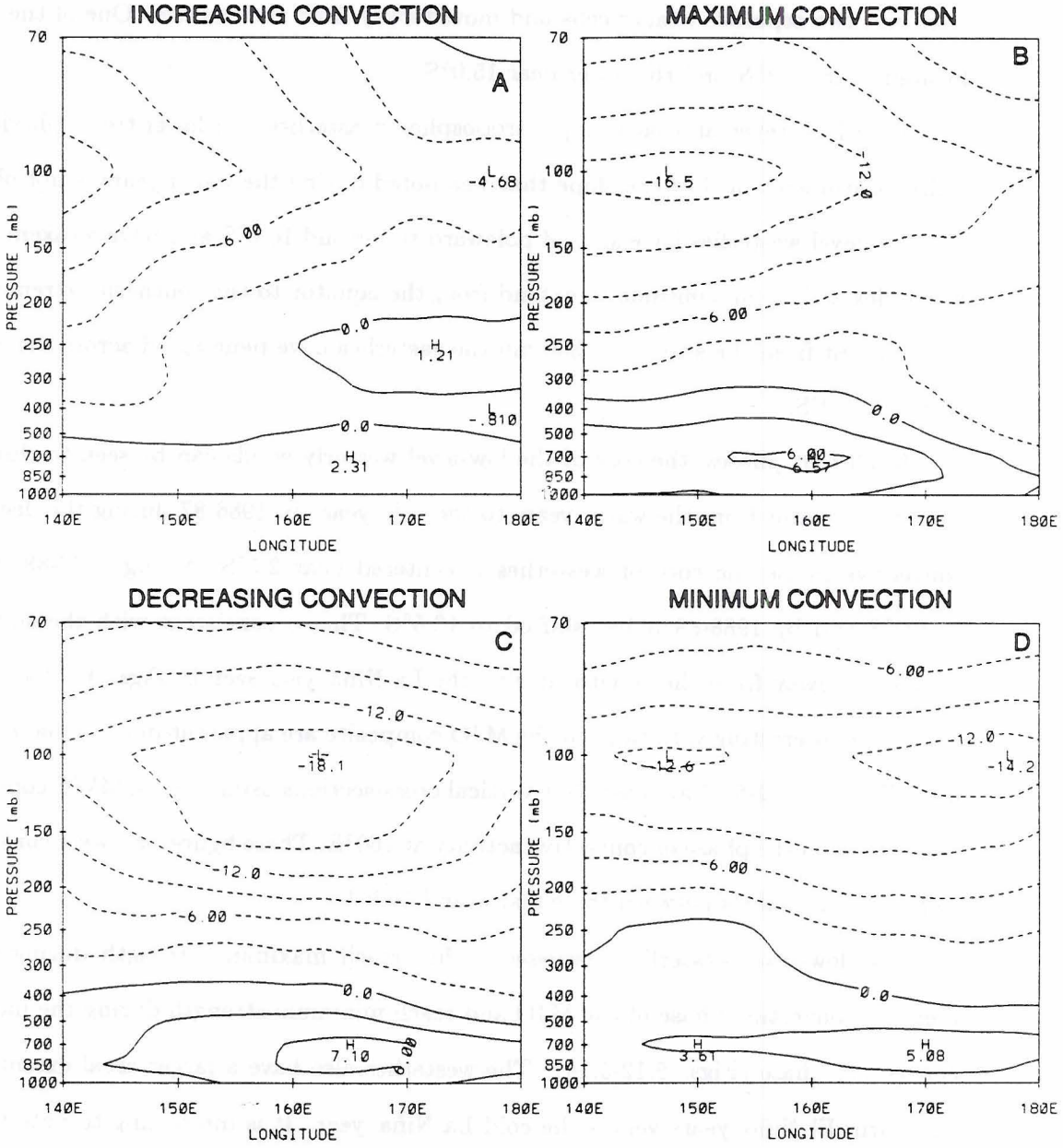

Figure 5.12: 1986-87 pressure versus longitude diagrams of ECMWF composited zonal wind (m s^{-1}) averaged from the equator to 10.0°S for the a.) increasing, b.) maximum, c.) increasing and d.) minimum convection phases of the MJO. Solid contours represent westerly winds and dashed represent easterlies. The contour interval is 3.0 m s^{-1} .

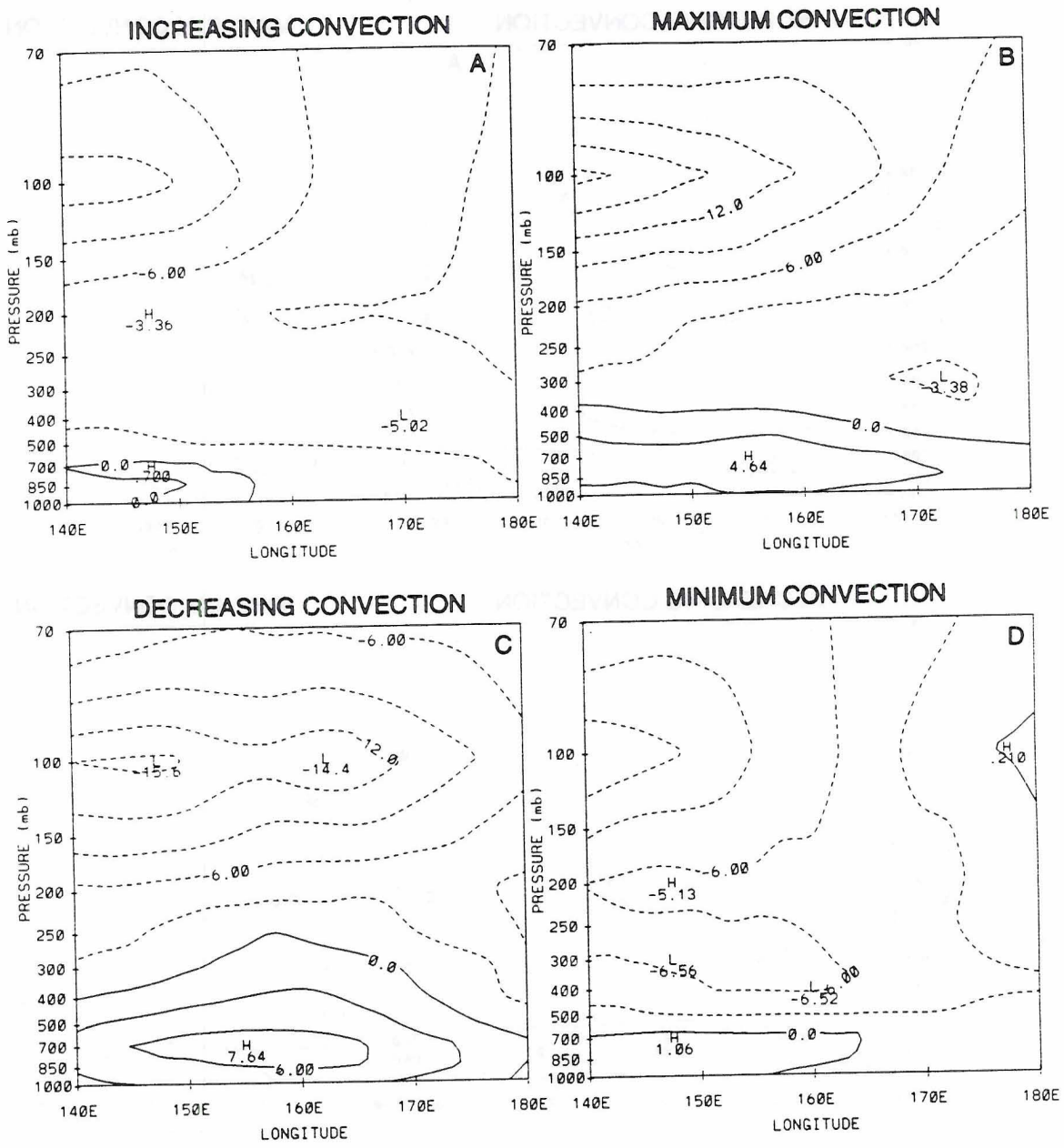

Figure 5.13: Same as Fig. 5.12, except for 1987-88.

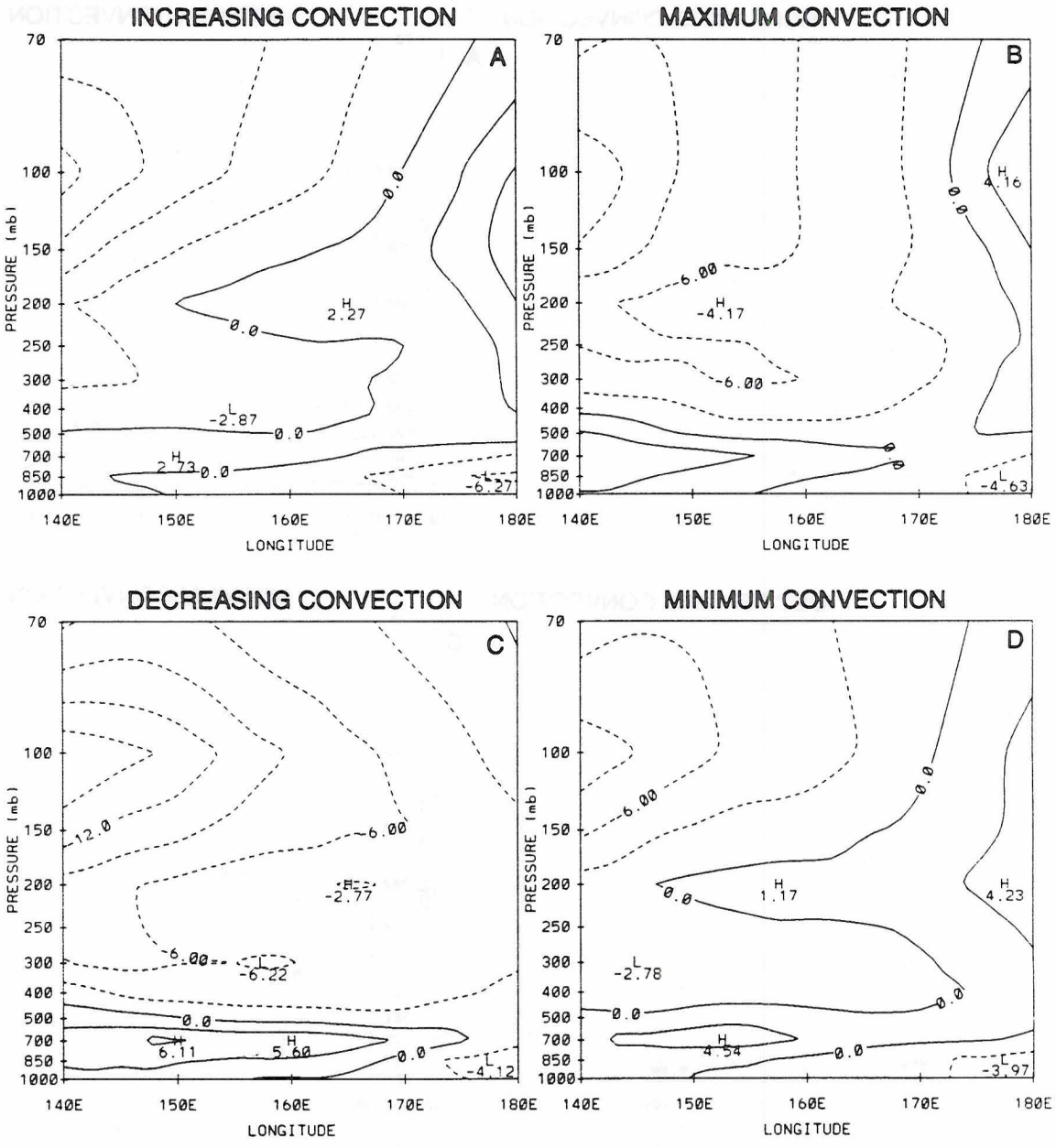

Figure 5.14: Same as Fig. 5.12, except for 1988-89.

during the decreasing convection phase and then shift eastward again and begin to weaken during the minimum convection phase. However, this propagation is not evident during 1987-88 nor 1988-89. In fact, the low-level westerly winds only occur across the entire domain during the maximum and decreasing phases of convective activity during 1987-88. In the other two phases the eastern portion of the domain, east of 160°E, easterly winds occur. There also appears to be more modulation in 1987-88. For example, the change in magnitude of maximum westerlies between the decreasing and minimum convection phase in 1986-87 is about 2.0 m s^{-1} , while in 1987-88 it is about 6.5 m s^{-1} .

As we move on to the La Niña year, 1988-89, the low-level westerlies are restricted to the western half of the domain for all convective phases, especially at the surface. Only during the decreasing convection phase, when the westerlies are strongest, does the main core extent east of 160°E.

Significant differences between the composite using ECMWF data and NMC data are seen in the lowest levels of the atmosphere (not shown, but the differences are indicated in Figs. 5.1 and 5.2). First, during the warm event years there are westerlies at the 1000 mb level over some portion of the domain during each phase of the oscillation in the ECMWF composite analysis. However, the NMC composite analysis shows no westerlies during the increasing convective phase in both 1986-87 and 1987-88 and no westerlies during the minimum convective phase during 1987-88. Second, there appears to be an abrupt increase in westerlies between phases of convective activity in the NMC composite. In 1986-87, during the increasing convective phase, weak easterlies exist from 140°E to the International Dateline. By the time the convection has maximized, virtually all the easterlies have been replaced by westerlies of at least 4.0 m s^{-1} . The same thing occurs during 1987-88, but initial onset of westerlies is somewhat slower. The ECMWF composite analysis shows a much more gradual increase in the westerlies as the convection approaches, reaches and passes maximum intensity. There is no clear explanation for these differences.

In the two El Niño years at the upper-levels, there appears to be a systematic eastward expansion of the main easterlies during and after the maximum convection has been realized followed by a retreat westward as the convection weakens. This signal is somewhat

evident in the NMC composite analysis, more so during 1986-87 than 1987-88. During the cold year (Fig. 5.14), the easterlies aloft do not occur over the complete domain for every phase of the oscillation and therefore, the eastward expansion is not seen. The main area of easterlies is restricted west of 160°E and they are significantly weaker than during the warm years.

There is also a noticeable change in the eastward extent of the core of the upper tropospheric easterlies. In 1986-87, during the decreasing convective phase, the easterlies are at their maximum intensity of 18 m s^{-1} between 160°-165°E. There are winds of 12.0 m s^{-1} across the entire domain. In 1987-88, for the same convective phase, there are dual maxima of 15.6 m s^{-1} and 14.4 m s^{-1} located between 145°-150°E and 160°-165°E, respectively. However, the 12.0 m s^{-1} region has shifted westward and is much smaller in coverage. By 1988-89, there are not any discernible maxima and the 12.0 m s^{-1} region is restricted to the area west of 150°E. The same arguments can be made to the NMC composited east-west cross-sections using an 8.0 m s^{-1} threshold.

To summarize this section, the low-level westerly wind maxima were found to lag the maximum convection by a quarter phase. That is, the maximum low-level westerlies occur during the decreasing convective phase of the composite (to the west of the deep convection) as shown in Fig. 5.1. The latitude versus longitude diagrams revealed that the low-level westerly winds are coincident with the minimum OLR and that the orientation of the axes of maximum westerlies are very similar to the orientation of the axes of minimum OLR or maximum convective activity. The upper-level easterlies were found to be strongest and to have the farthest eastward extent during 1986-87 and retreated westward in the following years. The north-south vertical cross-sections showed the migration of the lower tropospheric westerlies away from the equator from 1986-87 through 1988-89. Also evident is a distinct phase reversal with height such that there are upper-level easterlies over low-level westerlies with a south to north tilt, especially during the warm years. The east-west vertical cross-sections showed a systematic expansion of the core of the upper tropospheric easterly winds with the changes in convective activity. The strongest easterly flow occurred during the decreasing convective phase and as the convection continued to

decrease, reach a minimum and began to increase again, the core of the winds decreased in intensity and in areal coverage. Also, there was a distinct decrease in the intensity and coverage of upper tropospheric easterlies from 1986-87 to 1988-89. Overall, there was good agreement in the u-component composite analysis between the ECMWF and NMC data. Two notable exceptions are that the upper tropospheric equatorial easterlies are slightly weaker and at a lower level in the NMC composite and the lack of westerly winds at 1000 mb during all phases of the MJO in the NMC composite.

5.1.2 Meridional Winds

If the MJO were a pure Kelvin wave and the analysis technique employed here isolated only the MJO contribution to the flow, there should not be any meridional component. However, while the v-component signal is much weaker and a little less organized than the u-component, there are still some interesting features that are revealed by the meridional wind composite. The most prominent of these features are likely associated with convection within the MJO.

As was done in the previous section, vertical profiles of the v-component are examined in pressure versus convective phase diagrams first. Unlike the zonal wind analysis, there is a large latitudinal variation in the meridional winds, both within a particular winter season and between the three winter composites (see Fig. 5.15 at 5.0°N and Fig. 5.16 at 5.0°S). These latitudinal differences are mainly evident in the upper troposphere. In fact, the lowest levels, below 700 mb, appear to be very similar from 20.0°N to 5.0°S. At each of the latitudes within this band, the meridional winds averaged over all longitudes are weak and northerly as seen at 5.0°N and 5.0°S in Figs. 5.15 and 5.16. The speeds range from 1-3 m s^{-1} . South of 5.0°S (not shown), low-level southerly winds begin to occur during the minimum and increasing convective phases during the El Niño years, but not during the La Niña year. In 1988-89, northerly winds prevail to 15.0°S during all four convective phases.

The largest variability is seen in the upper troposphere. During the two El Niño years, southerly winds occur above 250 mb for all phases of convective activity at 5.0°N (Fig. 5.15). The core of the southerlies, with speeds greater than 5 m s^{-1} , occurs during

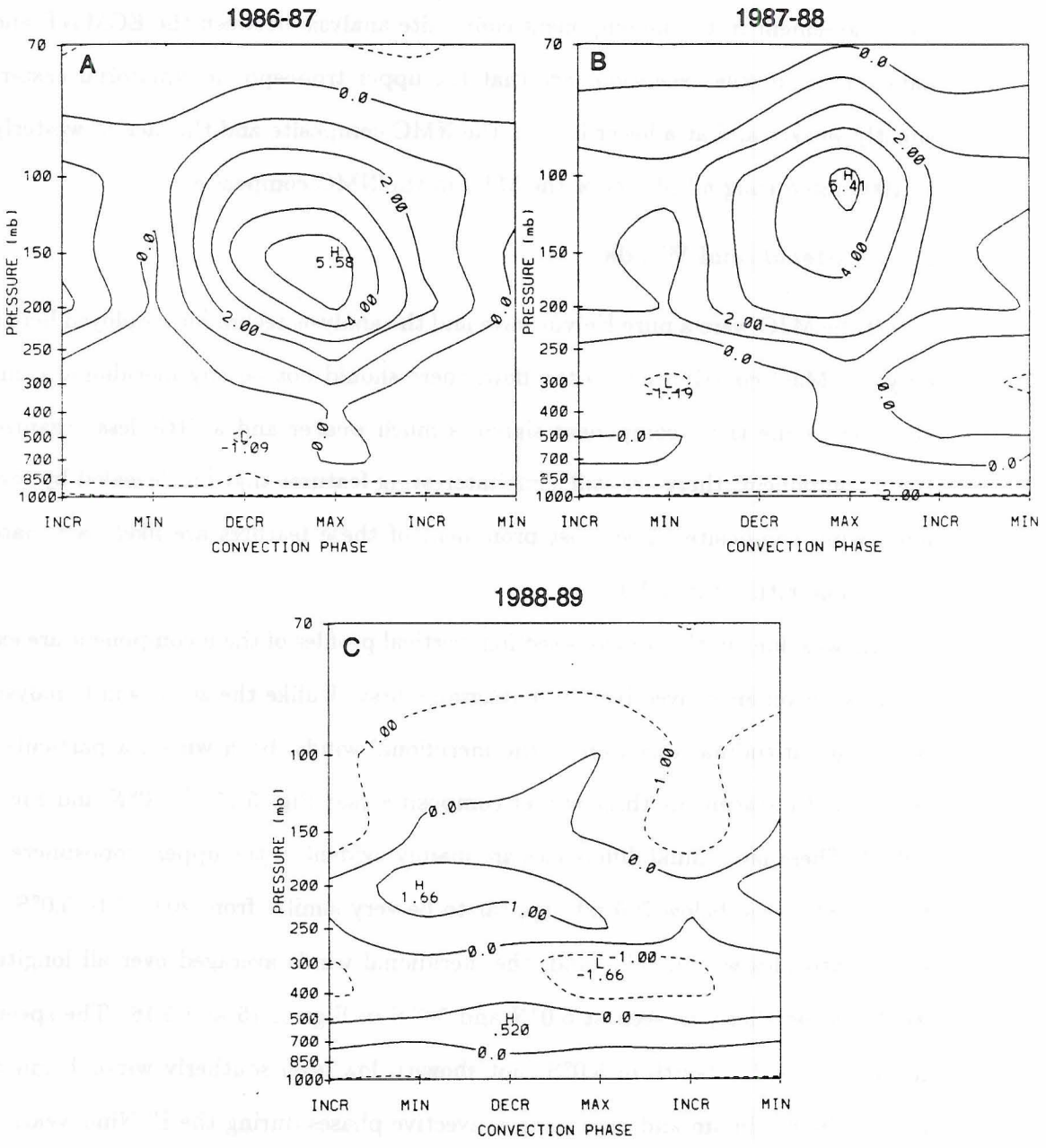

Figure 5.15: Pressure-phase diagrams of ECMWF composited meridional wind (m s^{-1}) at 5.0°N averaged from 140°E to 180° for a.) 1986-87, b.) 1987-88 and c.) 1988-89. Solid contours represent southerly winds and dashed represent northerlies. The contour interval is 1.0 m s^{-1} .

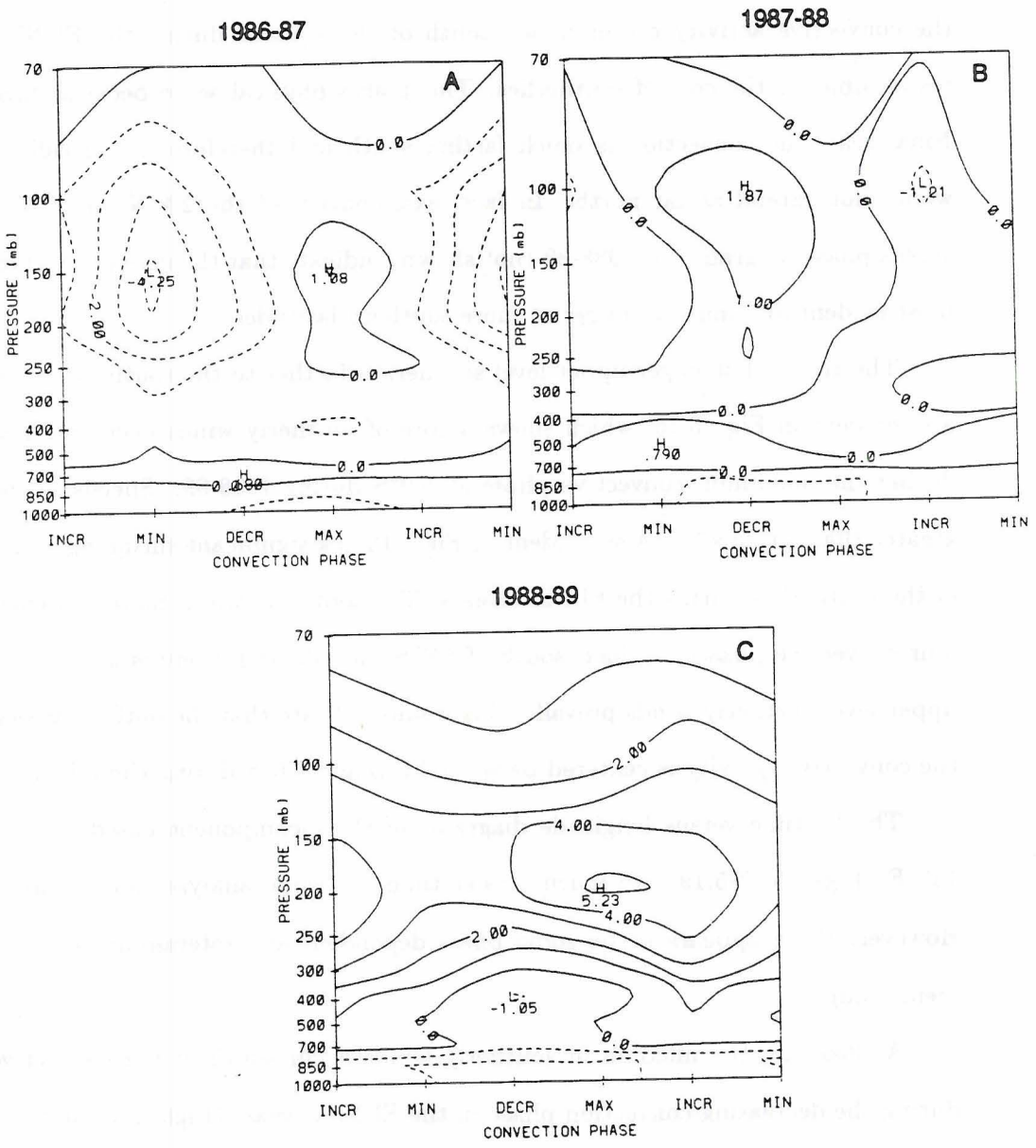

Figure 5.16: Same as Fig. 5.15, except at 5.0°S.

the maximum convective phase. In contrast, during the La Niña year when the convection has moved away from the equator, the core of the upper-level southerly winds occur during the minimum convective phases and a maximum in northerly winds appears near the 300-400 mb level during the maximum convective phase. It is believed that outflow from the convective activity centered just south of the equator during the El Niño years is responsible for the core of southerlies. This makes physical sense because during the La Niña year, the convection is much farther south and therefore the meridional outflow would not extend as far north. In fact, examination of the 2.5°N and 0.0°N pressure versus phase diagrams for 1988-89 (not shown) indicate that the core of southerly wind is most evident and much stronger at more southern latitudes.

The trend of stronger upper-level southerlies farther to the south in the cold year is also evident in Fig. 5.16, which shows a core of southerly winds occurring near 200 mb during the maximum convective phase at 5.0°S during 1988-89. Speeds in the core are greater than 5.0 m s^{-1} . Also evident in Fig 5.16 is a significant shrinking and weakening of the southerlies during the El Niño years. The southerly winds no longer encompass all four convective phases. In fact, south of 5.0°S (not shown), there is a reversal such that upper-level northerly winds prevail. This would indicate that the outflow associated with the convective activity is centered between 2.5°S and 5.0°S during these El Niño years.

The latitude versus longitude diagrams of the v-component based on the phase at 160°E (Figs. 5.17-5.19) are much noisier than the same analyses for the u-component. However, there appears to be some phase-dependent and interannual variations worth mentioning.

At 850 mb, the maxima in southerly winds occur south of the convective activity during the decreasing convection phase in the El Niño years (Figs. 5.17 and 5.18), which is the same phase that the maxima in low-level westerlies occur. This is not true during the La Niña year of 1988-89 (Fig. 5.19). In the cold year the southerly winds are confined to the southwestern corner of the domain, south of 10.0°S and west of 160°E.

A feature that is most evident in the La Niña year is revealed by comparing Fig 5.5 and Fig. 5.19. Close examination shows that the orientation of the axes of maximum

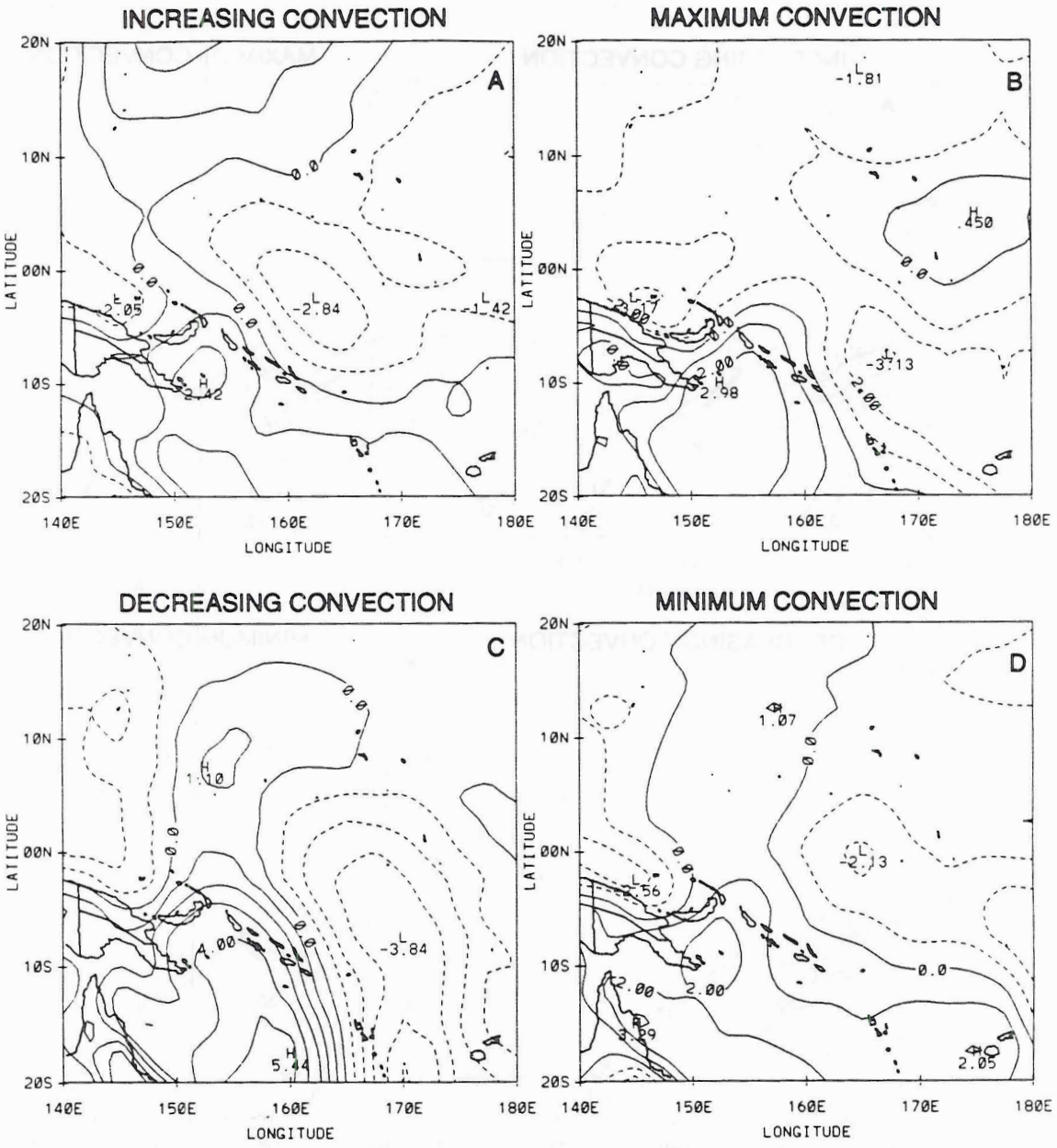

Figure 5.17: 1986-87 latitude-longitude diagrams of ECMWF composited meridional wind (m s^{-1}) at 850 mb for the a.) increasing, b.) maximum, c.) decreasing and d.) minimum convection phases of the MJO. Solid contours represent southerly winds and dashed represent northerlies. The contour interval is 1.0 m s^{-1} .

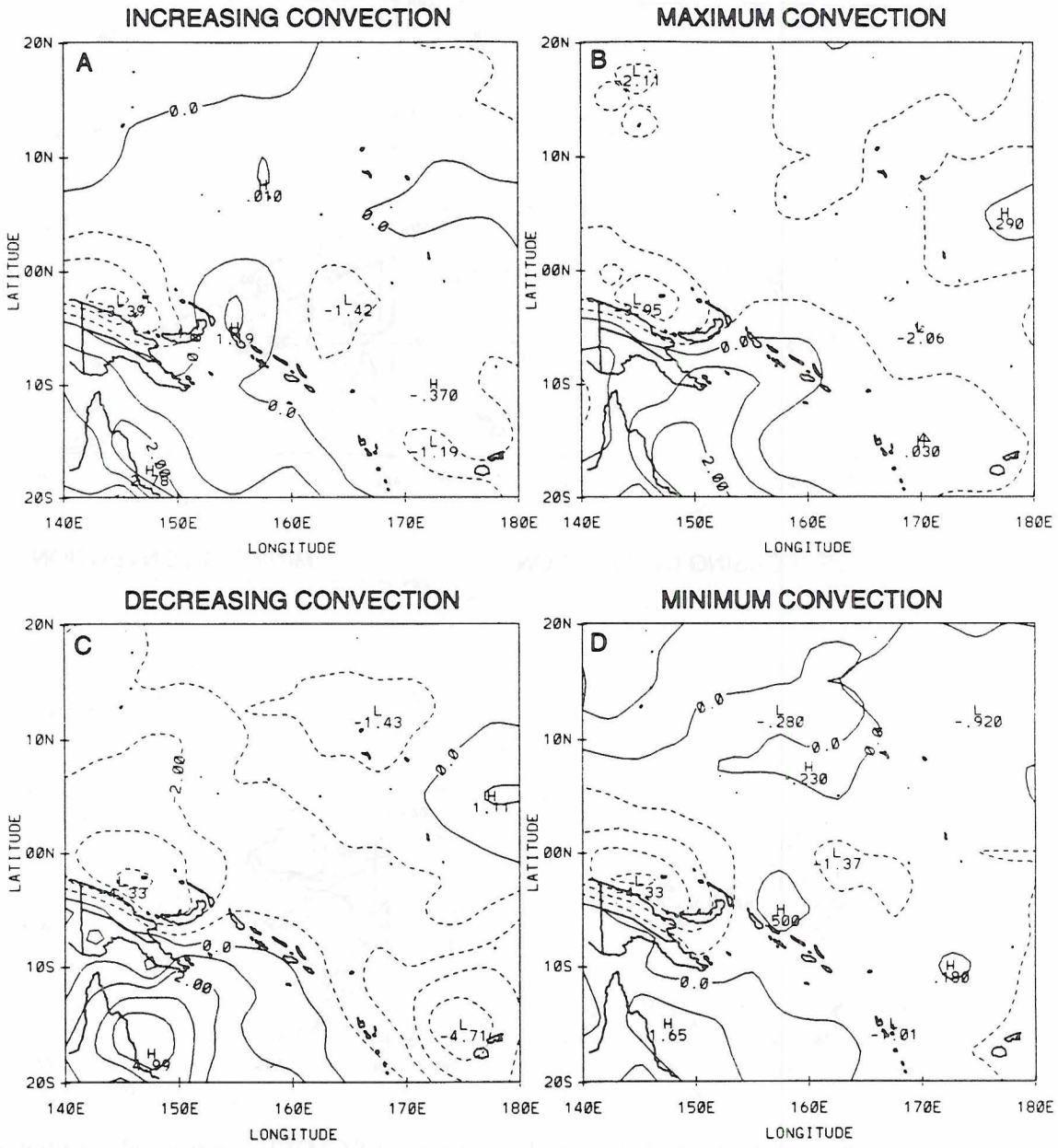

Figure 5.18: Same as Fig. 5.17, except for 1987-88.

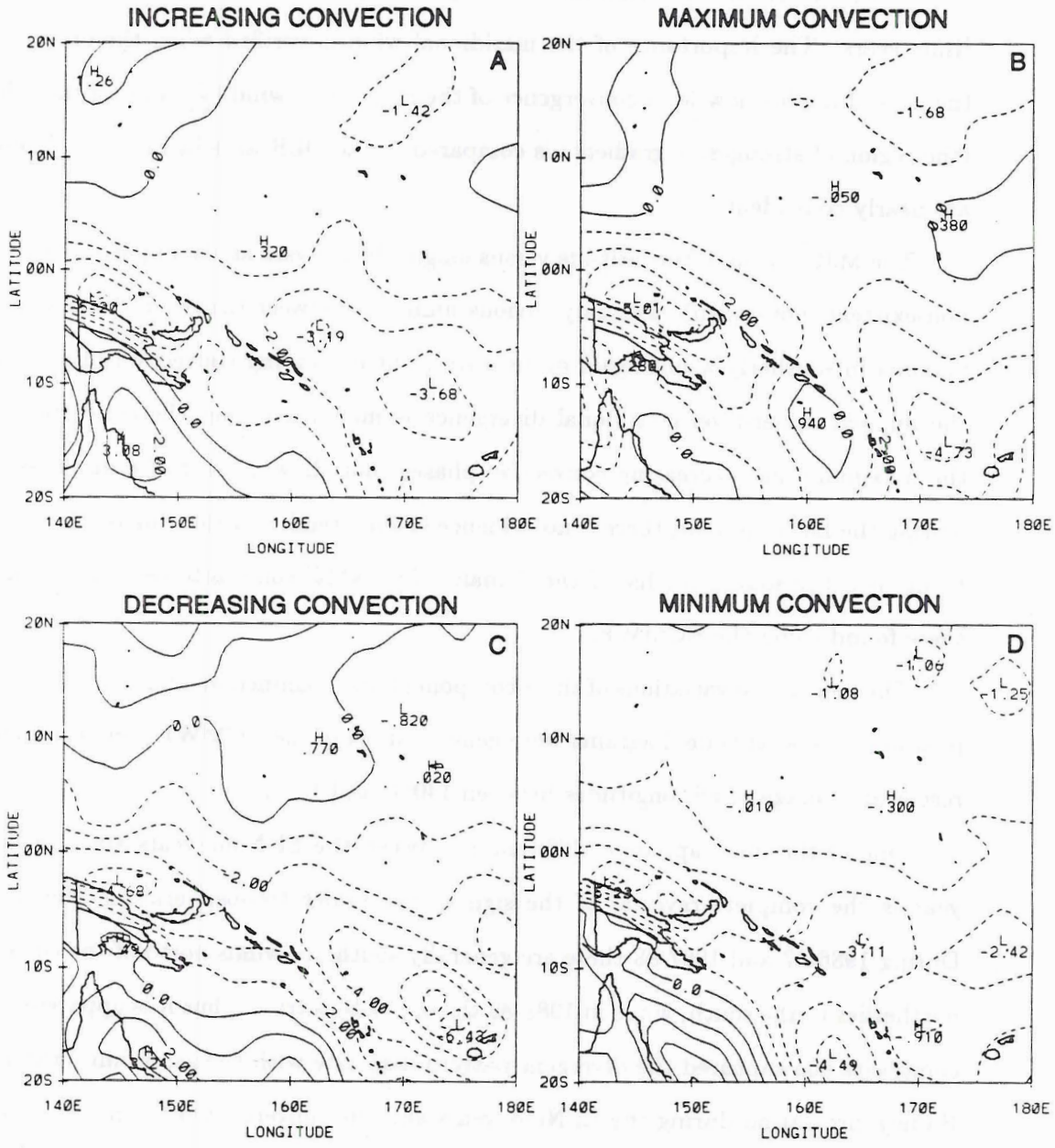

Figure 5.19: Same as Fig. 5.17, except for 1988-89.

southerly winds in Fig 5.19 closely matches the axes of maximum westerlies in Fig. 5.5 for all phases of convection. This is marginally visible in comparing Figs. 5.4 and 5.18 and not readily apparent in Figs 5.3 and 5.17. Thus, it is apparent that the v-component plays a larger role in the convective activity during the La Niña year than the two El Niño years. The importance of the meridional wind is verified when the orientation of the axes of implied low-level convergence of the meridional wind ($\frac{\partial v}{\partial y}$) during the cold year (the region of strongest v gradient) is compared to the OLR axes in Fig. 4.4. These axes are nearly coincident.

The MJO signal in the latitude versus longitude analyses at the upper-levels is almost non-existent (not shown). The only obvious similarity between the two El Niño years is the maxima in southerly winds again occur during the decreasing convection phase and that the implied upper-level meridional divergence is maximized over the convection during the maximum and decreasing convective phases (not shown, but to be discussed later). During the La Niña year, there is no evidence of this trend, possibly due to the convection being near the southern edge of the domain. The NMC composite results are similar to these found using the ECMWF.

The meridional variations of the v-component are examined in figures 5.20-5.22. These pressure versus latitude diagrams were generated using the ECMWF composite and represent an average of all longitudes between 140°E and 180°.

One of the most apparent differences between the El Niño years and the La Niña year is the complete reversal of the sign of the upper tropospheric meridional winds. During 1986-87 and 1987-88 there are generally southerly winds north of the equator and northerlies to the south, while in 1988-89 the opposite is true. Thus it is apparent that the composite has captured the divergent pattern associate with the ascending branch of the Hadley circulation during the El Niño years and the convergent pattern associated with the descending branch during the La Niña year. This result is supported by the vertical motion analysis (to be shown later) in that there are maxima in upward motion in the vicinity of the largest divergence of the meridional wind at upper-levels during 1986-87 and 1987-88 and a minima in upward motion near the largest upper-level convergence in 1988-89.

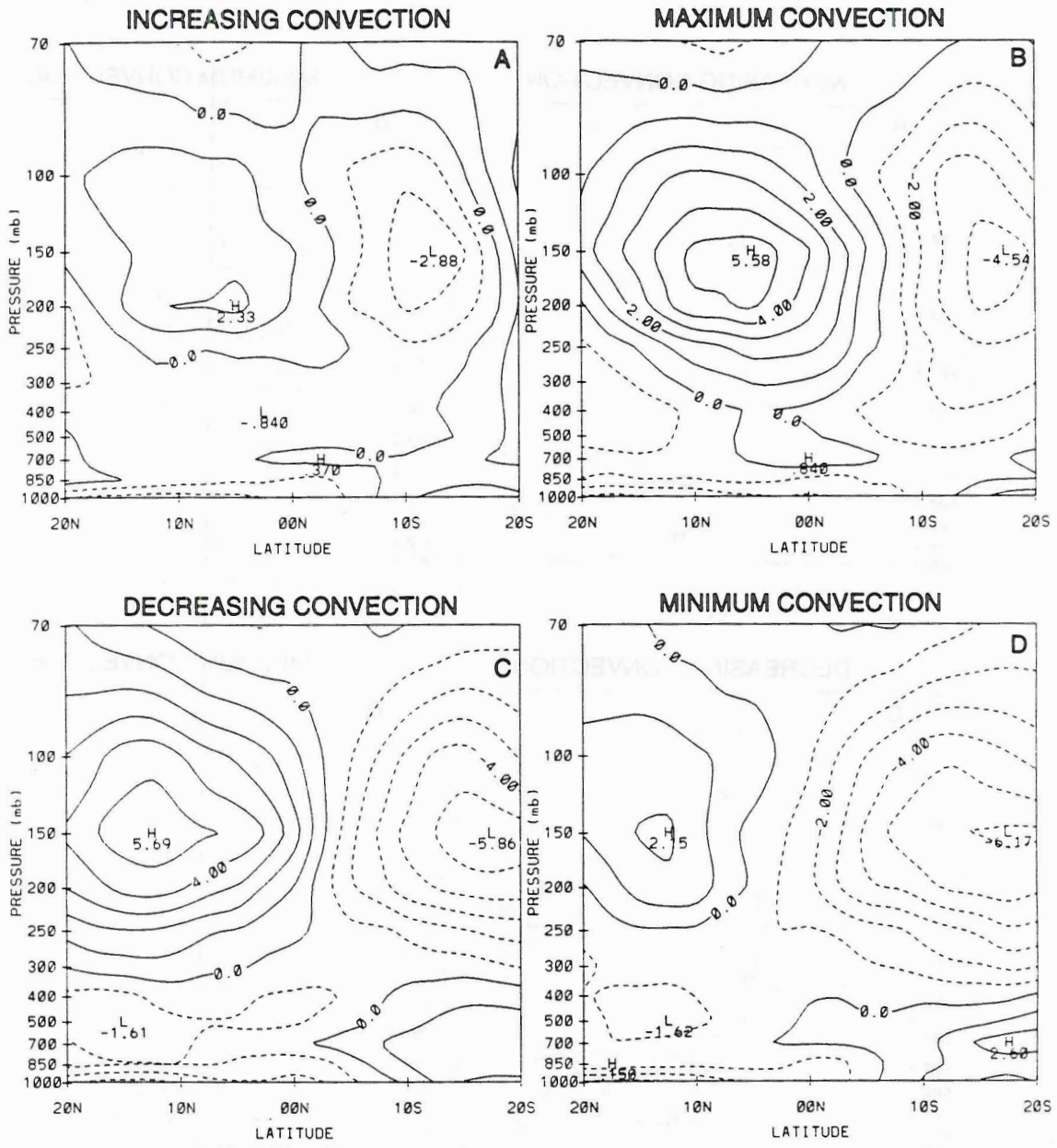

Figure 5.20: 1986-87 pressure-latitude diagrams of ECMWF composited meridional wind (m s^{-1}) averaged from 140°E to 180° for the a.) increasing, b.) maximum, c.) decreasing and d.) minimum convection phases of the MJO. Solid contours represent southerly winds and dashed represent northerlies. The contour interval is 1.0 m s^{-1} .

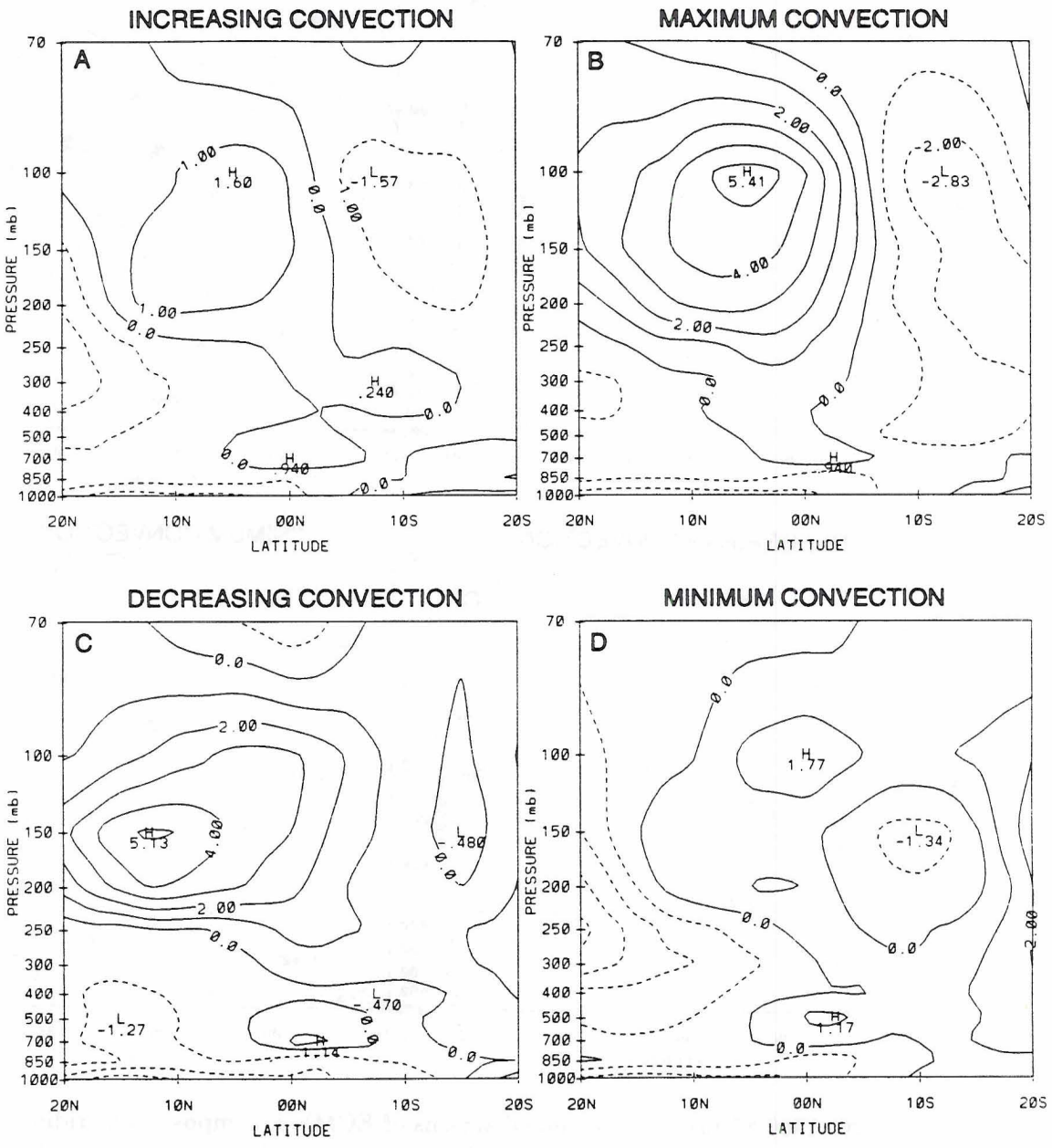

Figure 5.21: Same as Fig. 5.20, except for 1987-88.

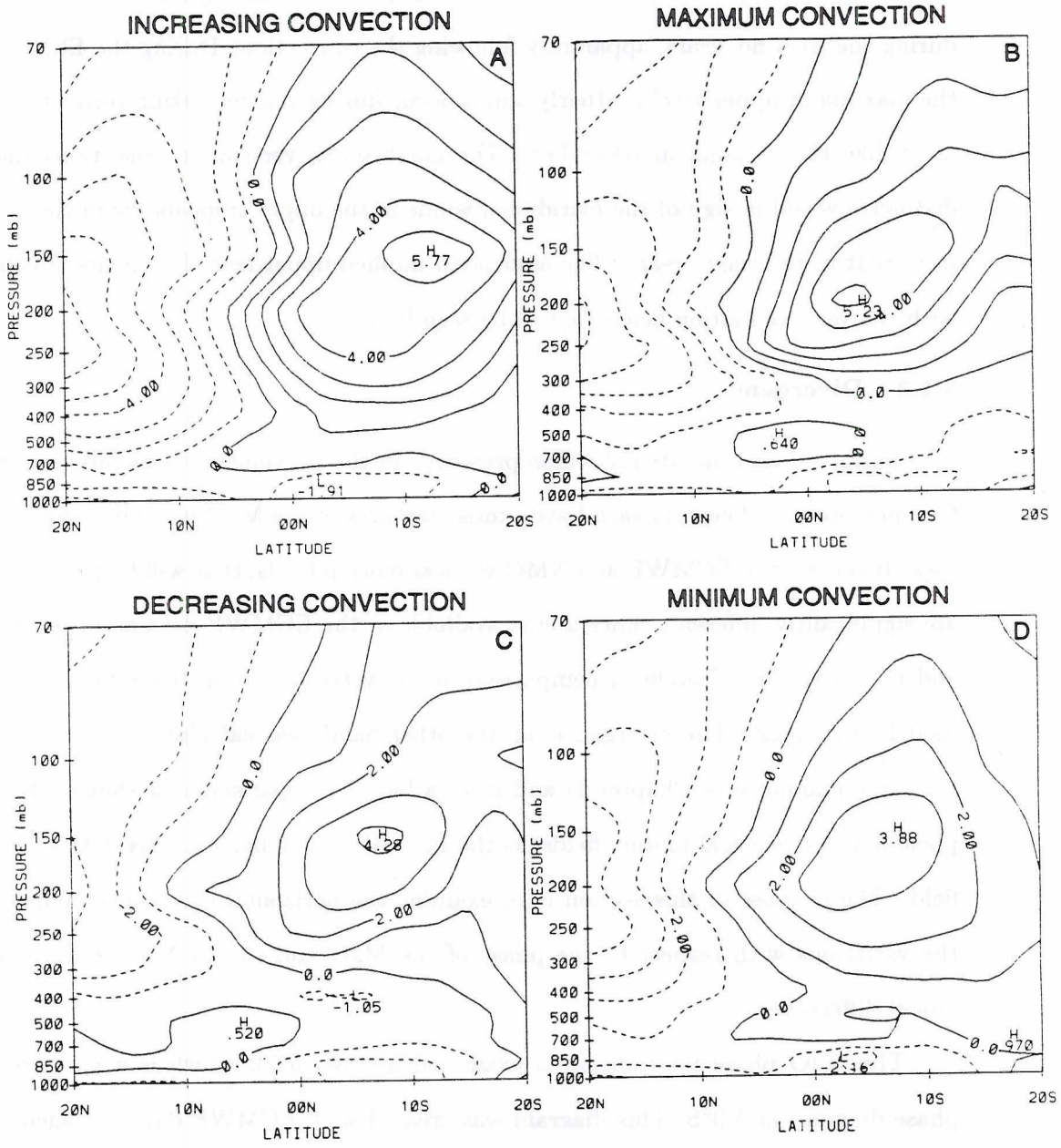

Figure 5.22: Same as Fig. 5.20, except for 1988-89.

To summarize this section, the v-component has a larger meridional variability than the u-component, especially at upper-levels. The low-levels were dominated by northerlies as far south as 5.0°S during all years. The latitude versus longitude analysis showed the maxima in upper-level southerlies occur farther south during the La Niña year than during the El Niño years, apparently following the convection. During the El Niño years the maxima in upper-level southerly winds occur during the decreasing convection phase, much like the maxima in westerlies. The north-south vertical cross-sections showed a distinct reversal in sign of the meridional winds in the upper troposphere in the cold year from that in the warm years. The associated implied upper-level divergence is consistent with the vertical motion fields, as will be seen later.

5.1.3 Divergence

The zonal and meridional winds presented in the previous sections indicate that the two meteorological centers each have similar features of the MJO in their respective analyses. However, the ECMWF and NMC vertical motion fields, that will be presented later, are significantly different. Since ω was available in the ECMWF data archives at NCAR and not in the NMC archive, comparison of the vertical motion fields between the two models is difficult. The divergence, on the other hand, was calculated for each model in the same manner (see Chapter 2) and gives a better comparison that should also be applicable to the vertical motion fields, as the vertical motion has its basis in the divergence field. The purpose of this section is to examine the horizontal divergence fields to show the variations with respect to the phase of the MJO and the El Niño and to examine model differences.

The MJO phase relationship is examined in Fig. 5.23, which is a pressure versus phase diagram at 5.0°S. This diagram was created with ECMWF data averaged over all longitudes between 140°E and the dateline. At first glance, it is apparent that in all three years there is weak convergence below about 400 mb and divergence above. This vertical profile is consistent with the cluster region findings of Gray (1973). He showed convergence of a nearly constant magnitude up to 400 mb and a concentrated region of

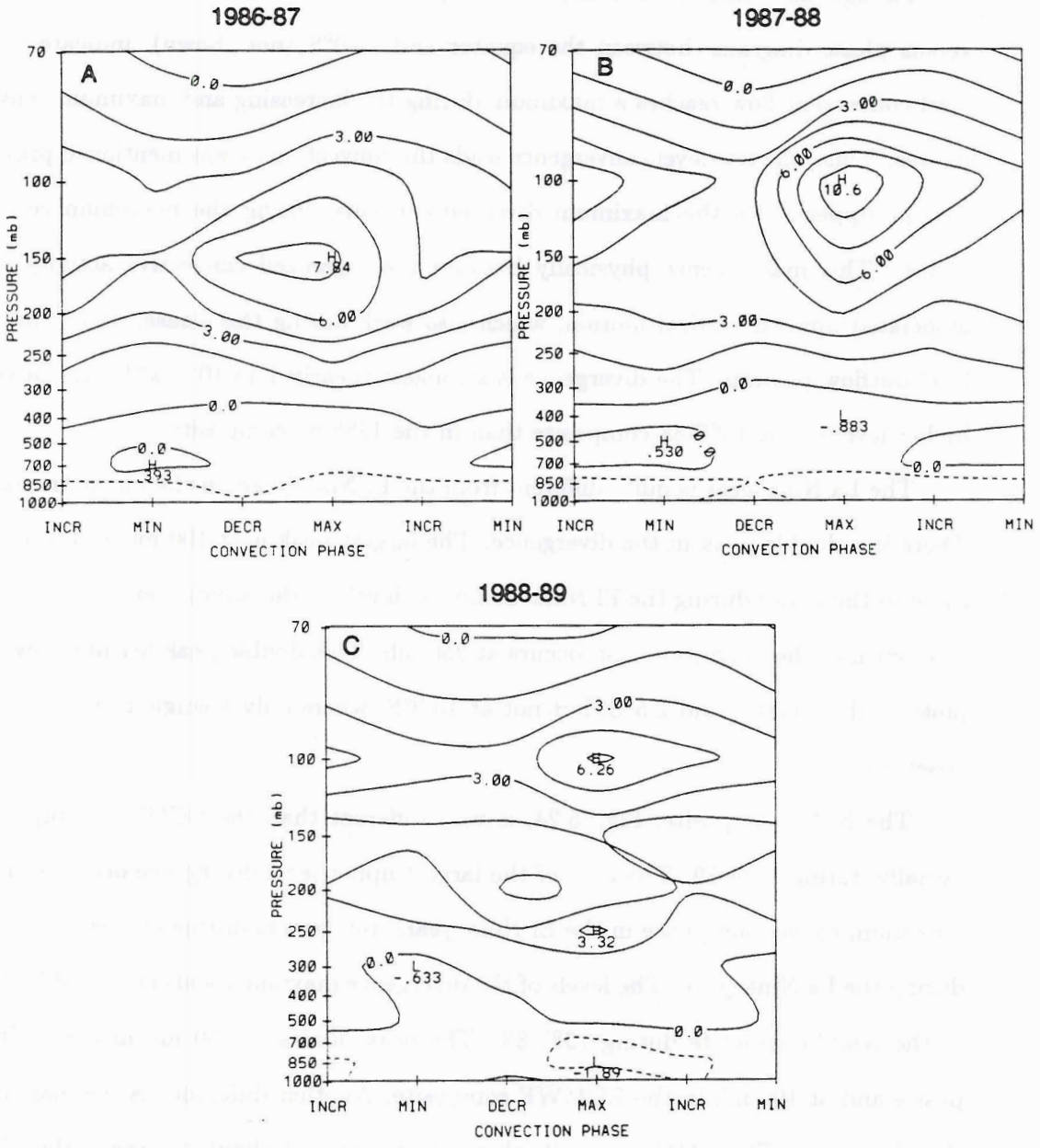

Figure 5.23: Pressure-phase diagrams of divergence at 5.0°S averaged between 140°E and 180° using the ECMWF data set for a.) 1986-87, b.) 1987-88 and c.) 1988-89. Solid lines indicate divergence and dashed lines indicate convergence. The units are $\times 10^{-6}$ s $^{-1}$ and the contour interval is 1.5 $\times 10^{-6}$ s $^{-1}$.

divergence centered at 200 mb. The level of maximum divergence is slightly higher in the present study.

Though not entirely obvious at 5.0°S (Fig. 5.23), examination of other pressure versus phase diagrams between the equator and 10.0°S (not shown), indicate the low-level convergent flow reaches a maximum during the increasing and maximum convective phases. Thus, the low-level convergence leads the convection as was mentioned previously.

At upper-levels the maximum divergence occurs during the maximum convection phase. This makes sense physically because the organized convective activity and its associated upward vertical motion, which also peak during this phase, drive this upper-level outflow pattern. The divergence is strongest (nearly 1.1×10^{-5} s^{-1}) and peaks at a higher level in the 1987-88 composite than in the 1986-87 composite.

The La Niña year is quite different from the El Niño years in the upper-troposphere. There is a double peak in the divergence. The largest peak is at 100 mb and it is comparable to the peaks during the El Niño at similar levels in the atmosphere. The other peak is about half the magnitude and occurs at 250 mb. This double peak feature is evident in plots at the equator and 2.5°S, but not at 10.0°S, where only a single peak at 200 mb is observed.

The NMC composite, Fig. 5.24, is very different than the ECMWF composite, especially during 1988-89. The area of the largest upper-level divergence occurs during the maximum convection phase in the El Niño years, but occurs during the decreasing phase during the La Niña year. The levels of the divergence maxima are also noticeably different in the NMC composite during 1987-88. The peak occurs at 150 mb in the NMC composite and at 100 mb in the ECMWF composite. Another difference is the magnitude of the divergence. The NMC composite shows magnitudes of about $\frac{1}{2}$ those of the ECMWF composite, leading to stronger vertical motion in the ECMWF model, as will be seen later.

The north-south cross-sections are relatively unrevealing and are omitted. However, one interesting aspect warrants some discussion. One would expect to find the maximum divergent region to be displaced poleward in the Southern Hemisphere during the La Niña year due to the shift of the main area of convective activity away from the equator

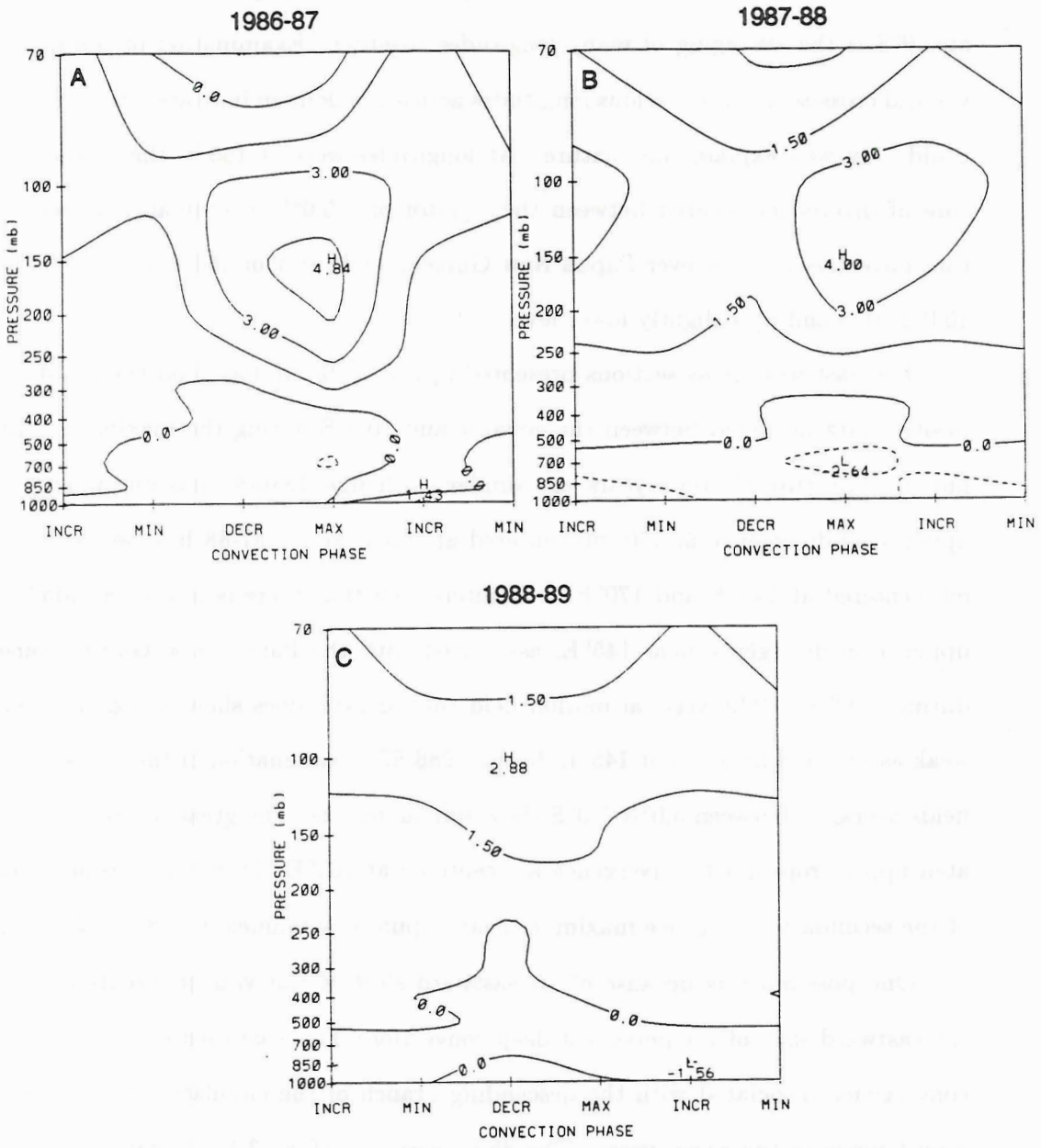

Figure 5.24: Same as Fig. 5.23, except for NMC composite.

as was shown in Figs. 4.2-4.4. Instead, the core of the divergence remains centered near 5.0°S during 1988-89. This is the same latitude as during both 1986-87 and 1987-88. There is, however, a smaller secondary maximum that is evident at a slightly lower level between 15.0-20.0°S. One possible explanation for the persistent core of divergence at 5.0°S is the averaging of many longitudes together. Examination of the north-south vertical cross-sections at various longitudes across the domain indicates that the averaging could very well explain this feature. At longitudes west of 150°E there is a persistent core of divergence located between the equator and 5.0°S, presumably associated with the convective activity over Papua New Guinea, while east of 160°E the core is between 10.0-20.0°S and at a slightly lower level.

The east-west cross-sections presented in Fig. 5.25 are based on the ECMWF composited data averaged between the equator and 10.0°S during the maximum convection phase. The two El Niño years are similar, although 1986-87 has one main region of upper-level divergence at 150 mb centered at 160°E and 1987-88 has two regions at 100 mb centered at 145°E and 170°E. It is interesting that there is not a secondary core of upper-level divergence near 145°E, associated with the Papua New Guinea convection, during 1986-87. The vertical motion field (not shown) does show a region of relatively weak ascent (0.8 μb s^{-1}) at 145°E during 1986-87. Examination of the ω and divergence fields averaged between 5.0°N-5.0°S show similar results. The greatest ascent and associated upper tropospheric divergence are centered at 160°E. Thus, the reason for the lack of the secondary divergence maximum near Papua New Guinea in 1986-87 is not clear.

One possibility is because of an eastward shift of the Walker circulation following the eastward shift of the persistent deep convection. This eastward shift would cause the convergence associated with the descending branch of the circulation to be near Papua New Guinea in the warm years. The SST anomalies (Fig. 3.1) indicate a rapid cooling of the ocean surface in Niño-4 between December 1987 and February 1988, which might explain the second divergence peak near Papua New Guinea in the 1987-88 composite. The region of divergence near 170°E could be due to convection that occurred near that longitude in November and December of 1987 and the region of divergence located near

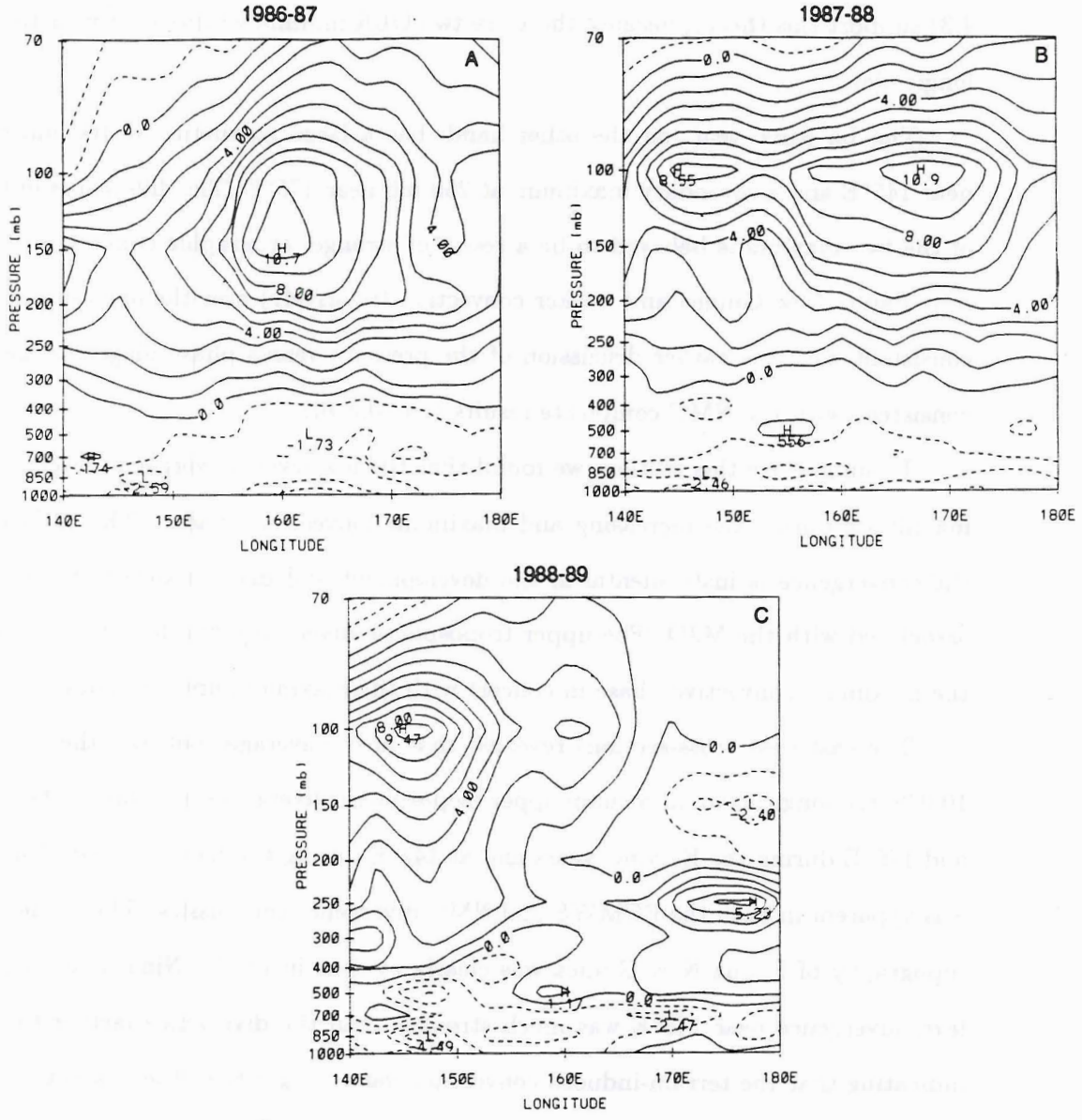

Figure 5.25: Pressure-longitude diagrams of divergence during the maximum convection phase of the MJO averaged between the equator and 10.0°S using the ECMWF data set for a.) 1986-87, b.) 1987-88 and c.) 1988-89. Solid lines indicate divergence and dashed lines indicate convergence. The units are $\times 10^{-6}$ s $^{-1}$ and the contour interval is 1.0 $\times 10^{-6}$ s $^{-1}$.

Papua New Guinea could be due to convection that occurred in January and February 1988. The westward shift of the thermally direct Walker circulation was driven by the rapid cooling of the SST's near the dateline. The composited OLR during 1987-88 (Fig. 4.3) support this theory, because there are two OLR minima which occur near these same longitudes.

The La Niña year, on the other hand, has a large maximum at 100 mb centered near 145°E and a secondary maximum at 250 mb near 175°E. The differences in the level of the two maxima is believed to be a result of stronger orographic convection occurring near Papua New Guinea and weaker convection (relatively) over the open ocean. This is consistent with the earlier discussion of the pressure versus phase diagrams and is also consistent with the NMC composite results (not shown).

To summarize this section, we found that the low-level convergence reaches its peak magnitude during the increasing and maximum convection phases. This indicates that the convergence is instrumental in the development and maintenance of the convection associated with the MJO. The upper tropospheric divergence was found to occur during the maximum convective phase in concert with the maximum upward motion.

The east-west cross-sections revealed that in the averages between the equator and 10.0°S, the longitude of maximum upper tropospheric divergence is located between 160°E and 170°E during the El Niño years and at 145°E during the La Niña year. This feature was apparent in both the ECMWF and NMC divergence composites. The influence of the topography of Papua New Guinea was clearly evident in the La Niña year. The upper-level divergence near 145°E was much stronger than the divergence farther to the east, indicating that the terrain-induced convection was stronger than the convection over the open ocean.

5.1.4 Vertical Motion

One of the indicators of the strength of convective activity is vertical motion. That is, where there are deep cumulus clouds there is strong ascending air and where there are shallow cumulus clouds or no clouds there is weak ascending or descending air. The vertical motion fields presented in this section from the ECMWF data set are those that were

calculated within the model analysis and those from the NMC data set were calculated using the technique described in Chapter 2.

The purpose of this section is to examine the relationship between the vertical motion field and the convective activity within the MJO. As will be shown, there are significant differences in the vertical profiles of ω from one phase of the MJO to another, from one year to another and from one model to another. The differences seen between the models are no doubt caused by many factors including different analysis schemes. We are unable to get a true measure of how these two centers differ from the vertical motion field due to reasons described earlier, but the differences in the divergence fields discussed in the previous section are applicable here as well.

The pressure versus convection phase vertical cross-sections are useful in describing the large-scale characteristics of the vertical motion field. As with the horizontal wind component diagrams, the cross-sections represent an average of all longitudes from 140°E to the International Dateline. The profiles at latitudes north of the equator are all very similar, so we chose to use the ECMWF composite at 5.0°N (Fig. 5.26) to describe the vertical motion in the trade wind regime. The analyses in the region from the equator to 10.0°S are also very similar. For this portion of the domain, we chose to use 5.0°S (Fig 5.27 for ECMWF and Fig. 5.28 for NMC) in order to be consistent with the previous sections.

Examination of Fig. 5.26 indicates that the strongest vertical motions occur during the maximum convection phase of the MJO. This result should not be surprising; however, it does give an indication of the consistency of the model[1]. There is a trend for the center of the maxima in ω to occur during other convection phases north of 5.0°N and south of 10.0°S (not shown). An explanation for the shift of the strongest vertical velocities to the other phases away from the equatorial region is not clear, but it could be because the main convection is located between 5.0°N and 10.0°S.

---

[1]The OLR and model data may actually not be independent. If cloud-drift winds are used in the models, then it is plausible for OLR and divergence maxima to be highly correlated.

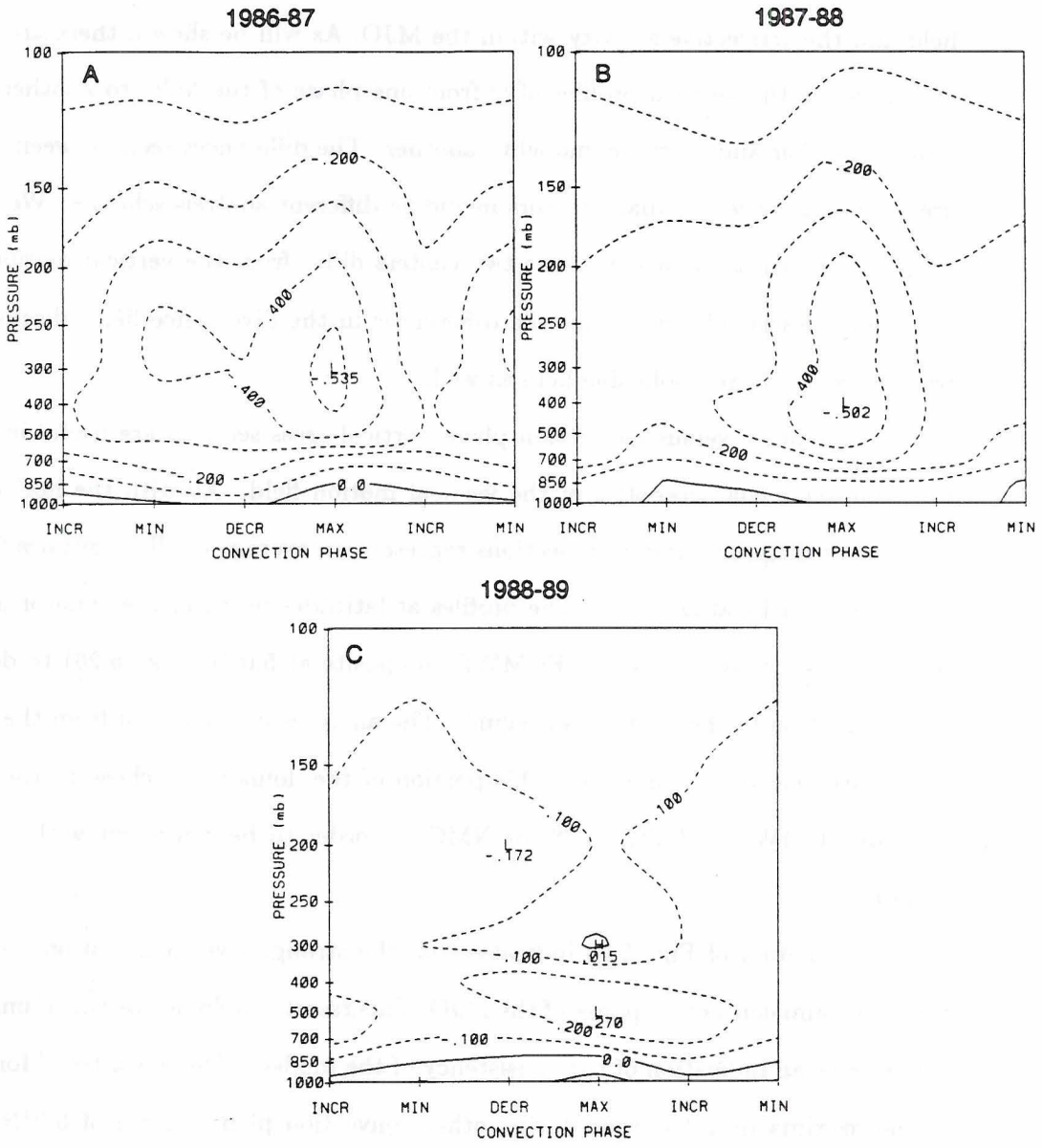

Figure 5.26: Pressure-phase diagrams of ECMWF composited vertical motion (μb s^{-1}) averaged from 140°E to 180° at 5.0°N for a.) 1986-87, b.) 1987-88 and c.) 1988-89. Solid contours represent downward motion and dashed represent upward motion. The contour interval is 0.1 μb s^{-1} .

In the 1986-87 composite at 5.0°N, the maximum ascending motion is located near 300 mb and has a magnitude greater than 0.5μb s^{-1} . There is also weak ($< 0.1\mu$b s^{-1}) descending air from the surface to about 850 mb during all but the decreasing convection phase. The 1987-88 composite is similar in appearance, but the maximum ascending motion is near 400 mb, slightly lower than the other El Niño year. However, there does appear to be a secondary maximum near 250 mb. In the lower troposphere there is weak descending motion ($< 0.1\mu$b s^{-1}) during the decreasing and minimum convection phases. The La Niña year is characterized by very weak vertical motions in all phases. There is a maximum in upward motion during the maximum convective activity which is located near 500 mb and a relative maximum in downward motion near the surface during the same convective phase. There is also a weak region of subsidence at 300 mb during the maximum convective phase. All of these maxima have absolute values of less than half those described in the other two years. At low-levels, below 850 mb, downward motion is seen during all convection phases, with the greatest descent during the maximum convection. It is important to remember that for all three years the convection was centered on or south of the equator (see Figs. 4.2-4.4), this is especially true during 1988-89.

To better contrast the El Niño years and the La Niña year, the vertical motion at 5.0°S is presented. This latitude is near the center of the maximum in convection for the two El Niño years as depicted in the OLR composite diagrams (Figs. 4.2-4.4). The latitude of the maxima in convective activity for the La Niña year is about 10.0°S. Thus, the diagram of vertical motion presented in Fig. 5.27 and Fig. 5.28 are on the northern fringe of the deep convection for the La Niña year. A discussion of the characteristics of ω at 10.0°S will also be included for 1988-89.

In general, the vertical motion fields from the ECMWF (Fig. 5.27) appear to be much more organized at this latitude, for all three years. There is one distinct maximum in upward motion that occurs consistently during the maximum convection phase. There are, however some differences in the location, magnitude, and extent of the core of the ascending and descending air.

The two El Niño years show a peak in upward motion near the 300 mb level and the peak during the La Niña year is near 500 mb, significantly lower. Also, the magnitude

of the vertical motion is 1.5 to 2.0 times greater during the warm years. The differences in magnitude might be explained as a result of the convection in the La Niña year being farther south, but the vertical cross-section at 10.0°S (not shown) shows the maximum vertical motion of 0.6 μb s^{-1} , which is nearly the same as that shown in Fig 5.27. Therefore, we conclude that the convective activity during the El Niño years is stronger than the convective activity during the La Niña year. This result is consistent with the findings of Deser and Wallace (1990), in that the convection associated with the tropical convergence zones intensifies with increased positive SST anomalies. The divergent structure functions introduced into the mass and wind field analysis of the ECMWF (Trenberth and Olson 1988) in January 1988 might also explain the magnitude differences, but this could not be substantiated.

Another feature that differentiates the warm years from the cold year is evident at low-levels. Recall from Fig. 5.24, that there was subsidence in the lower troposphere during at least some phase of the MJO at 5.0°N. However, at 5.0°S there is no indication of descending air in either 1986-87 or 1987-88. In fact, the upward motion in the low-levels is nearly as strong as the maxima that were described at 5.0°N. There remains a shallow subsidence layer (surface to about 900 mb) during 1988-89. This subsidence layer begins to disappear at 7.5°S and is completely replaced by rising motion at 10.0°S (not shown).

There are also some subtle differences between the two El Niño years. The most obvious difference, evident in both models, is the narrowness of the core of rising motion during 1987-88 compared to the broad core during 1986-87. The magnitude of ω is about 22% greater in the 1987-88 composite than the 1986-87 composite. These results indicate that the convection is stronger at this latitude during 1987-88 (assuming no changes in the model analysis procedures), but that it is shorter lived because it only persists for one phase of the MJO. In 1986-87, the convective activity is slightly weaker, but it persists for nearly three phases of the MJO. Recall from Fig. 3.1 that the positive SST anomalies in Niño-4 are actually slightly larger in 1987-88 than in 1986-87, which could contribute to the stronger vertical motion. However, as will be seen in the north-south cross-sections (Fig. 5.29), the maximum ascent during 1986-87 is located at 2.5°S and is actually larger than the maximum ascent during 1987-88, which is located at 5.0°S.

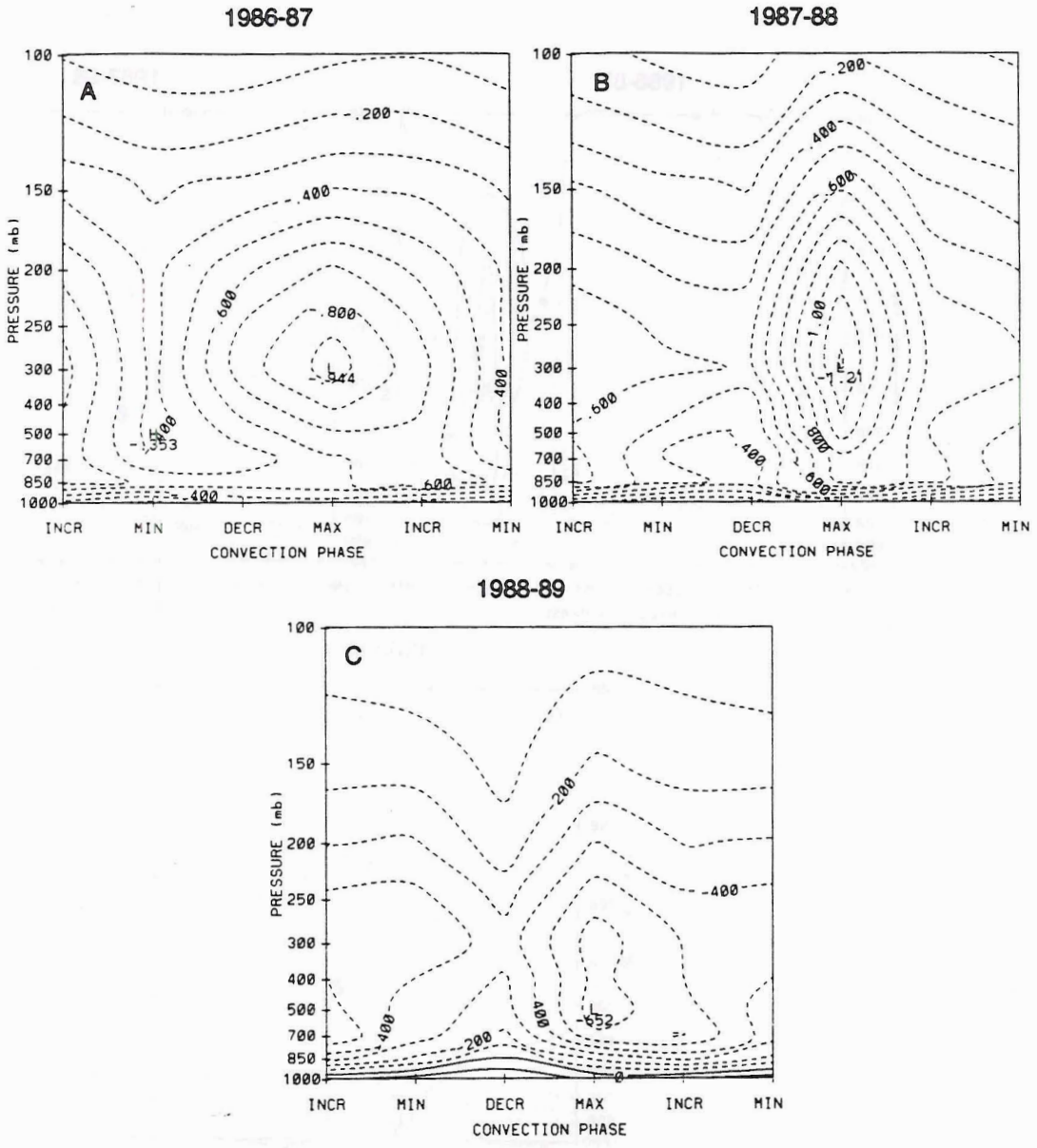

Figure 5.27: Pressure-phase diagrams of ECMWF composited vertical motion (μb s^{-1}) averaged from 140°E to 180° at 5.0°S for a.) 1986-87, b.) 1987-88 and c.) 1988-89. Solid contours represent downward motion and dashed represent upward motion. The contour interval is 0.1 μb s^{-1} .

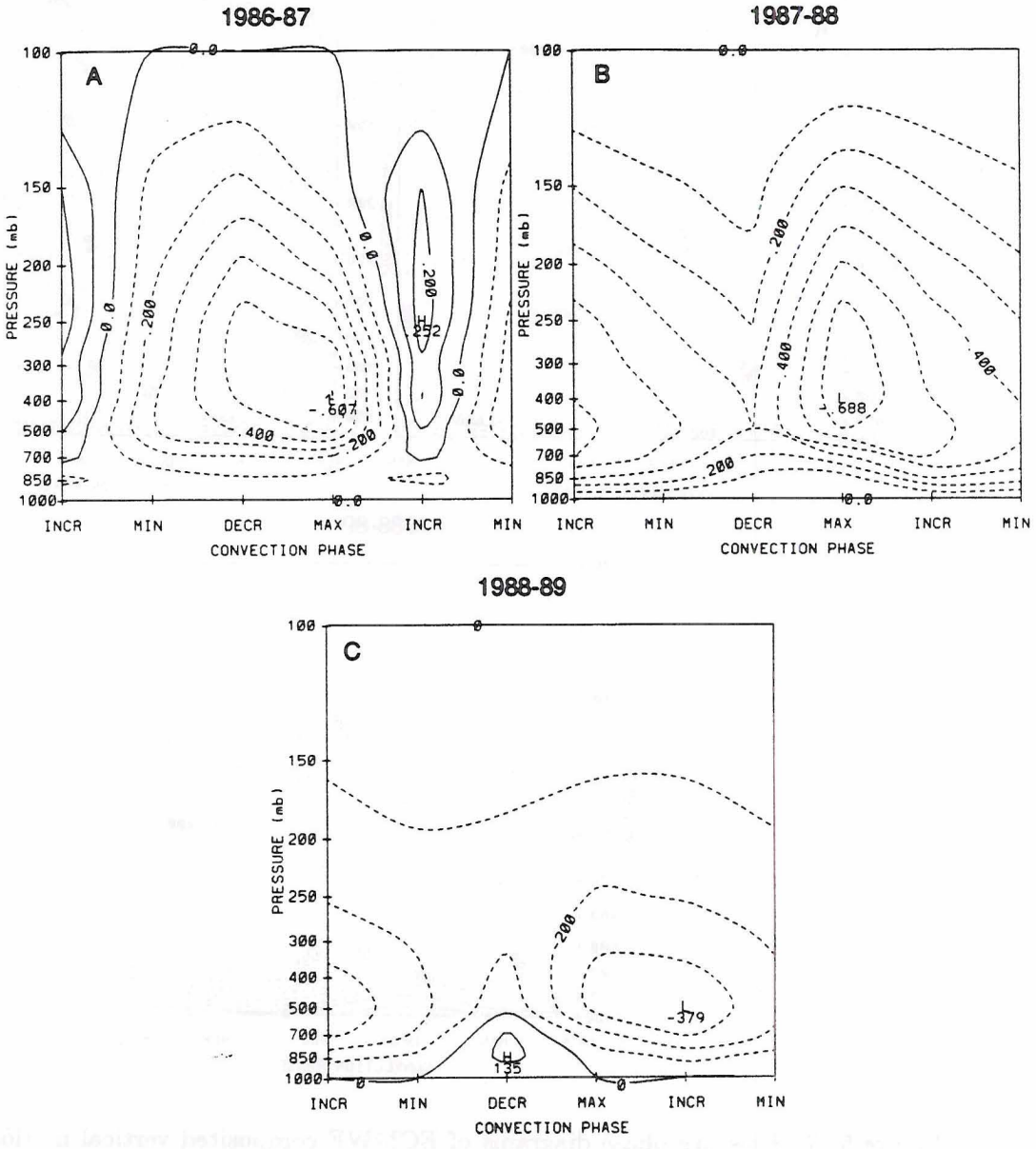

Figure 5.28: Same as in 5.27, except for NMC composite.

Comparing Figs. 5.27 and 5.28, one can see fairly large differences in the vertical motion fields between the two different centers. In the NMC composite during the El Niño years, the maxima in upward vertical motion occur during the maximum convection phase, but they are centered at 400 mb. This is 100 mb lower than in the ECWMF composite. Another apparent difference is seen in the 1986-87 composite. The NMC composite shows an area of subsidence during the increasing convection phase that does not exist in the ECMWF composite. The cause of this region of subsidence is not clear, but it is visible in the north-south vertical cross-section during the increasing convection phase between 2.5°S and 10.0°S (not shown).

The magnitudes of ω are also significantly different between the two models. The ascending motion is stronger in the ECMWF composite by a factor of 1.5 in 1986-87 and 1.8 in 1987-88. These differences can be attributed to the differing model analysis schemes.

During the La Niña year, the differences between the two models become even greater. The NMC composite (Fig. 5.28) shows the maximum in upward motion occurring during the increasing convection phase. The character of the core of the ascending air is also different. The ECMWF composite shows a narrow vertical column of ascent extending well into the upper-troposphere during the maximum convection phase, while the NMC composite shows a rather broad flat region restricted to the mid-troposphere.

One similarity that is evident in the two models during the La Niña year is at low-levels. Both show subsidence of nearly the same intensity during the decreasing convection phase, although the NMC composite has a deeper layer than the ECMWF composite.

The meridional variations in ω are presented during the maximum convection phase for the ECMWF and NMC composites in Fig. 5.29 and Fig. 5.30, respectively. These diagrams are north-south vertical cross-sections based on the average of all longitudes between 140°E to 180°. The inter-phase variations, though evident, are not as significant as the inter-annual variations, and are not presented.

The two El Niño years show upward vertical motion from about 10.0°N to 15.0°S in the ECMWF model with the primary maxima south of the equator. In 1986-87 there are multiple centers of ascent, both north and south of the equator. During 1987-88,

however, there is only one main region of ascent. This suggests, because this is an average of many longitudes, that during 1986-87 the latitude that deep convection occurred varied with longitude and in 1987-88 the latitude remained fairly regular across the 40° domain. Examination of the north-south vertical cross-sections along various longitude belts (not shown) indicates that this is in fact the case. This is also consistent with the composited OLR (Figs. 4.2 and 4.3) because during the maximum convection phase (minimum OLR) for 1986-87 the amount of OLR is highly variable across the domain, while in 1987-88 there is a persistent band of low OLR across the entire domain indicating persistent convective activity.

The 1986-87 ECMWF composite (Fig. 5.29) is suggestive of the double ITCZ structure that is often found in the equatorial Pacific Ocean, although there are multiple centers of upward motion on both sides of the equator. Examination of north-south cross-sections along individual longitude belts (recall Fig. 5.29 is an average of all longitudes from 140°E-180°) indicates that the multiple centers on each side of the equator are a result of this longitudinal averaging. The vertical motion associated with the Northern Hemisphere trade wind trough is indicated by the two peaks at 2.5°N and 7.5°N and the Southern Hemisphere SPCZ is indicated by the two peaks at 2.5°S and 7.5°S. During 1987-88 this double ITCZ structure is not obvious during the maximum convection phase, but it is apparent in the other three phases near 10.0°N (not shown). In each of the two warm years, the level of maximum upward vertical motion is between 300-400 mb. Also, in both years the region of subsidence associated with the Northern Hemisphere subtropical ridge is confined north of 15.0°N.

In the ECMWF composite, the La Niña year shows two primary centers of upward vertical motion south of the equator located near 7.5°S and 15.0°S and a relatively weak center at about 5.0°N. There is some evidence of the double ITCZ structure during this cold year during the maximum convection phase, but it is more apparent in the other three phases (not shown) with a zone of upward motion near 7.5°N. The two maxima in the Southern Hemisphere peak between 500-700 mb and are smaller in magnitude than the peaks in the El Niño years. One possible explanation for this difference is that the

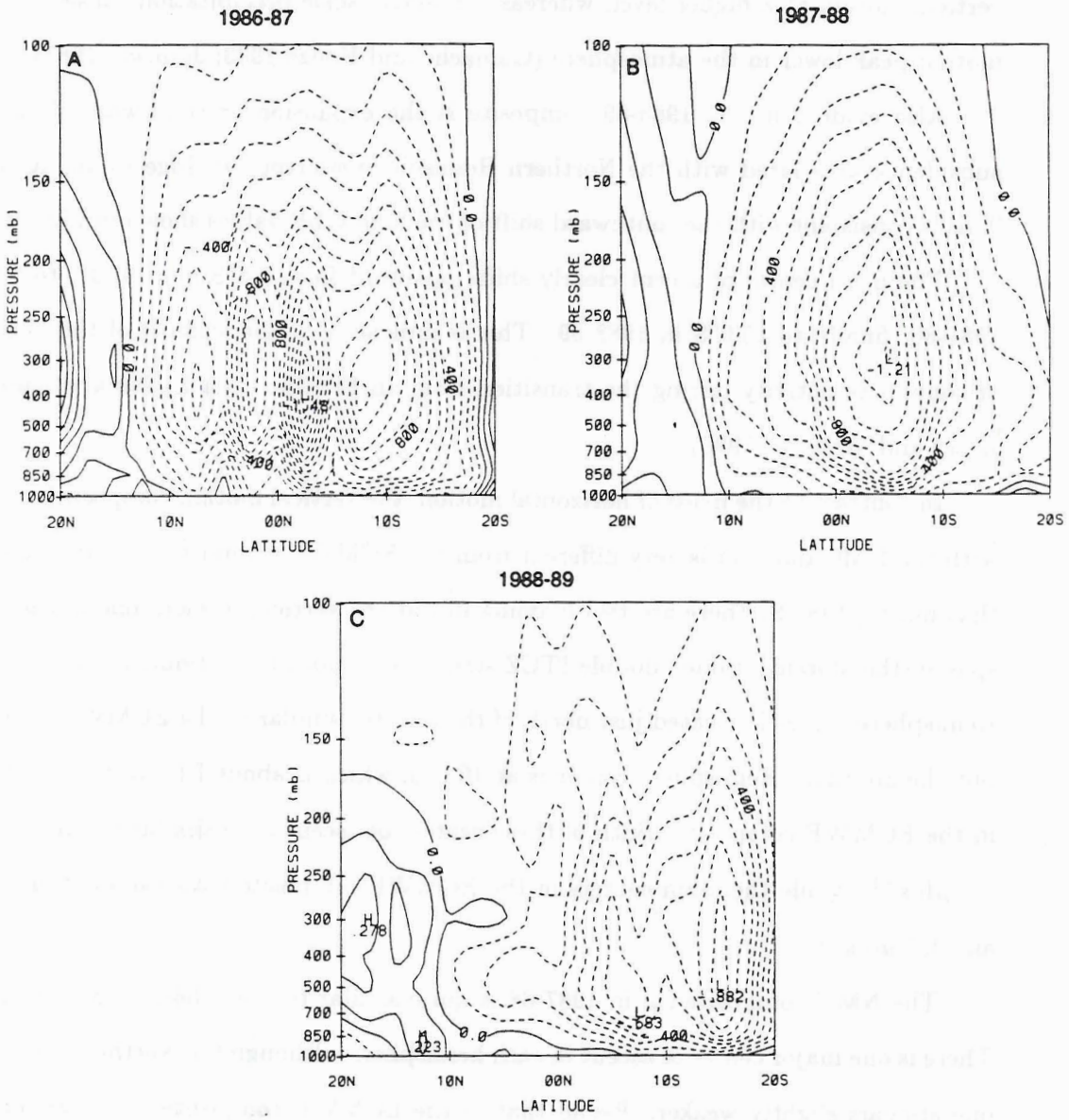

Figure 5.29: Pressure versus latitude diagrams of ECMWF composited vertical motion (μb s^{-1}) averaged from 140°E to 180° for the maximum convective phase for a.) 1986-87, b.) 1987-88 and c.) 1988-89. Solid lines represent downward motion and dashed lines represent upward motion. Contour interval 0.1 μb s^{-1} .

convection is shallower and weaker during the this La Niña year than during the two El Niño years. Another possibility is that during the El Niño years there is a larger fraction of upper-level stratiform precipitation in the composite, which would cause a peak in vertical motion at a higher level, whereas convective scale precipitation causes a vertical motion peak lower in the atmosphere (Gamache and Houze 1983; Johnson 1982).

Also evident in the 1988-89 composite is the expansion or southward shift of the subsidence associated with the Northern Hemisphere subtropical ridge to about 10.0°N. This is consistent with the southward shift of the high OLR values shown in Figs. 4.2-4.4.

The main center of ascent clearly shifts poleward from 2.5°S in 1986-87, to 5.0°S in 1987-88, finally to 15.0°S in 1988-89. This is indicative of the shifting of the main area of convective activity during the transition from an El Niño to a La Niña discussed by Deser and Wallace (1990).

In contrast to the fields of horizontal motion, the vertical motion composite computed with the NMC data set is very different from the ECMWF composite. Figure 5.30 shows that during 1986-87 there are two maxima in upward vertical motion, one in each hemisphere (the aforementioned double ITCZ structure is much more evident). The Northern Hemisphere center is located just north of the equator similar to the ECMWF composite, but the Southern Hemisphere center is at 10.0°S, which is about 7.5° farther south than in the ECMWF composite. Both of these centers of ascent have similar magnitudes near 0.7 μb s^{-1} , while the main centers in the ECMWF composite have values of around 1.0 and 1.5 μb s^{-1} .

The NMC composited ω in 1987-88 is quite similar to the 1986-87 NMC composite. There is one major center of ascent in each hemisphere, although the Northern Hemisphere one appears slightly weaker. Recall that in the ECMWF composite there was only one main core of ascending air. The core of the Southern Hemisphere upward vertical motion is located near 7.5°S, which is 2.5° south of the main center in the ECMWF composite.

During the La Niña year the NMC pattern continues to be different from the ECMWF composite. There is one center of ascent in each hemisphere, one located at 5.0°N and another at 10.0°S. In this year, however, the Southern Hemisphere center is more than twice as strong as the Northern Hemisphere one.

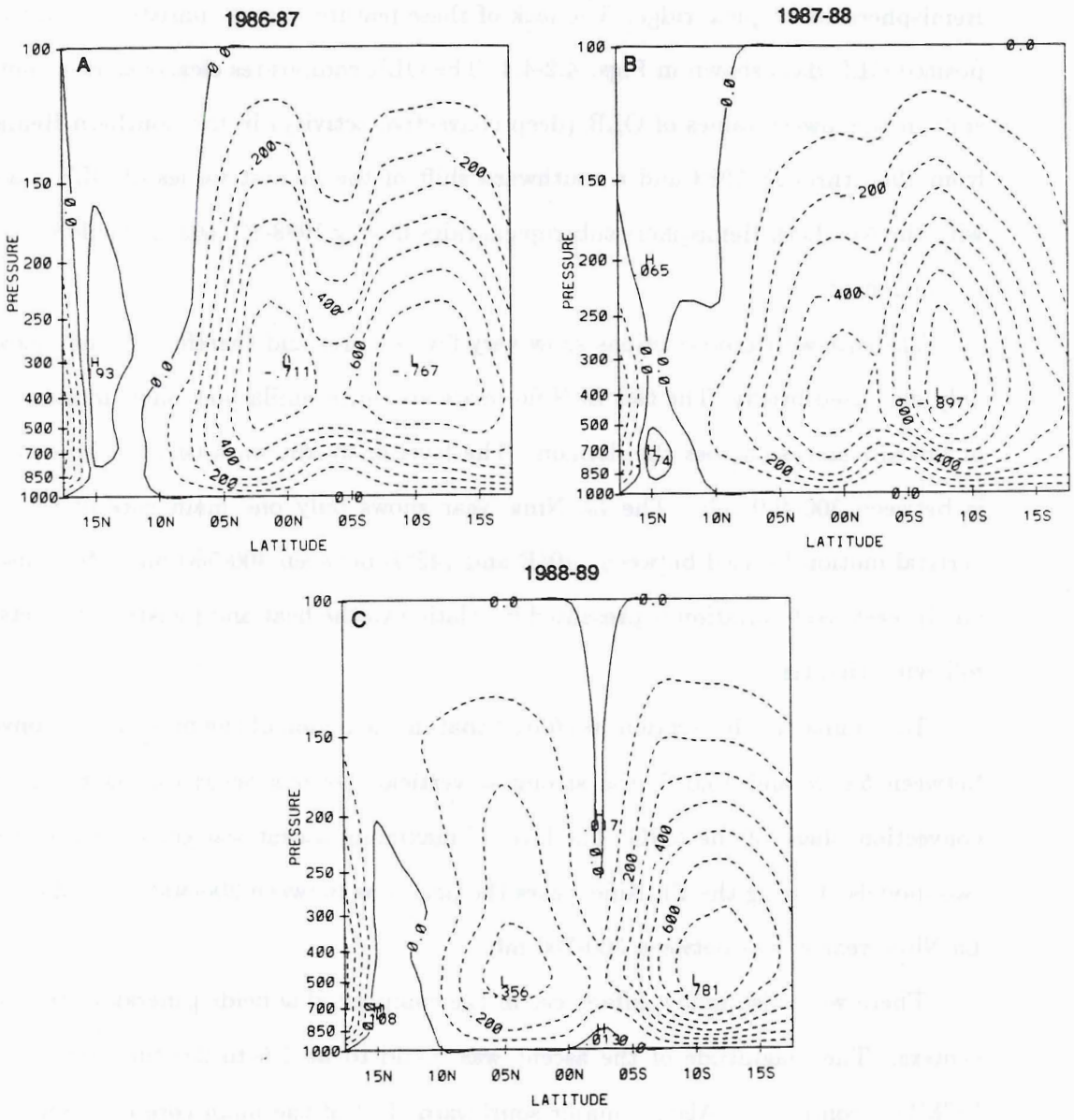

Figure 5.30: Same as Fig. 5.29, except for NMC composite.

Despite other differences, the level of strongest vertical motion is consistent in both of the models for all three years. However the southward shift of the core of the ascending motion during the La Niña year is not as clearly evident in the NMC composited ω field, nor is the expansion or southward shift of the subsidence associated with the Northern Hemisphere subtropical ridge. The lack of these features is not consistent with the composited OLR data shown in Figs. 4.2-4.4. The OLR composites clearly show a southward shift in the lowest values of OLR (deep convective activity) in the Southern Hemisphere from 1986 through 1989 and a southward shift of the highest values of OLR associated with the Northern Hemisphere subtropical ridge during 1988-89, which should be reflected in the ω field.

The east-west cross-sections show very few features and therefore are not shown and only discussed briefly. The two El Niño years are quite similar and show multiple centers of upward motion across the domain. The level of maximum ascent in these two years is between 300-400 mb. The La Niña year shows only one main core of the upward vertical motion located between 140°E and 145°E between 400-500 mb. More discussion on the east-west variation is presented in relation to the heat and moisture budgets in the following chapter.

To summarize this section, we found that in the region of the most active convection, between 5.0°N and 15.0°S, the strongest vertical motions occur during the maximum convection phase of the MJO. The level of maximum ascent was consistent between the two models. During the EL Niño years the peak was between 300-400 mb and during the La Niña year it was between 500-700 mb.

There were also many differences in the composited ω fields generated from the two centers. The magnitude of the ascent was found to be 1.5 to 2.0 times greater in the ECMWF composite. Also, a major southward shift of the main core of upward motion (from near the equator in 1986-87 to about 15.0°S during 1988-89) was only apparent in the ECMWF composite. The NMC composite showed the main core of ascent remaining near 10.0°S in all three years. The magnitude of the vertical motion was 1.5-2.0 times stronger during the warm years than the cold year in the ECMWF composite and of equal strength for all three years in the NMC composite.

5.2 Thermodynamic Fields

The purpose of this section is to present the surface pressure, atmospheric temperature and relative humidity fields in relation to the MJO composite. The small daily, and even monthly, variability of these parameters makes it necessary to show anomalies rather than total fields. The means for each grid point in the domain for the four month period (Nov-Feb) for each year are subtracted from the composited data to arrive at these anomalies.

5.2.1 Surface Pressure Anomalies

The spatial variations in surface pressure anomalies are shown in Figs. 5.31-5.33. These figures were generated using the ECMWF data composited based on the convective phase at 160°E longitude. The NMC composite results are not presented because they are very similar to the ECMWF composite.

In the 1986-87 composite (Fig. 5.31) the pattern north of the equator shows negative anomalies of about 0.8 mb centered at 10.0°N across most of the domain during the decreasing and minimum convection phases and a mixture of weaker positive and negative anomalies during the other two phases. A stronger more revealing signal exists in the Southern Hemisphere. Positive pressure anomalies dominate during the minimum convection phase and negative pressure anomalies dominate during the maximum convection phase. This makes physical sense because during the periods of minimum convective activity, the pressure perturbations associated with the low-level divergent flow within the MJO wave would be positive and during the maximum convective activity the opposite would be true.

Also apparent in Fig. 5.31 is a west to east propagation of the centers of anomalous pressures. The positive anomaly near 10.0°S and 145°E in the decreasing convection diagram appears to move south-eastward across the domain during the minimum and increasing phases and is completely out of the domain by the maximum convection phase. Lau and Lau (1986) also noted an eastward propagation in the surface pressure field in their composite study. This propagation is evident in the NMC composite as well (not shown).

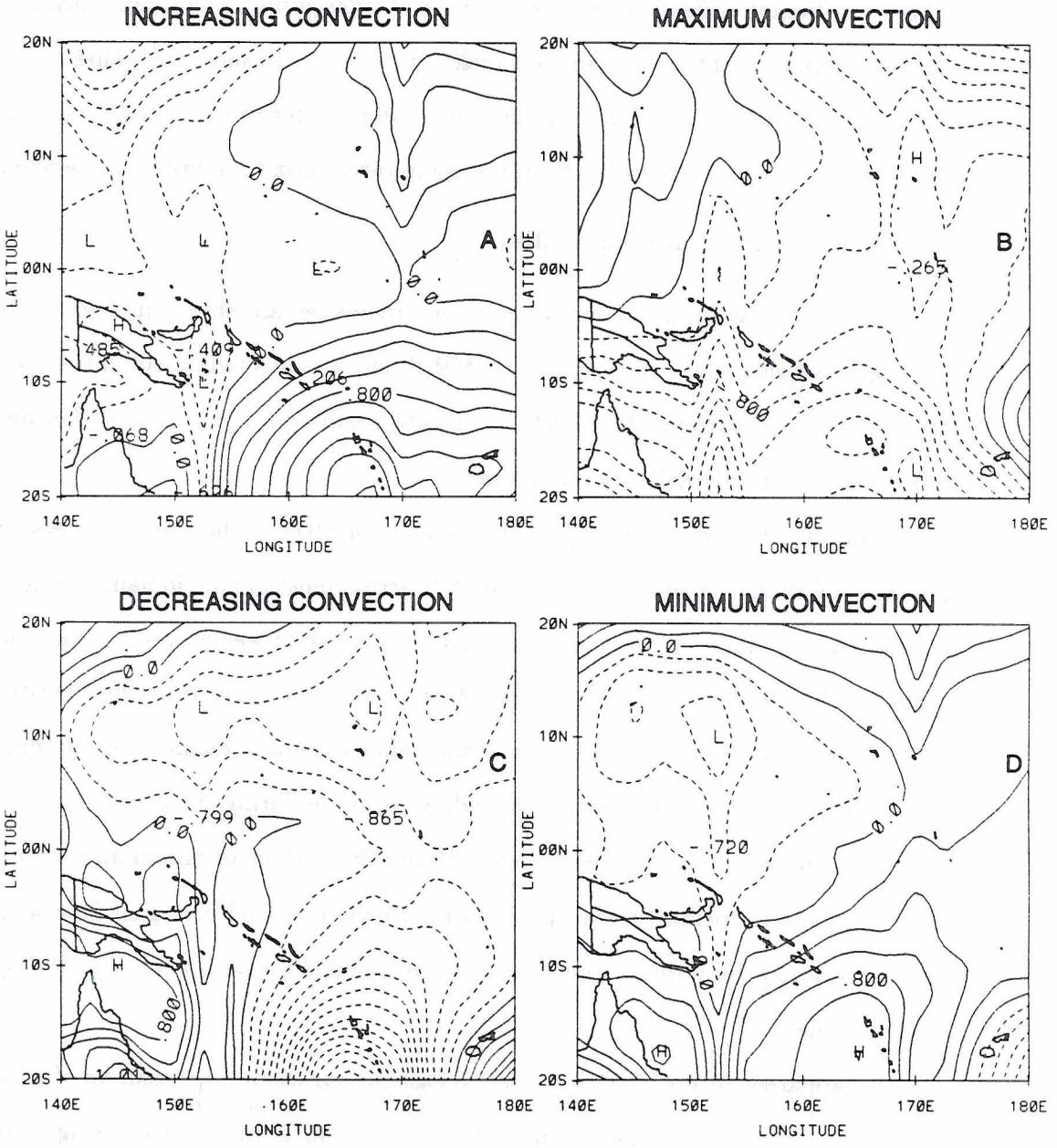

Figure 5.31: 1986-87 latitude-longitude diagram of anomalous surface pressure based on the phase of the MJO at 160°E using the ECMWF data set for the a.) increasing, b.) maximum, c.) decreasing and d.) minimum convective phases. Solid (dashed) lines are positive (negative) pressure anomalies and the contour interval is 0.1 mb.

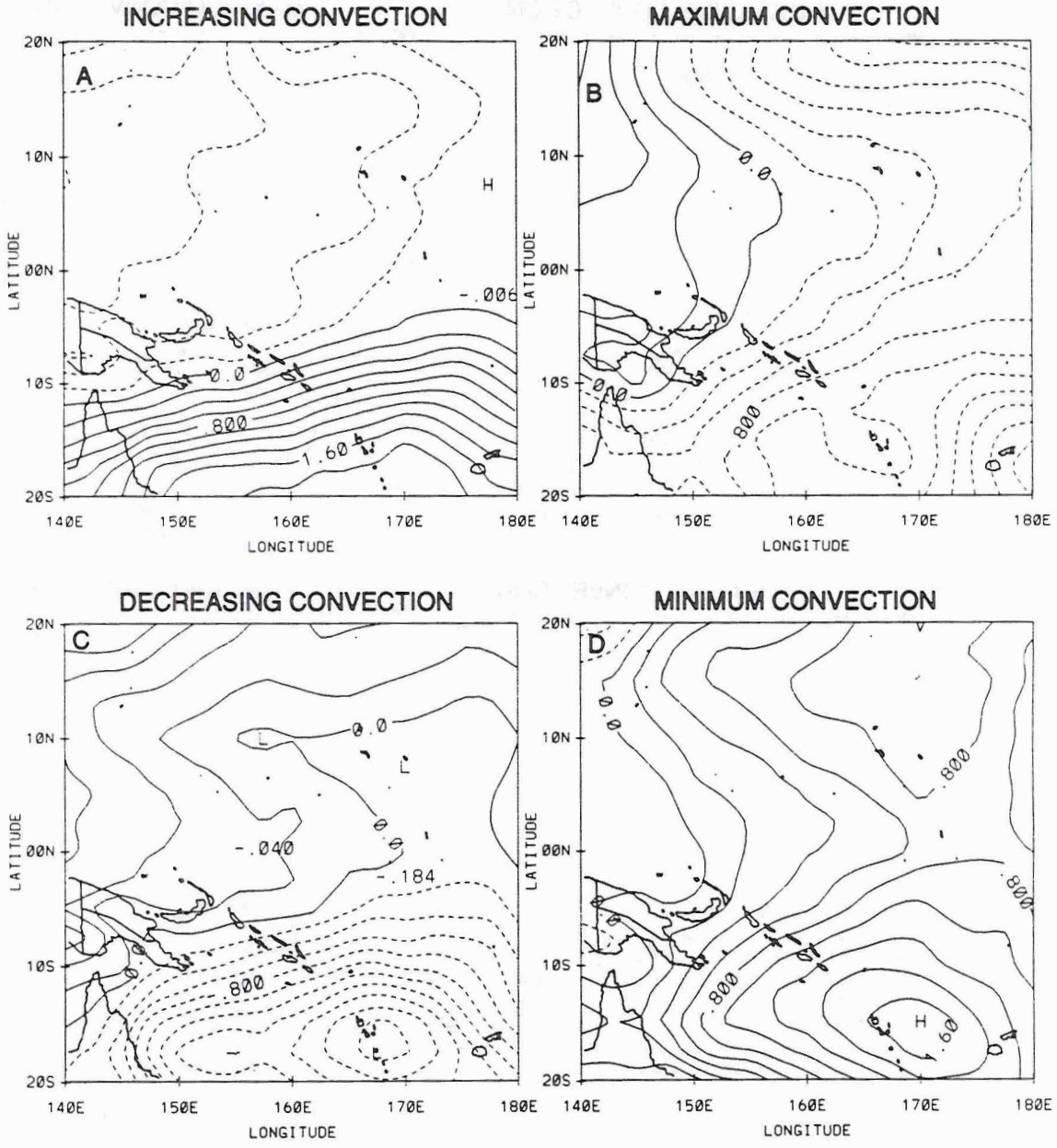

Figure 5.32: Same as Fig. 5.31, except for 1987-88

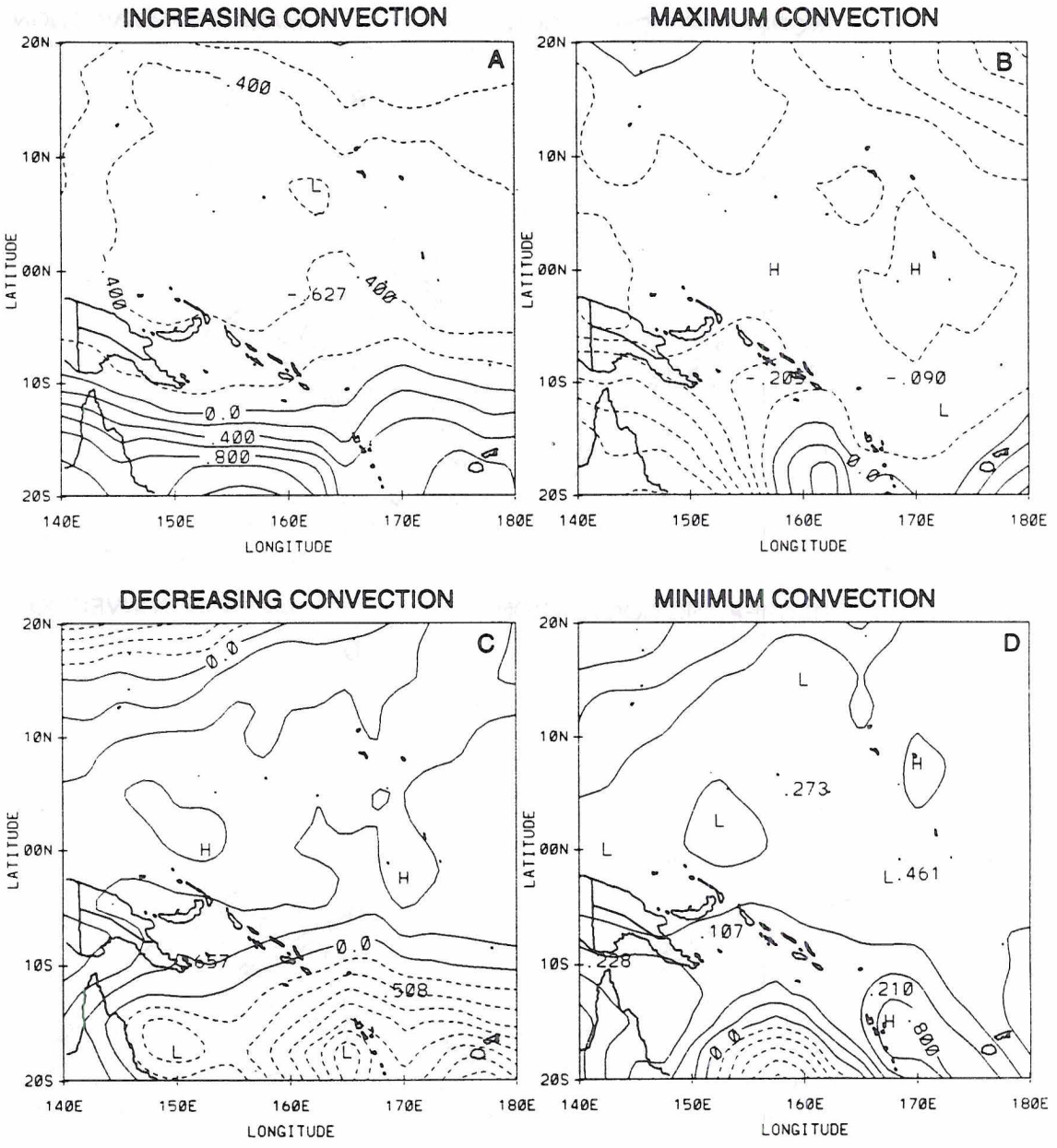

Figure 5.33: Same as Fig. 5.31, except for 1988-89.

North of the equator, the 1987-88 composite (Fig. 5.32) is drastically different from the 1986-87 composite. The pressure anomalies during the decreasing and minimum convection phases are positive and during the increasing and maximum convection phases the anomalies are predominately negative. Intuitively this makes better physical sense as lower surface pressures are expected to accompany higher convective activity as explained above. The NMC composite results indicate the same tendency. Attempts to explain the differences between these two years have been difficult and inconclusive.

The anomalous pressure patterns south of the equator are somewhat similar in both the 1986-87 and 1987-88 composites. However, the pattern south of 10.0°S during 1986-87 appears to have pressure variations on a smaller scale than the MJO, as seen best in the decreasing convection phase. Investigation into the number of tropical cyclones in the region between 155°E and 175°E (JTWC, 1986-89) indicates more cyclones occurred in during 1986-87 than the other two years. It is, therefore, likely that the surface pressure anomalies have been biased by these cyclones.

The composited surface pressure anomalies for the La Niña year, 1988-89, are shown in Fig 5.33. During this cold year, the convection was found to be shifted well south of the equator. The surface pressure anomalies north of the equator are similar to those shown in Fig. 5.32. Positive anomalies occur when convection is decreasing and at a minimum and negative anomalies occur as the convection increases and reaches a maximum. South of the equator the patterns are also similar, but there are some differences evident during the transition phases, when the anomalies are greatest. The regions of anomalous pressures are shifted farther south and are smaller in magnitude in the 1988-89 composite year, consistent with the more southerly track of convection in the La Niña year.

A feature that is apparent in all three years is that the maximum and minimum anomaly values occur during the two transition phases. The highest surface pressure anomalies occur during the increasing convective phase and the lowest anomalies occur during the decreasing phase. Thus, there appears to be a phase lag between the occurrence of maximum (minimum) convection and vertical motion and the minimum (maximum) surface pressure. The fact that the minimum in surface pressure anomalies occur during

the same phase as the maximum in low-level westerlies and vice versa is consistent with the results presented in Lau and Lau (1986). In their GCM simulation, they showed for the western Pacific Ocean area, strong low-level easterlies were associated with positive surface pressure anomalies south of the equator and strong low-level westerlies were associated with negative surface pressure anomalies.

To summarize this section, we found that there is good agreement between the ECMWF and NMC surface pressure composite results. Both composites show that the surface pressure anomaly pattern in the Northern Hemisphere during 1986-87 is very different than the patterns in 1987-88 and 1988-89. The patterns in the Southern Hemisphere are quite similar in all three years, although the centers of the anomalies are shifted farther away from the equator during the cold year. The Southern Hemisphere results are similar to the results of Lau and Lau (1986).

5.2.2 Temperature Anomalies

The temperature deviations for the ECMWF data are presented in order to examine how the MJO modifies the thermal structure of the atmosphere. The temperatures in the NMC archives at NCAR were found to be virtual temperature (Jenne, 1991) and are not presented because large mixing ratios in the tropics makes the recovery of accurate temperature anomalies problematic.

Figure 5.34 is a pressure versus phase diagram of temperature anomalies at 5.0°S averaged over all longitudes from 140°E to 180°. In the lower troposphere, there are negative anomalies during the decreasing phase of the MJO. These anomalies may be due evaporational cooling of the residual precipitation in the unsaturated downdrafts associated with the decaying convective towers. This region of negative anomalies is also apparent just east of the trough axis in the composite of westward propagating synoptic-scale disturbances accomplished by Reed and Recker (1971) (their Fig. 5) and in the Australian summer monsoon onset composite done by Hendon and Liebmann (1990) (their Fig. 5d). The same speculation as to the source of this low-level cooling anomaly was forwarded by Reed and Recker and Hendon and Liebmann, although the former used the precipitation pattern to substantiate their conclusion. In the El Niño years there are

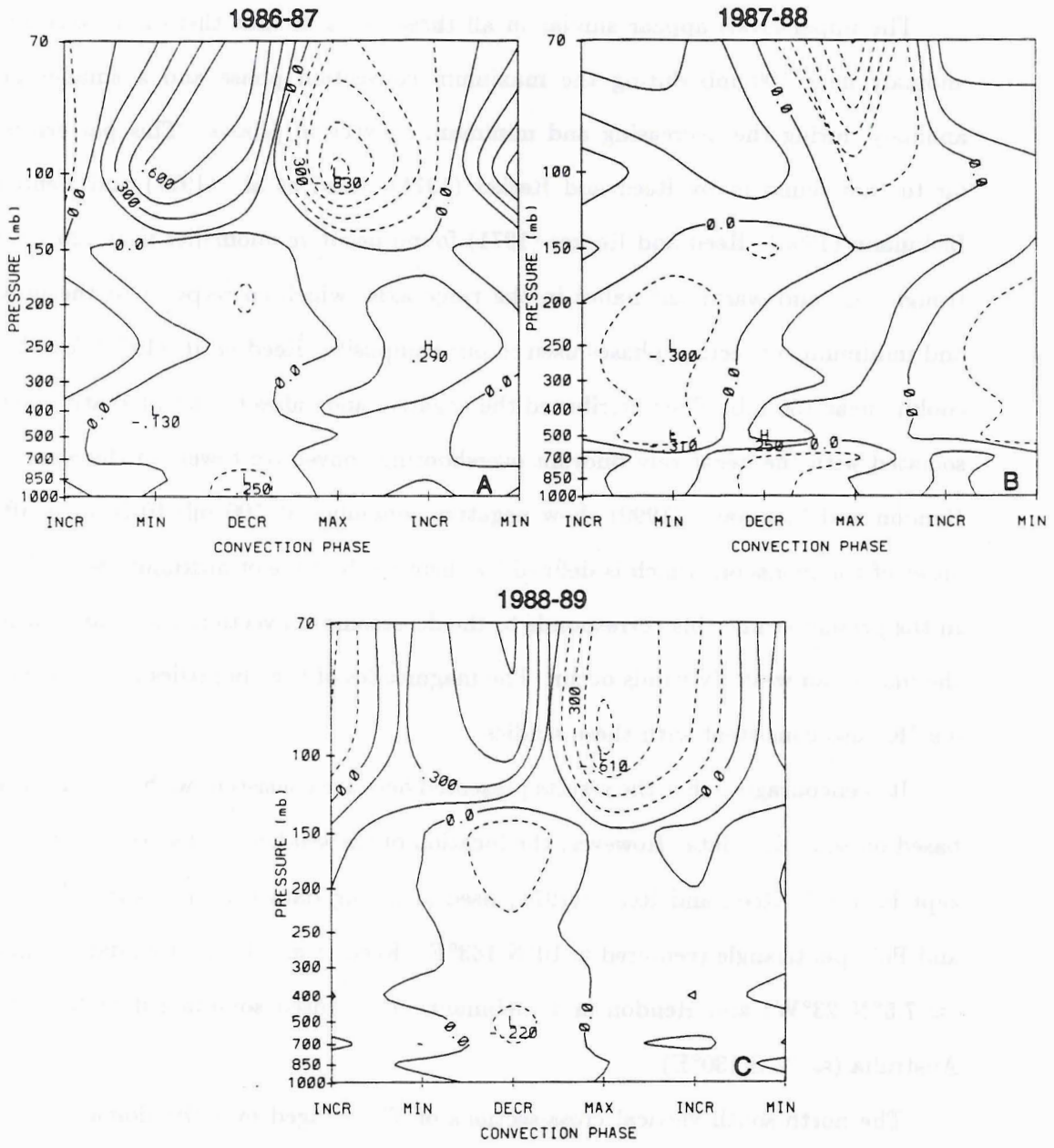

Figure 5.34: Pressure-phase diagram of temperature anomalies (°K) at 5.0°S averaged from 140°E to 180° for a.) 1986-87, b.) 1987-88 and c.) 1988-89. The solid lines are warm anomalies and the dashed are cool. The contour interval is 0.15 °K.

weak warm anomalies between 200 and 500 mb in the increasing, maximum or decreasing convection phases. These warm anomalies are presumably associated with latent heat release (similar to the results of Reed and Recker 1971 and Reed *et al.* 1977).

The upper-levels appear similar in all three years in that there is a large negative anomaly near 100 mb during the maximum convection phase and a smaller positive anomaly during the decreasing and minimum convection phases. This pattern is similar to that found in by Reed and Recker (1971), Reed *et al.* (1977) and Hendon and Liebmann (1990). Reed and Recker (1971) found negative anomalies near 125 mb in the trough axis and warm anomalies in the ridge axis, which correspond to the maximum and minimum convection phases used in our composite. Reed *et al.* (1977) found similar cooling near 150 mb. They attributed the negative anomalies to the adiabatic cooling associated with the negatively buoyant overshooting convective towers in the wave trough. Hendon and Liebmann (1990) show negative anomalies at 100 mb 10-20 days after the onset of the monsoon, which is defined by them as the time of maximum westerly winds. In the present study, this corresponds to the decreasing convection phase, as that is when the maximum westerly winds occur. The magnitudes of the anomalies are between 0.6 to 0.9 °K, also consistent with these studies.

It is encouraging that the results presented here are consistent with those from studies based on sounding data. However, the location of the studies referenced above should be kept in mind. Reed and Recker(1971) used sounding data from a Kwajalein, Eniwetok and Pohnpei triangle (centered $\approx$ 10°N 163°E), Reed *et al.* (1977) used data from GATE ($\approx$ 7.5°N 23°W) and Hendon and Liebmann (1990) used sounding data from Darwin, Australia ($\approx$ 12°S 130°E).

The north-south vertical cross-sections of T' averaged over the domain for 1987-88 are presented in Fig. 5.35. Because the anomalous temperature patterns are quite similar in all three years, we chose this year examine the meridional thermal structure.

There is a dramatic reversal in the temperature anomalies with the change in convective phase south of the equator. During the increasing convection phase, the lower troposphere shows warm anomalies, the middle and lower portion of the upper troposphere have

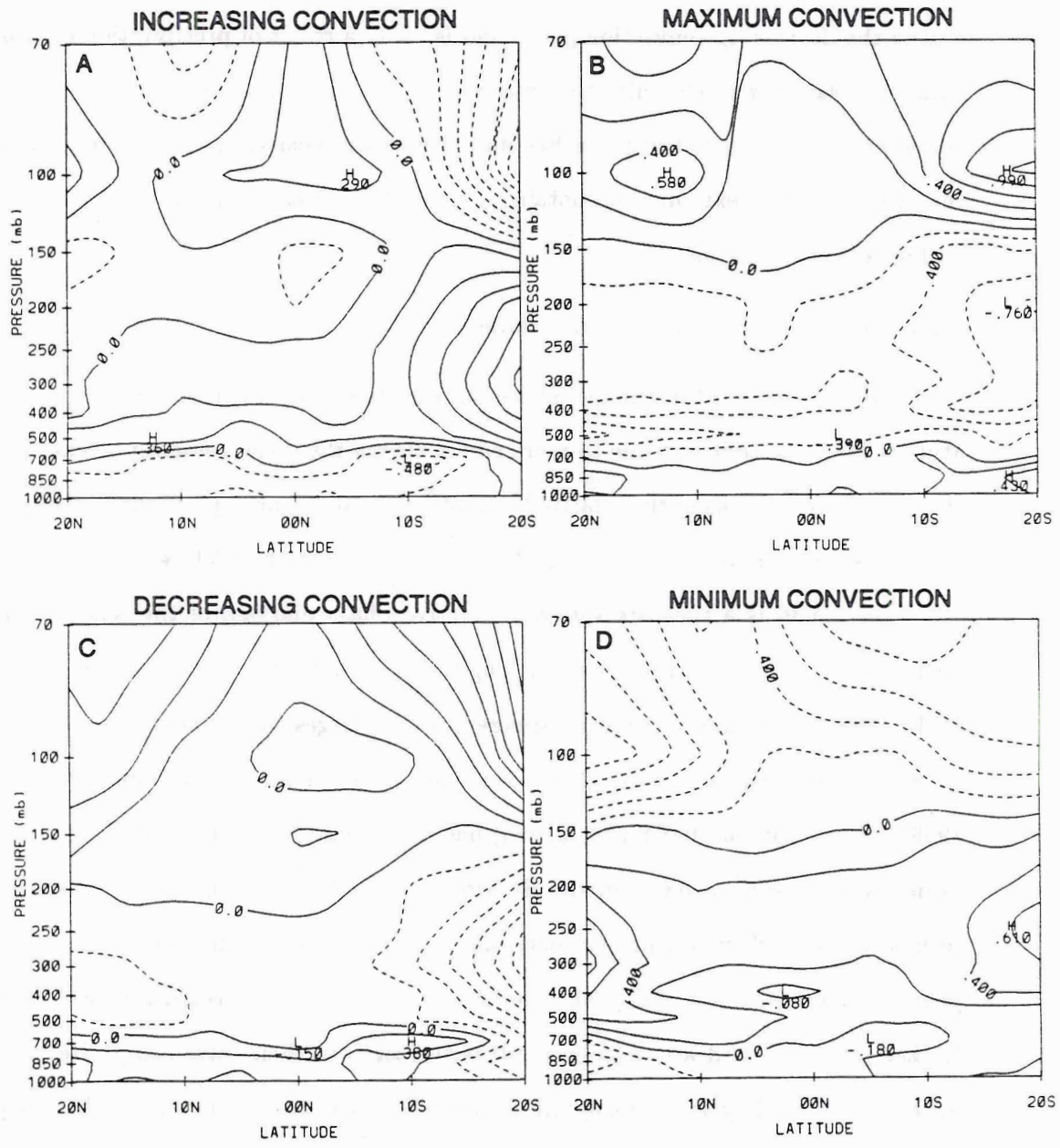

Figure 5.35: Pressure-latitude diagram of temperature anomalies (°K) averaged from 140°E to 180° for the a.) increasing, b.) maximum, c.) decreasing and d.) minimum convection phase of the MJO. The solid lines are warm anomalies and the dashed are cool. The contour interval is 0.15 °K.

cold anomalies and the remainder of the upper troposphere has warm anomalies. When the convection reaches a maximum and begins to decrease, there is a complete reversal of the temperature anomaly profile. The maximum negative anomaly in the low-levels peaks during the decreasing convection phase and is likely a result of precipitation evaporation, while the warming in the mid- to upper troposphere is likely due to latent heat release. When the convective activity reaches its minimum intensity, the profile reverts back to the original. The next chapter contains a complete discussion about the heating profiles and is deferred until then.

5.2.3 Relative Humidity Anomalies

The moisture field in the model was anticipated to be less reliable than the temperature fields because it is prone to more errors during the measurement process. However, the composite analysis of the relative humidity anomalies shows good physical consistency and has some similar characteristics of the Reed and Recker (1971) wave composite.

Figure 5.36 is a pressure versus convective phase diagram of the relative humidity anomalies at 5.0°S averaged over all longitudes from 140°E to the dateline (as in Fig. 5.34). The middle and upper troposphere have the largest modulations, especially in the El Niño years. During the La Niña year the modulation is weaker and lower, but the 1988-89 composite at 10.0°S (not shown) has anomalies of the same magnitude and at the same levels as seen at 5.0°S in the El Niño years. Positive anomalies (moistening) are seen near the surface during the increasing convection phase and shift to the maximum phase in the mid-levels and peak near 200 mb during the decreasing phase. Reed and Recker (1971) showed a west-to-east tilt with height in their wave composite (their Fig. 6), but because they were examining westward propagating disturbances their slope was from the front of the wave to the rear. In the present study of eastward propagating disturbances the slope is also front to rear, but because the disturbance is moving in the opposite direction, the slope is actually east-to-west. This front-to-rear slope is evident in Fig. 5.36. The slope is better defined in the 1988-89 composite at 10.0°S (not shown). No slope is indicated in the results of Hendon and Liebmann (1990).

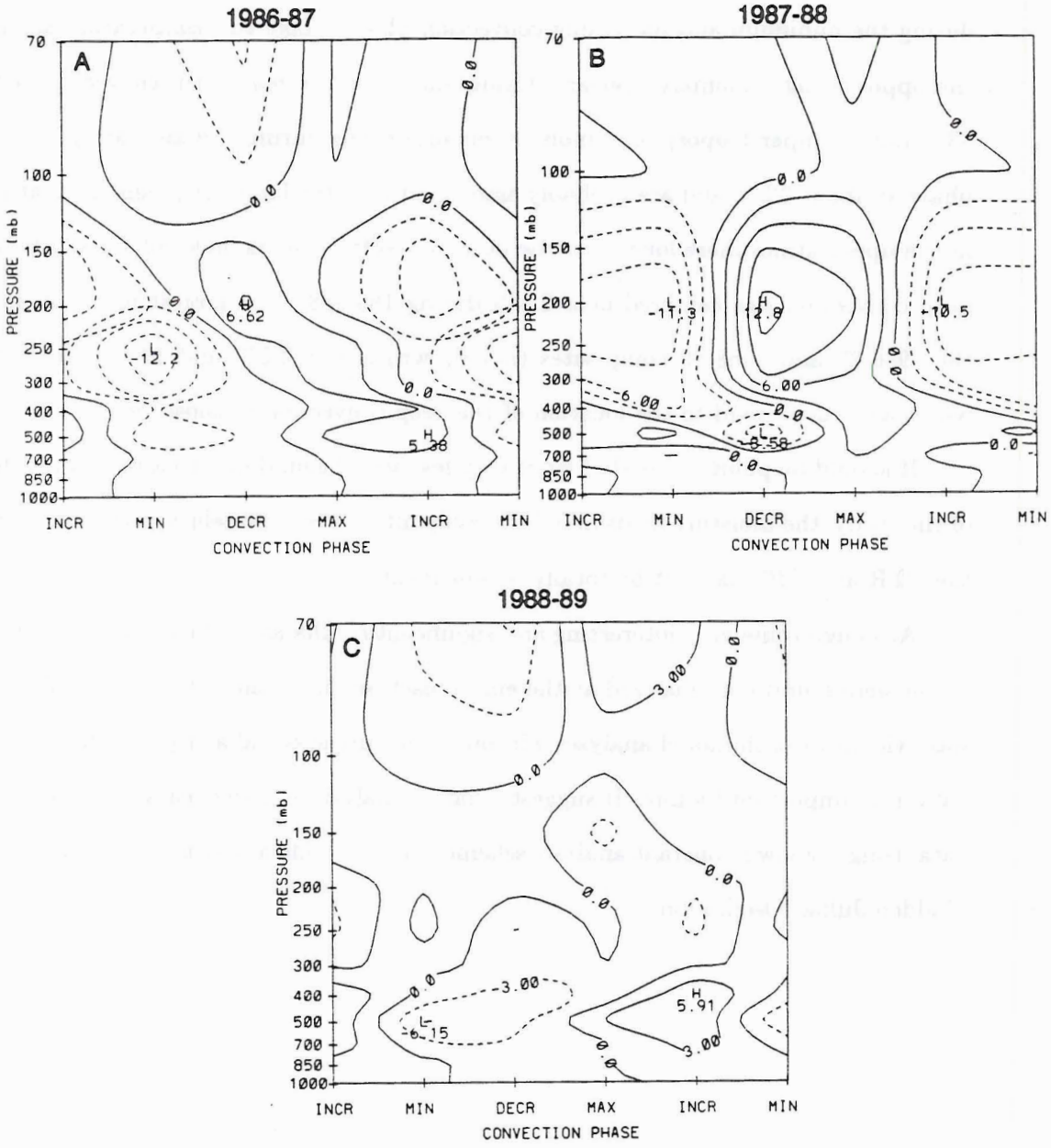

Figure 5.36: Pressure-phase diagram of relative humidity anomalies (%) at 5.0°S averaged from 140°E to 180° for a.) 1986-87, b.) 1987-88 and c.) 1988-89. The solid lines are moist anomalies and the dashed are dry. The contour interval is 3.0%.

For consistency, we present the relative humidity anomalies in a north-south vertical cross-section for 1987-88 averaged over the entire domain (Fig. 5.37). The most dramatic changes are evident in the upper-levels. There are negative anomalies above about 400 mb during the minimum and increasing convection phases. Like the temperature anomalies, the opposite sign anomaly appears during and after the maximum convective activity. The largest upper tropospheric moist anomalies occur during the decreasing convection phase at about 2.5°S and are probably associated with the large cirrus shields that persist in the upper atmosphere long after the deep convective towers have collapsed. Recall the deep convection was centered near 2.5°S during 1987-88. The largest moist anomaly in the 1986-87 and 1988-89 composites (not shown) are at 2.5°S and 12.5°S, respectively, which also correspond to the location of the deep convection in those years.

It should be pointed out that since very few actual soundings exist within the domain of the study, the moisture fields may be heavily influenced by satellite data and, therefore, the OLR and RH′ may not be totally independent.

Although some very interesting and significant results as to the structure of the oscillation were found (summarized at the end of each section), the fact that the MJO signal was evident in both model analyses without using any spectral analysis or filtering of the data is an important finding. It suggests that re-analysis of many years of model analyzed data using a known constant analysis scheme could provide a better understanding of the Madden-Julian Oscillation.

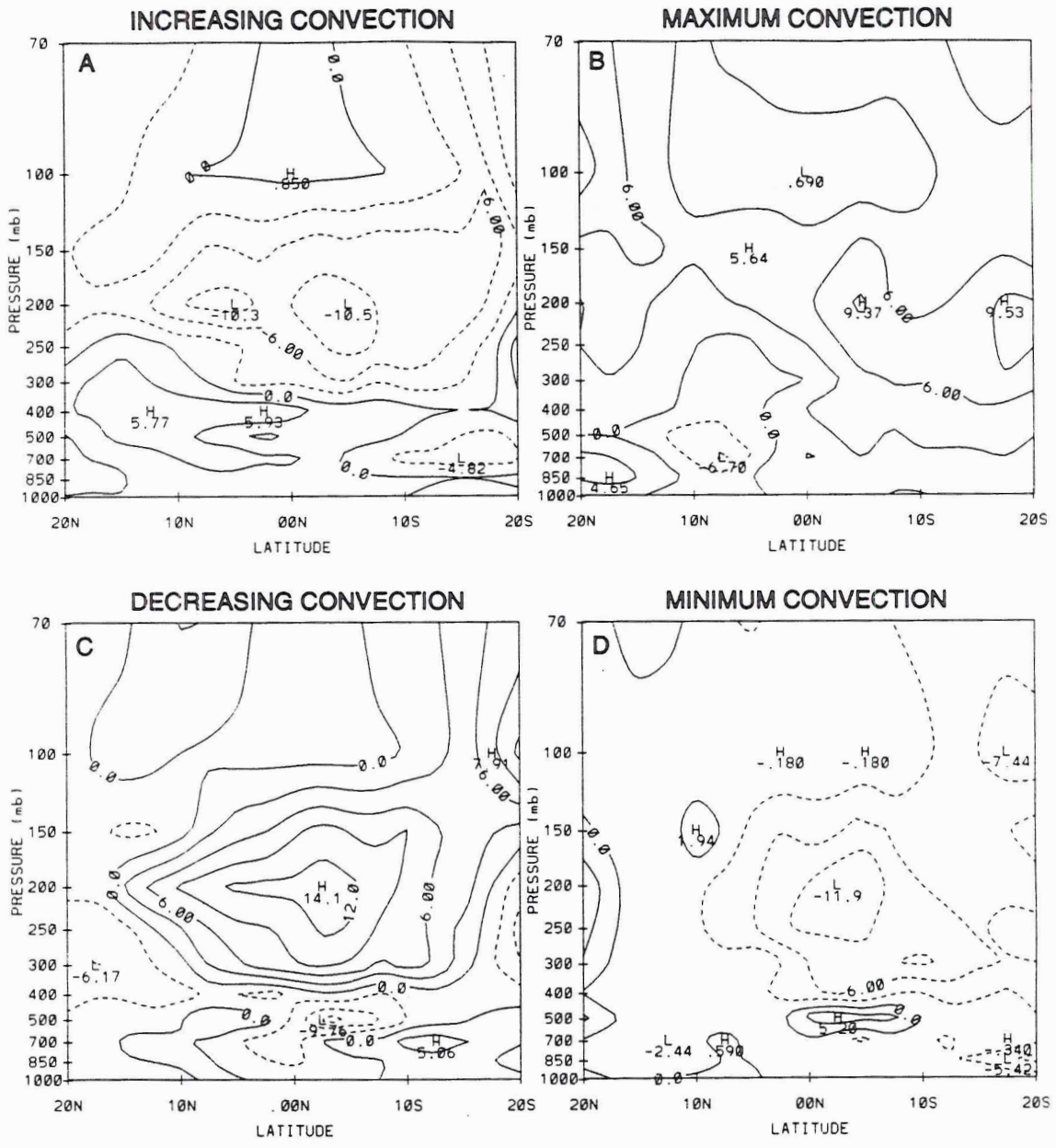

Figure 5.37: Pressure-latitude diagram of relative humidity anomalies (%) averaged from 140°E to 180° for the a.) increasing, b.) maximum, c.) decreasing and d.) minimum convection phase of the MJO. The solid lines are moist anomalies and the dashed are dry. The contour interval is 3.0%.

Chapter 6

COMPOSITE HEAT AND MOISTURE BUDGETS

Heat and moisture budgets, were first applied to precipitation features in the tropics (Yanai *et al.* 1973). More recently there has been a shift to the middle latitudes. Gallus and Johnson (1991) used heat and moisture budgets to characterize a squall line that traversed Kansas and Oklahoma during the 1985 PRE-STORM experiment. In the latter, the data resolution was fine enough to allow partitioning of the storm into the convective line and the stratiform regions. The resolution of the data in the following composite results is nowhere near as fine as in the squall line study, but the MJO is on a much larger scale than a squall line. It is therefore believed that 2.5° resolution composited data captures this large-scale feature rather well.

The budget results are presented in a manner similar to the previous chapter. Only the results of the ECMWF composite are presented because of the difficulty in recovering NMC temperatures. The variation of the Q_1 (the apparent heat source) and Q_2 (the apparent moisture sink) as a function of MJO phase is shown in Figs. 6.1 and 6.2. These figures are based on an average of all longitudes between 140°E and 180° at 2.5°S. We chose this latitude because during the El Niño years the convection is centered near this latitude. Similar figures at 7.5°S will be shown later to illustrate the heating rates associated with the convection during the La Niña year (Figs. 6.3 and 6.4).

The terms involving the vertical derivatives in Eqs. (2.1) and (2.2) dominate the local change and horizontal advection terms in the tropics due to temporal and horizontal homogeneity. Thus, the Q_1 and Q_2 profiles should resemble the vertical motion field to some degree. As can be seen from a comparison of Figs. 6.1 and 6.2 with Fig. 5.27, this is generally the case. Recall from Fig. 5.27 that the maximum vertical motion occurred

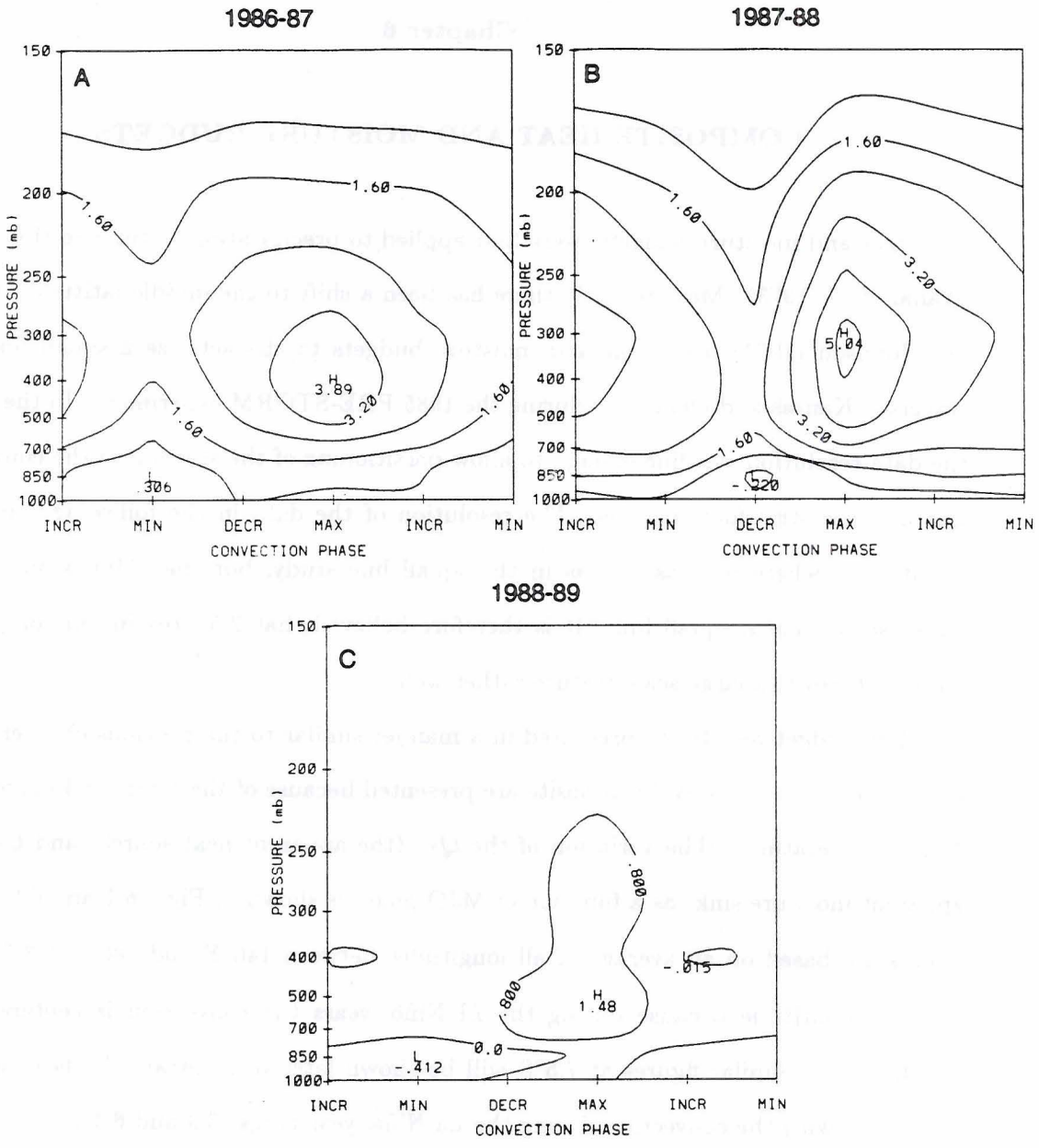

Figure 6.1: Pressure-convective phase of Q_1 averaged from 140°E to 180° at 2.5°S for a.) 1986-87, b.) 1987-88 and c.) 1988-89 in units of °K day^{-1}. The solid lines indicate the apparent heat source and the dashed lines indicate the apparent heat sink. The contour interval is 0.8°K day^{-1}

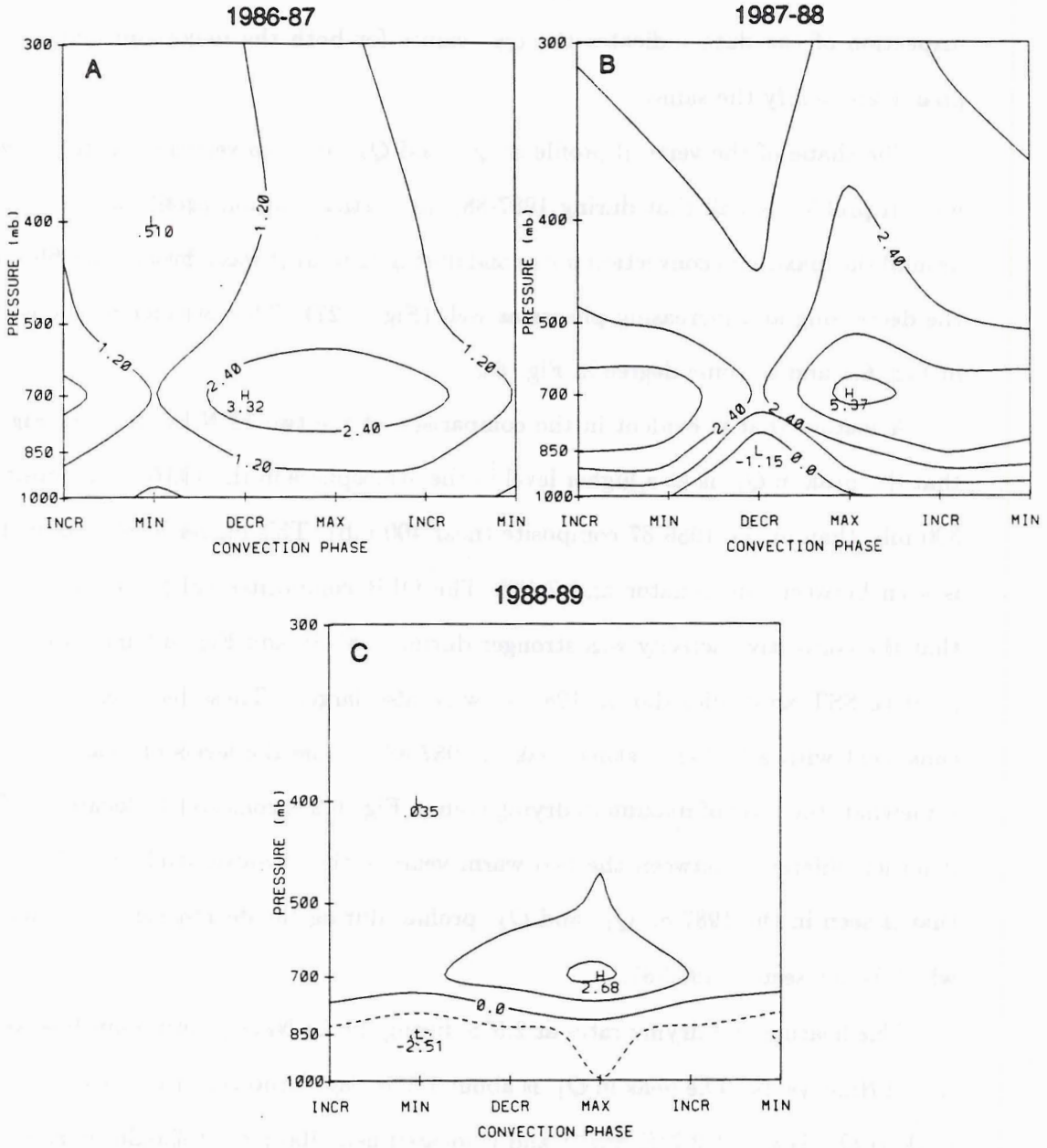

Figure 6.2: Pressure-convective phase of Q_2 averaged from 140°E to 180° at 2.5°S for a.) 1986-87, b.) 1987-88 and c.) 1988-89 in units of °K day^{-1}. The solid lines indicate the apparent moisture sink and the dashed lines indicate the apparent moisture source. The contour interval is 1.2°K day^{-1}

during the maximum convection phase. In all three years the maximum Q_1 occurs during this phase and the maximum Q_2 occurs during the maximum convection phase in 1987-88 and 1988-89. The maximum Q_2 in 1986-87 occurs during the decreasing phase, but inspection of the data indicates the Q_2 values for both the maximum and decreasing phases are nearly the same.

The shape of the vertical profile of Q_1 and Q_2 are also very similar to the vertical motion profile. Recall that during 1987-88, the vertical motion profile was concentrated around the maximum convection phase and during 1986-87 it was a broader profile covering the decreasing and increasing phases as well (Fig. 5.27). This broader profile is evident in Fig. 6.1 and to some degree in Fig. 6.2.

A feature that is evident in the comparison of the two El Niño years in Fig. 6.1 is that the peak in Q_1 is at a higher level in the atmosphere in the 1987-88 composite (near 300 mb) than in the 1986-87 composite (near 400 mb). This higher level peak in 1987-88 is seen between the equator and 7.5°S. The OLR composites (Figs. 4.2-4.4) indicated that the convective activity was stronger during 1987-88 and Fig. 4.1 indicated that the positive SST anomalies during 1987-88 were also larger. These features are physically consistent with a higher heating peak in 1987-88. While the levels of peak heating vary somewhat, the level of maximum drying seen in Fig. 6.2 is consistently located at 700 mb. Another difference between the two warm years is the low-level cooling and moistening that is seen in the 1987-88 Q_1 and Q_2 profiles during the decreasing convection phase, which is not seen in 1986-87.

The heating and drying rates at 2.5°S during the La Niña year are much weaker than the El Niño years. The peak in Q_1 is about 1.5°K day^{-1} and is located near 500 mb. The peak in Q_2 is about 2.7°K day^{-1} and is located near 700 mb. It should be kept in mind that the core of the convection is centered near 10.0°S during 1988-89, so the magnitude of heating and drying rates at 2.5°S are not representative of the deep convection in this year. However, as will be seen later, the level of maximum heating and drying is typical of the La Niña year. The La Niña year also shows moistening below 850 mb during all phases of the MJO. The cause of this low-level moistening cannot be determined from

the data, but since there is heating aloft, it is speculated that its origin is mainly the evaporation of precipitation.

Luo and Yanai (1984) pointed out that profiles of Q_1 and Q_2 will be similar if the heating and drying resulted from non-convective precipitation and the profiles will be different if the heating resulted from cumulus convection (provided Q_R is small). The deep cumulus convection and the associated strong vertical convergence of the vertical eddy transport of sensible heat in the upper-levels leads to the peak of Q_1 in the upper-levels. If the eddy vertical motions are stronger, the separation of the maxima in Q_1 and Q_2 will be greater. That is, stronger convection will result in stronger fluxes of sensible heat and larger vertical flux divergences ($\frac{\partial \overline{s'\omega'}}{\partial p}$ term in Eq. (2.1)) at higher levels, thereby leading to a higher level peak of Q_1 . The separation between the peaks of Q_1 and Q_2 is evident in Fig. 6.3, which shows vertical profiles of Q_1 (curve A) and Q_2 (curve B) for the maximum convection phase of the MJO at 2.5°S averaged between 140°E and 180°. In comparing the two El Niño years, we see that the peaks in Q_1 and Q_2 during 1986-87 are at 400 mb and 700 mb, respectively and during 1987-88 they are at 300 mb and 700 mb, respectively.

The profiles for the La Niña year show much less vertical separation with the Q_1 maximum at 500 mb and the Q_2 maximum at 700 mb. This indicates that either the convection is weaker and/or there is more low-level stratiform cloudiness in the cold year. The low-level cooling and moistening during 1988-89 is indicative of stratiform precipitation, although the heating and drying peaks aloft are at a lower level than are commonly observed (eg. Johnson and Young 1983). Precise inferences reguarding the nature of convection are difficult since the heating and drying are obviously closely dependent on the schemes for representing convective and non-convective precipitation in the model. The ECMWF model uses a modified Kuo scheme to parameterize penetrative cumulus convection and the shallow non-precipitating cumulus are parameterized using a quasi-equilibrium state between the moistening and cooling within the turbulent mixed boundary layer balancing the warming and drying due to large scale subsidence (Tiedtke *et al.* 1988).

Many authors have shown the vertical profile of Q_2 to have a double maxima. The mechanism for the double peak in Q_2 remains unresolved. Johnson (1984) and Esbensen

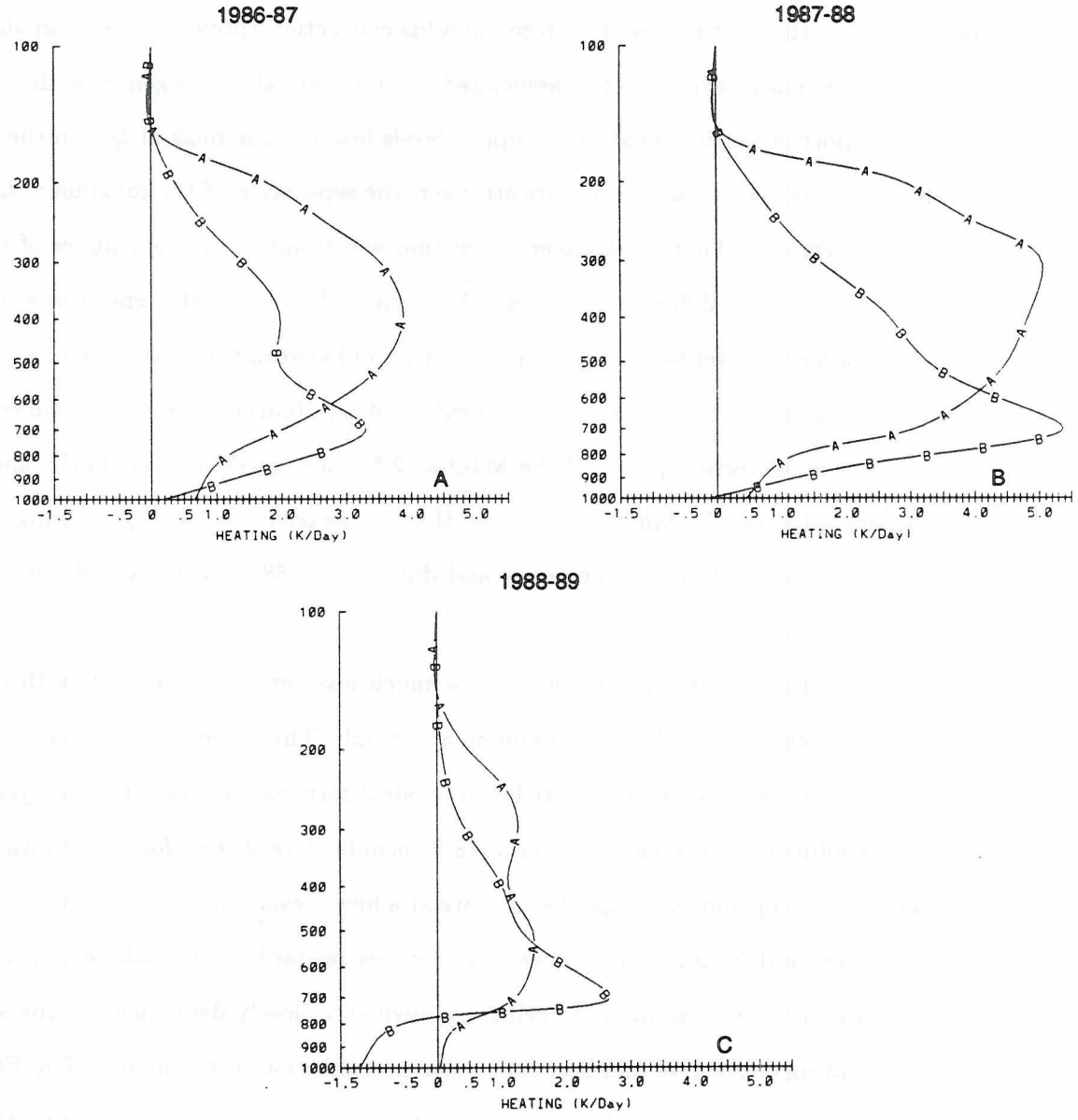

Figure 6.3: Vertical profile of Q_1 (curve A) and Q_2 (curve B) for the maximum convective phase of the MJO averaged from 140°E to 180° at 2.5°S for a.) 1986-87, b.) 1987-88 and c.) 1988-89 in units of °K day^{-1}.

et al. (1988) argue that the coexistence of convective towers and stratiform clouds lead to moistening in the lower- and upper-levels, respectively, thereby giving a double peak in Q_2 . However, Dudhia and Moncrieff (1987) and Lafore *et al.* (1988) suggest that double peak appears as a result of the vertical eddy flux convergence of moisture in the convective towers. Figure 6.3 indicates this double peak structure is most apparent during 1986-87.

If we now look at the vertical profile of the heating rates at 7.5°S shown in Figs. 6.4 and 6.5, we see the Q_1 profiles in the two El Niño years look very similar to the profiles at 2.5°S, although the magnitudes are slightly larger. The Q_2 profiles, on the other hand, are much different. The maxima occur lower in the atmosphere (850 mb) and in 1986-87 the peak occurs during the increasing convection phase. The reason for the shift to this phase is not clear, but it is also seen at 10.0°S (not shown). As with Q_1 , the magnitudes of Q_2 are larger at this latitude.

The La Niña year is also quite different at 7.5°S. The peak in Q_1 has more than doubled in magnitude and has shifted to a higher level in the atmosphere (near 400 mb). This shift to a higher level peak is possibly due to the fact that the core of the convection during 1988-89 is centered nearer 7.5°S, but examination of east-west cross-sections of Q_1 (Fig. 6.9) indicates it is most likely due to the inclusion of the high level heating peak associated with terrain-induced convection near Papua New Guinea. The east-west cross-section of ω averaged between the equator and 10.0°S (not shown) also indicates a maximum near 400 mb near Papua New Guinea. The Q_2 profile also reflects a large change. The maximum in Q_2 occurs at the same level (700 mb), but occurs during the increasing and maximum convection phases. The plot indicates the maximum occurs during the increasing phase, but inspection of the data shows the values during the maximum phase are nearly the same. Another noticeable difference is the larger vertical extent of the drying and less low-level moistening at 7.5°S. This is indicative of the stronger convective activity and/or less stratiform clouds.

McBride and Frank (1991) give a good summary of the Q_1 and Q_2 profiles produced from various composite data sets in tropical regions around the world (their Fig. 5). They show the Pacific cloud clusters have a maximum heating rate between 300-400 mb and

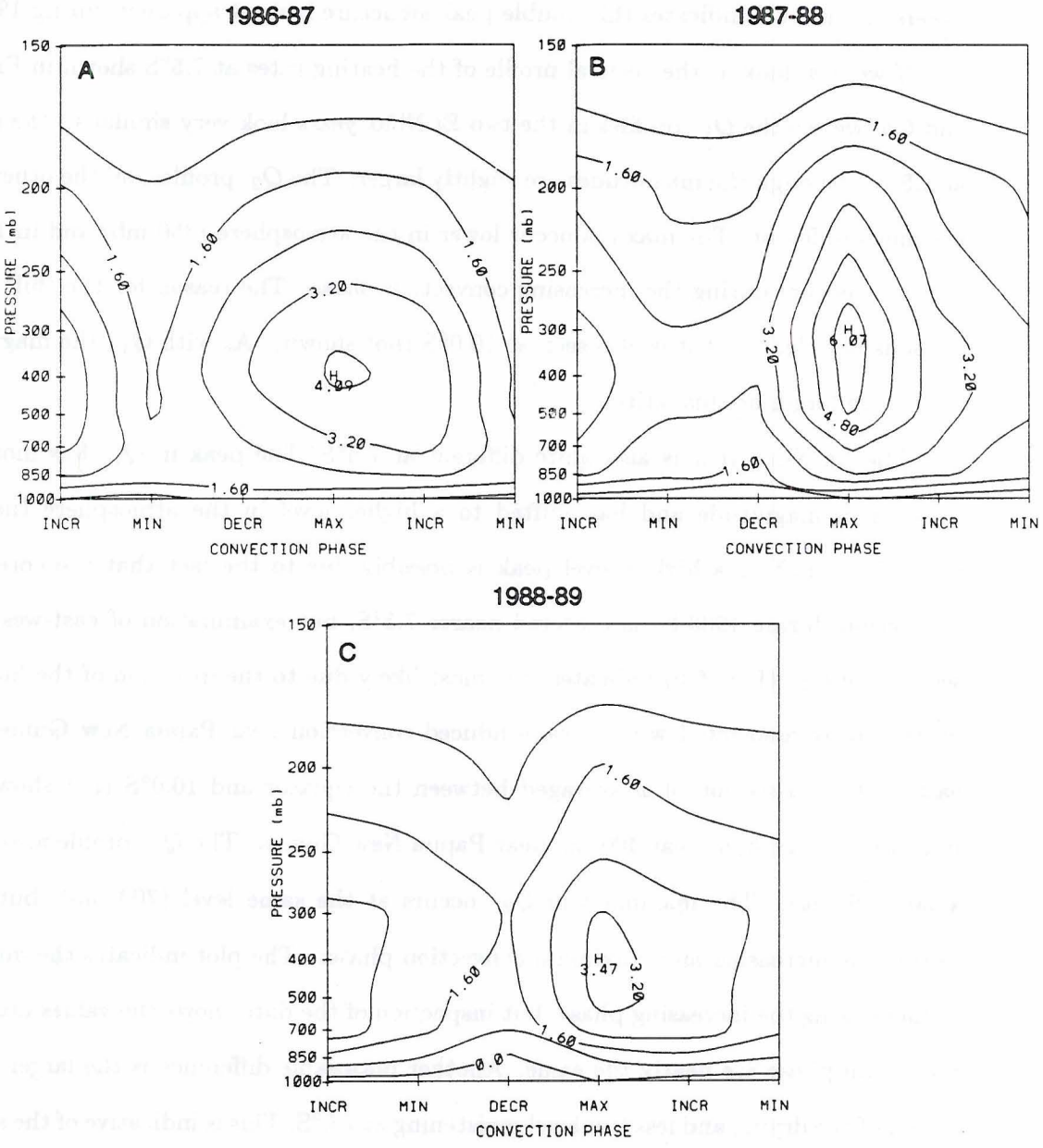

Figure 6.4: Same as Fig. 6.1, except at 7.5°S.

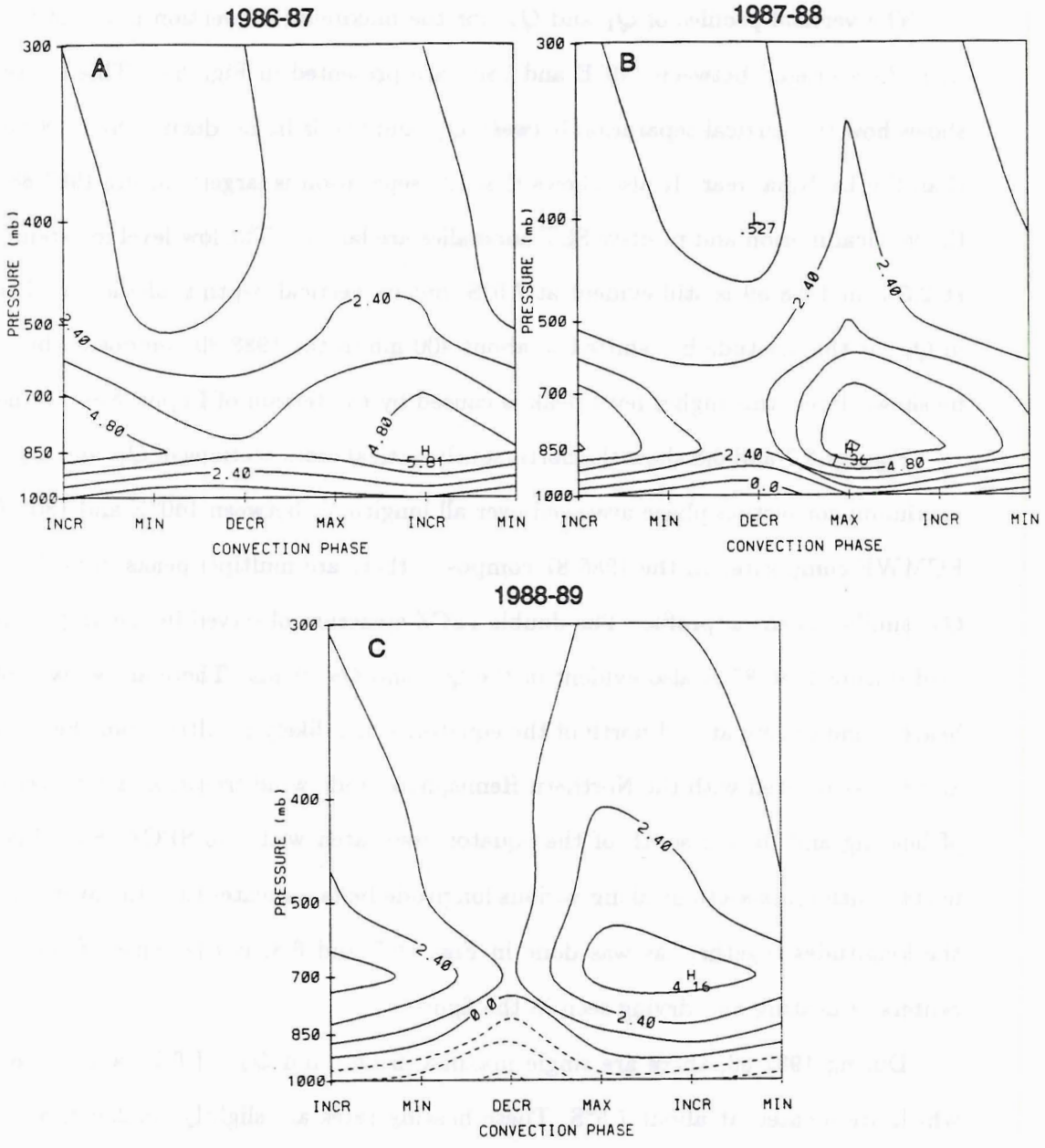

Figure 6.5: Same as Fig. 6.2, except at 7.5°S.

the western Atlantic cloud clusters have a maximum heating rate at about 400 mb. The results shown here are in good agreement with these levels of peak heating. McBride and Frank also show the Atlantic ITCZ during GATE had a maximum heating just below the 500 mb level.

The vertical profiles of Q_1 and Q_2 for the maximum convection phase of the MJO at 7.5°S averaged between 140°E and 180° are presented in Fig. 6.6. This figure again shows how the vertical separation between Q_1 and Q_2 is larger during the El Niño years than the La Niña year. It also shows that the separation is largest during 1987-88, when the vertical motion and positive SST anomalies are largest. The low-level moistening seen at 2.5°S in 1988-89 is still evident at 7.5°S, but its vertical depth is shallower. The peak in Q_1 at this latitude has shifted to about 400 mb in the 1988-89 composite, but as will be shown later, this higher level peak is caused by the terrain of Papua New Guinea.

Figures 6.7 and 6.8 show the north-south vertical cross-sections of Q_1 and Q_2 for the maximum convection phase averaged over all longitudes between 140°E and 180° for the ECMWF composite. In the 1986-87 composite there are multiple peaks in both Q_1 and Q_2 similar to the ω profile. The double ITCZ structure observed in the vertical motion field during 1986-87 is also evident in the Q_1 and Q_2 fields. There are weak centers of heating and drying at and north of the equator, which likely resulted from the convective activity associated with the Northern Hemisphere trade-wind trough and stronger centers of heating and drying south of the equator associated with the SPCZ. Examination of north-south cross-sections along various longitude belts indicates that the averaging of all the longitudes together, as was done in Figs. 6.7 and 6.8, is the cause of the multiple centers of heating and drying seen in the figures.

During 1987-88, there are single maxima in Q_1 and Q_2 of 6.1° and 7.4°K day^{-1} which are located at about 7.5°S. These heating rates are slightly smaller than the two mentioned in the 1986-87 results. However, the peak in Q_1 is at a higher level in the atmosphere.

The La Niña composite indicates that in the main convective region near 7.5°S, the peaks in the heating and drying are at comparable levels to the El Niño year, although

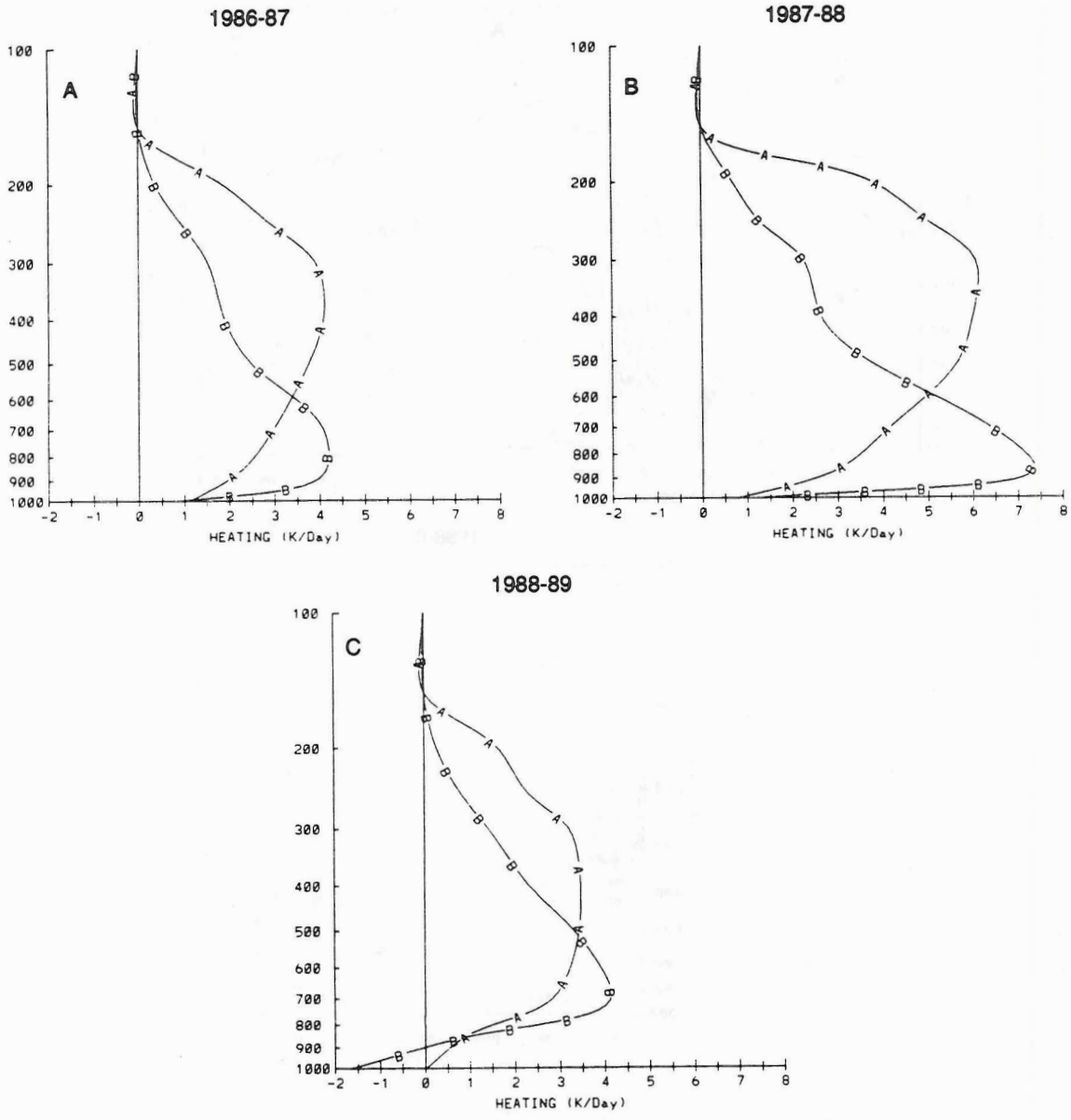

Figure 6.6: Same as Fig. 6.3, except at 7.5°S.

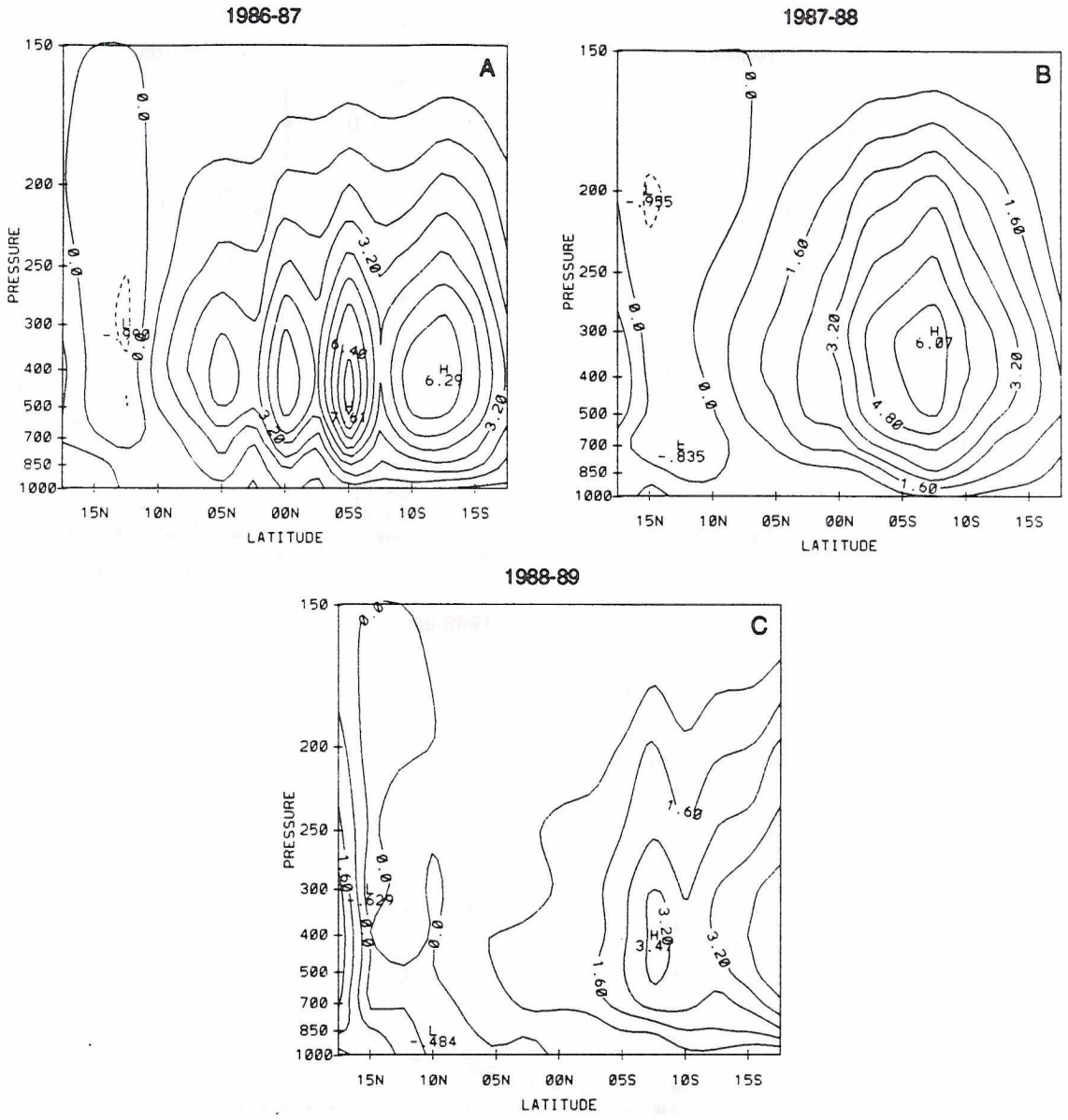

Figure 6.7: Pressure-latitude diagram of Q_1 in °K day^{-1} for the maximum convection phase of the MJO averaged between 140°E and 180° using the ECMWF data set for a.) 1986-87, b.) 1987-88 and c.) 1988-89. Solid lines indicate an apparent heat source and dashed lines indicate an apparent heat sink. The contour interval is 0.8°K day^{-1}.

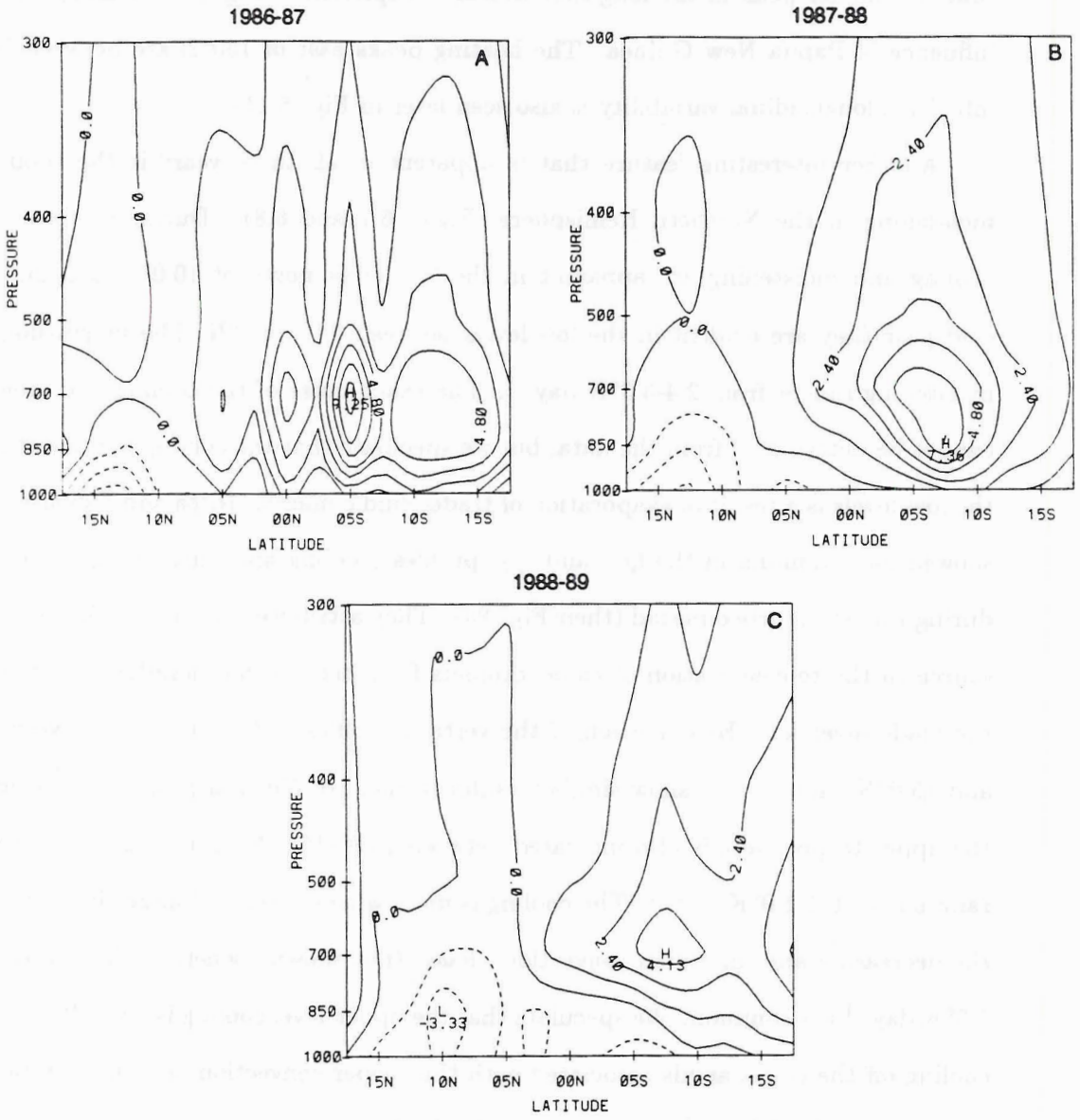

Figure 6.8: Pressure-latitude diagram of Q_2 in °K day^{-1} for the maximum convection phase of the MJO averaged between 140°E and 180° using the ECMWF data set for A.) 1986-87, b.) 1987-88 and c.) 1988-89. Solid lines indicate an apparent moisture sink and dashed lines indicate an apparent moisture source. The contour interval is 1.2°K day^{-1}.

the magnitudes are about half that of the warm years. Recall that the vertical motions in the cold years were also weaker. However, the east-west profiles of Q_1 (Fig.6.9) indicate that this higher peak in the longitude-averaged depiction of Fig. 6.7c is likely due to the influence of Papua New Guinea. The heating peaks east of 150°E are between 500-700 mb (This longitudinal variability is also seen later in Fig. 6.11).

Another interesting feature that is apparent in all three years is the cooling and moistening in the Northern Hemisphere (Figs. 6.7 and 6.8). During the warm years cooling and moistening are apparent in the low-levels north of 10.0°N and during the cold year they are evident in the low-levels between 5.0°-15.0°N. The magnitude of the moistening ranges from 2.4-3.3°K day^{-1}. The exact cause of the cooling and moistening cannot be determined from the data, but we speculate that the cooling and moistening in the low-levels is a result of evaporation of trade-wind cumulus. Nitta and Esbensen (1974) showed local minima in the Q_1 and Q_2 profiles (cooling and moistening) near 800 mb during the undisturbed period (their Fig. 8a). They attributed the heat sink and moisture source to the re-evaporation of cloud droplets from trade-wind cumulus near the top of the trade inversion. Examination of the vertical profiles of Q_1 and Q_2 between 10.0°N and 15.0°N (not shown) show similar results to those of Nitta and Esbensen. Cooling in the upper troposphere is also indicated between 10.0°-15.0°N. The magnitude of cooling ranges from 0.5-1.0°K day^{-1}. The cooling is more wide spread and larger in magnitude in the decreasing and minimum convection phases (not shown), where cooling rates of over 1.5°K day^{-1} are common. We speculate that the upper-level cooling is a result of longwave cooling off the cirrus anvils associated with the deeper convection as well as tropospheric losses in the cloud-free regions. The magnitude of cooling is consistent with the mean net radiative cooling rate of about 1.6°K day^{-1} in the upper troposphere between 10.0°-20.0°N presented by Dopplick (1972).

Comparison of Figs. 6.7 and 6.8 and Fig. 5.29 again shows how the vertical motion profile is instrumental in the Q_1 and Q_2 profiles. One feature that we are unable to explain is why the peaks in Q_1 and Q_2 are displaced south of the peaks in the vertical motion fields during the El Niño years and not during the La Niña year.

The pressure versus longitude diagrams averaged from the equator to 10.0°S show multiple centers of heating and drying and that the level at which the maxima in Q_1 and Q_2 occur is more consistent across the domain during 1987-88 than either of the other two years (Figs. 6.9 and 6.10). We chose to only show the maximum convection phase again. The figures show that the two warm years are similar in that the centers of maximum Q_1 and Q_2 are between 160°E and 180°. In 1987-88 these multiple centers of maximum Q_1 and Q_2 are of similar magnitude and occur between 300-400 mb and at 700 mb, respectively. In 1986-87, however, the largest Q_1 heating rate (10.4°K day^{-1}) is seen at 500 mb near 160°E and the largest Q_2 drying rate (13.4°K day^{-1}) is seen at 850 mb, also near 160°E. There are also weaker regions of heating and drying that are at higher levels (400 mb and 700 mb, respectively) at other longitudes. Thus, when all the longitudes are averaged together, as was done in Figs. 6.7 and 6.8, the larger peaks lower in the atmosphere have the effect of lowering the zonally averaged levels of peak heating.

The cold year is very different. The largest heating and drying occur between 140°E and 150°E. At this longitude, the terrain-induced convection around Papua New Guinea is believed to be the major cause of the persistent high level peaks of Q_1 and Q_2 (400 mb and 700 mb, respectively). The centers farther to the east are quite weak and, in the case of Q_1, much lower in the troposphere. A comparison of the El Niño years and the La Niña year indicates that, over the open ocean away from the influence of land, the heating rates are largest and at higher levels in the atmosphere when the SST anomalies (Fig. 3.1) are positive (during warm events). The higher level heating peaks in the El Niño years is an indication that the convective activity was stronger during the warm years and/or that there was a larger fraction of upper tropospheric stratiform precipitation (eg. Houze 1982; Johnson 1984).

Though not shown, the minimum convection phase does warrant some discussion. In all three years, most of the centers of maximum Q_1 are lower in the atmosphere during this phase than during the maximum convective phase. The major exception to this trend occurs in 1988-89 between 140°E and 150°E. The terrain of Papua New Guinea is again believed to be the cause of a persistent large heating peak between 300-400 mb that occurs

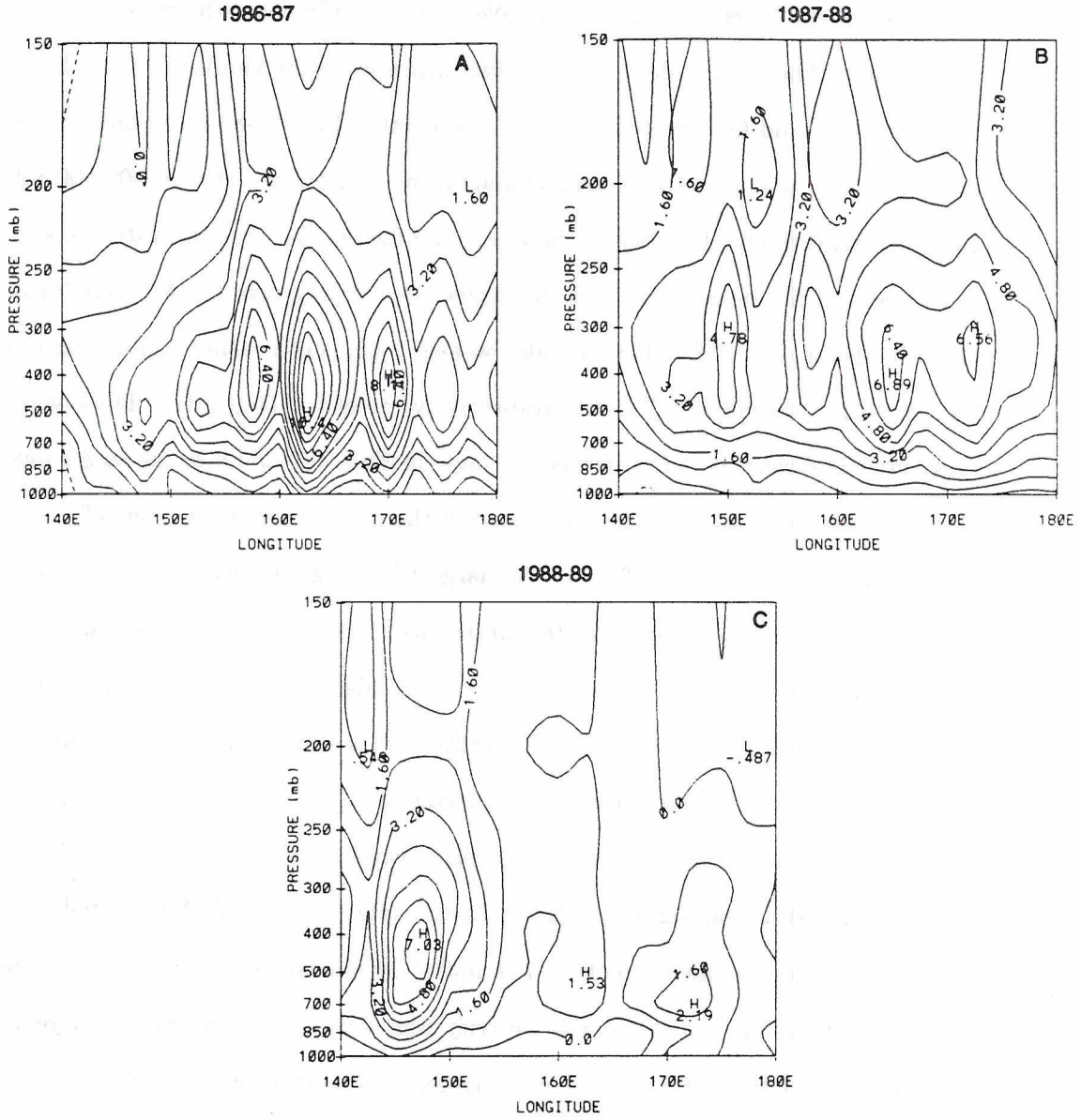

Figure 6.9: Pressure- longitude diagram of Q_1 in °K day^{-1} for the maximum convection phase of the MJO averaged between the equator and 10.0°S using the ECMWF data set for a.) 1986-87, b.) 1987-88 and c.) 1988-89. Solid lines indicate an apparent heat source and dashed lines indicate an apparent heat sink. The contour interval is 0.8°K day^{-1}.

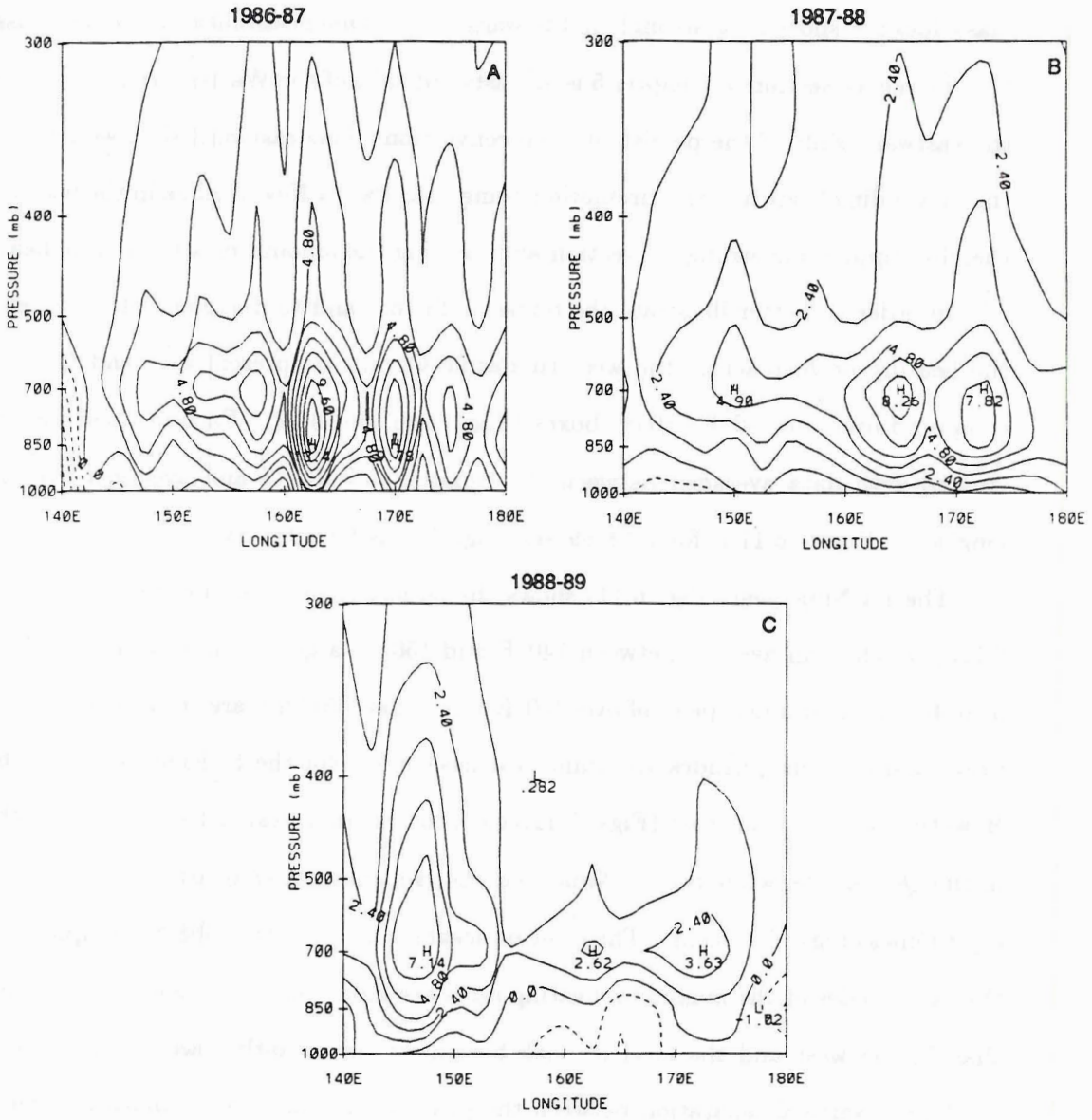

Figure 6.10: Pressure-longitude diagram of Q_2 in °K day^{-1} for the maximum convection phase of the MJO averaged between the equator and 10.0°S using the ECMWF data set for a.) 1986-87, b.) 1987-88 and c.). 1988-89. Solid lines indicate an apparent moisture sink and dashed lines indicate an apparent moisture source. The contour interval is 1.2°K day^{-1}.

during all four MJO phases in 1988-89. The terrain influence does not appear as large in the El Niño years. In fact, the centers of the largest Q_1 are well to the east of Papua New Guinea. It is not clear why a strong heating peak associated with this mountainous land mass does not show up as strongly in the warm years. One possibility that was discussed in the divergence section of Chapter 5 is an eastward shift of the Walker circulation following the eastward shift of the persistent deep convection. This eastward shift would result in the descending branch of the circulation being near Papua New Guinea in the warm years, thereby suppressing strong convection and limiting the amount of atmospheric heating.

In order to better illustrate the terrain influence and to document the differences in the heating profiles across the western Pacific Ocean, we present Q_1 and Q_2 profiles computed over four $10.0° \times 10.0°$ boxes (Figs. 6.11 and 6.12). Each of these figures was created with data averaged between the equator and 10.0°S and averaged over 10° of longitude. Figure 6.11 is for 1988-89 and Fig. 6.12 is for 1987-88.

The La Niña year (Fig. 6.11) shows the largest changes across the domain. In Fig. 6.11a, which is an average between 140°E and 150°E, a Q_1 peak of nearly 6.0°K day^{-1} near 400 mb and a Q_2 peak of over 6.0°K day^{-1} near 700 mb are seen. The levels of the peaks and their magnitudes are similar to those shown for the El Niño year (Fig. 6.12a). However, farther to the east (Figs. 6.12b,c,d), the El Niño year shows only minor changes in the Q_2 profile, while the La Niña year shows significant changes in both the Q_1 and Q_2 profiles (Figs. 6.11b,c,d). The most noticeable change in the 1988-89 composite is that the magnitudes of the maximum heating rates are much smaller in the eastern longitudes than in the west and the level of peak heating is significantly lower in the east. As a result, the vertical separation between the peaks of Q_1 and Q_2 is much smaller in the east than in the west. In contrast, the 1987-88 composite shows the magnitudes are larger in the east, the level of the maxima in Q_1 remains between 300-400 mb and the level of the maxima in Q_2 lowers from 700 mb to 850 mb. An explanation for the lowering of the Q_2 peak in the 1987-88 composite (it also occurs in the 1986-87 composite) is not clear. However, the large west-to-east changes seen in the 1988-89 composite are likely due to the affects of Papua New Guinea and the Solomon Islands. The convection near

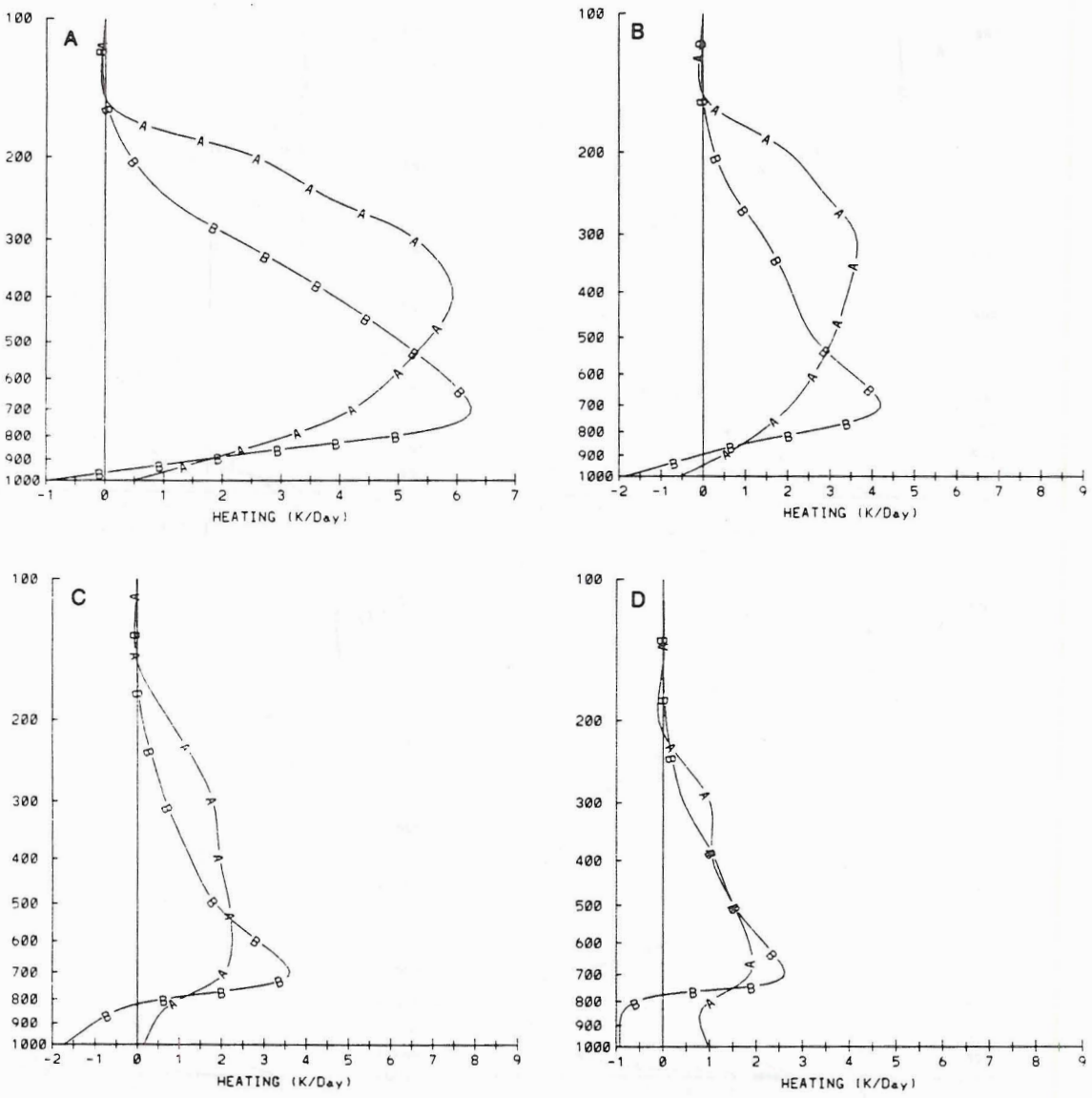

Figure 6.11: Vertical profiles of Q_1 and Q_2 during the maximum convection phase averaged from the equator to 10.0°S for 1988-89 averaged between a.) 140-150°E, b.) 150-160°E, c.) 160-170°E and d.) 170-180°E.

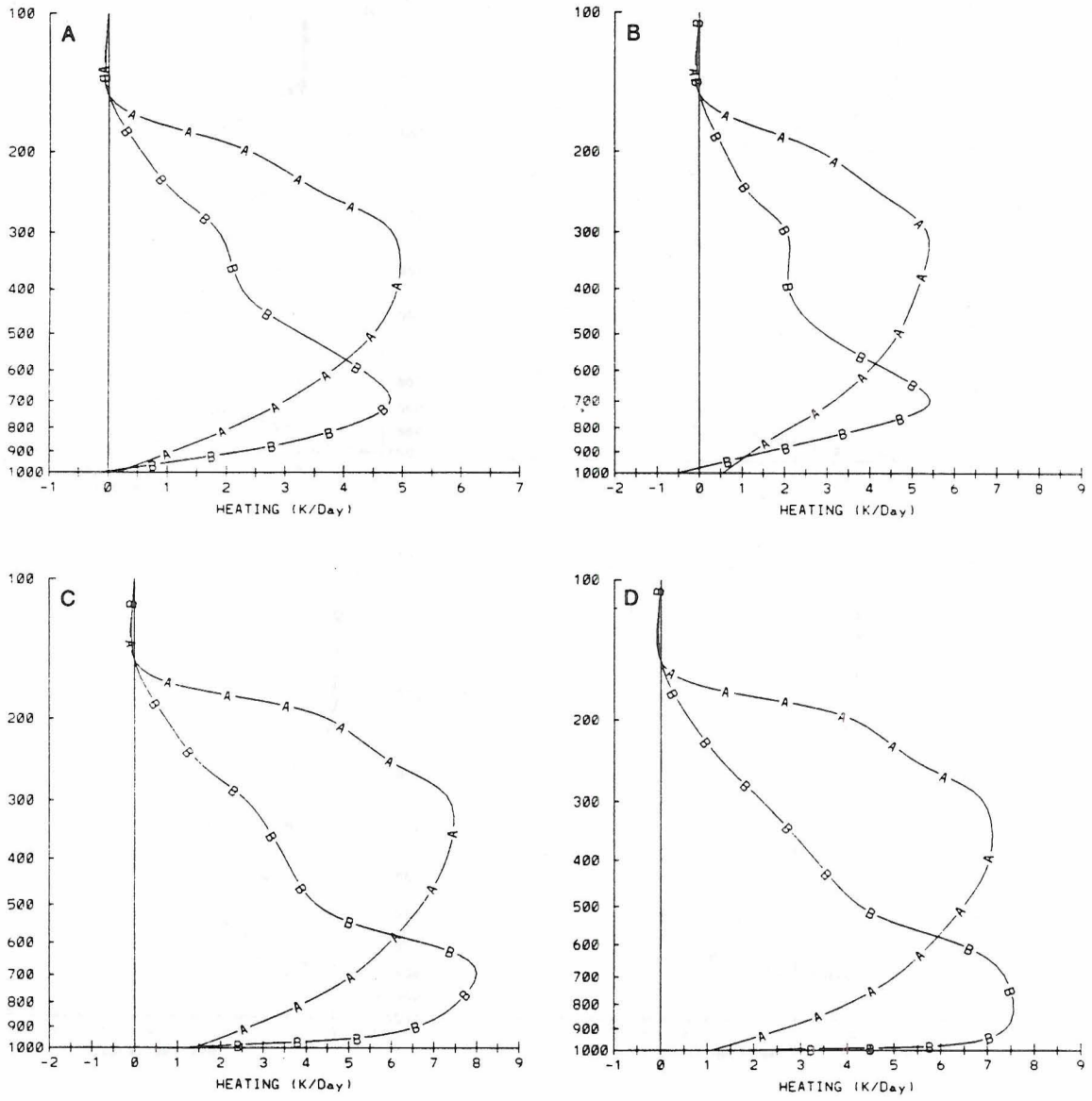

Figure 6.12: Same as Fig.6.11, except for 1987-88.

these land masses appears to be quite different than the convection over the open ocean and these differences are being captured in the heating profiles shown in Figs. 6.11a-d.

To summarize this chapter, we found that the centers of maximum heating and drying occurred during the maximum convection phase of the MJO. The vertical profiles of Q_1 and Q_2 were found to be very similar to the vertical motion profiles found in the previous chapter. The double ITCZ structure was evident in 1986-87 as multiple centers of heating and drying on both sides of the equator.

The El Niño years showed large peaks in Q_1 and Q_2 between 300-400 mb and 700-850 mb, respectively. The east-west cross-sections during the warm years showed the magnitude and level of the peak in heating and drying was not influenced by the high terrain of Papua New Guinea in the western portion of the domain.

During the maximum convective phase of the MJO, the level of maximum Q_1 occurred at a higher level and was more uniformly distributed longitudinally across the domain in the 1987-88 composite than the other two years, a trend that was also seen in the vertical motion field. This was attributed to more intense convection and/or more upper-level stratiform precipitation in 1987-88, possibly due to larger positive SST anomalies.

By examining the divergence fields, we suggest that the lack of a large upper-level peak in heating near Papua New Guinea during the El Niño years was due to an eastward shift of the Walker circulation. This shift resulted in the descending branch of the circulation being between 140°-150°E, thereby suppressing the deep convection.

The cold year was characterized as having much weaker Q_1 and Q_2 profiles, with the centers of the largest heating and drying rates occurring near Papua New Guinea. The level of the peak heating near Papua New Guinea was comparable to the levels found in the warm years (between 300-400 mb), but over the open ocean to the east, the heating peaked at a much lower level (between 500-700 mb). This is an important finding because, as was presented in Chapter 1, the speed of the MJO wave in model simulations was found to be very sensitive to the level of maximum heating. The wave speed in the model simulations of the MJO were found to be too fast with heating peaks in the upper troposphere, yet the observations in this and many other studies indicate that the heating peak does occur

in the upper troposphere. This suggests that the models used to simulate the MJO may not be accurately representing the oscillation even though the modeled kinematic fields are realistic.

The classical double peak in the vertical profile of Q_2 was somewhat evident in the composite, but was not as pronounced as that observed in rawinsonde-based studies. A large low-level peak occurred between 700-850 mb and much smaller upper-level peak occurred between 300-400 mb.

Finally, cooling in both the upper and lower troposphere and moistening in the lower troposphere north of 10.0°N were shown. The low-level cooling and moistening were attributed to re-evaporation of trade-wind cumulus cloud drops and the upper-level cooling was believed to be due to radiational cooling off cirrus anvils combined with tropospheric radiative losses.

Overall, the results presented in this chapter are quite similar to those found in heat and moisture budgets computed with tropical western Pacific data by many previous authors. This in itself is an interesting finding because it shows that reliable results can be acquired from budget studies of large-scale phenomena using coarse resolution model analysis data. Even some local effects, such as the influence of Papua New Guinea, can be isolated.

Chapter 7

SUMMARY

This study has been directed at an examination of the structure and properties of the Madden-Julian Oscillation (MJO) in the western Pacific Ocean. To construct a composite of the MJO, outgoing longwave radiation (OLR) data were analyzed in a longitude versus time format. These Hovmöller diagrams showed a west-to-east progression in the OLR from the eastern Indian Ocean to the central Pacific Ocean. The axes of minimum (maximum) OLR were used infer the location of the axes of maximum (minimum) convective activity. With these axes identified, the regions between them were divided into four equal sections and then grouped into four convective phases of the MJO. The days corresponding to each phase were then used as the basis for compositing European Center for Medium Range Weather Forecasts (ECMWF) and National Meteorological Center (NMC) model analysis data. Various kinematic and thermodynamic variables, including component winds, vertical motion and temperatures anomalies, were examined in the composite, which encompassed the period of November through February for 1986-89. Finally, heat and moisture budget analyses were conducted and compared to other budget studies.

Sea surface temperature analyses indicated that during the period of this study, both 1986-87 and 1987-88 had positive anomalies in Niño-4 (defined by the Climate Analysis Center (CAC) as the region between 5.0°N-5.0°S and 160.0°E-150.0°W) and 1988-89 had negative anomalies of nearly the same magnitude (see Fig. 3.1). We, therefore, refer to the former two years as El Niño years and the latter as a La Niña year. Emphasis was placed on comparisons between the composites during the warm events and the cold event.

The OLR analyses confirmed the results of many previous authors. An eastward propagating disturbance with a period similar to the MJO (30-60 days) was clearly evident

in the Hovmöller diagrams. We found that the MJO signal in the OLR consistently began near 90°E in all three years and propagated across the eastern Indian and western Pacific Oceans. The longitudinal extent of the propagation and the propagation speeds found were consistent with those found by Knutson and Wieckmann (1987) and Wieckmann and Khalsa (1990).

The OLR data were subjected to the composite and proved to be consistent with other studies as well. A very distinct difference in the location and intensity of the the deep convection (OLR used as a proxy) was found between the warm years and the cold year. During the warm years the convection was centered between 2.5°S and 5.0°S and was quite vigorous. During the cold year it was located between 10.0°S and 15.0°S and was noticeably weaker. This is consistent with the findings of Liebmann and Hartmann (1982) and Deser and Wallace (1990).

The MJO signal was found to be very strong in the zonal winds for both the ECMWF and NMC composites. One of the most significant results was that the maximum westerly winds (westerly wind bursts) occurred during the decreasing convection phase or, if viewed spatially, to the west of the trough in the MJO wave. This is consistent with the schematic depiction of the MJO presented by Lau *et al.* (1989) (Fig. 1.2). The orientation of maximum lower tropospheric westerly winds were nearly identical to the orientation of the maximum convective activity on the composited OLR diagrams. The north-south vertical cross-sections showed the migration of the low-level westerly winds away from the equator from 1986-87 through 1988-89 and, as was found in the initial investigations of Madden and Julian (1971), there was a phase reversal with height. That is, there were upper-level easterlies over low-level westerlies and vice versa. The east-west vertical cross-sections showed the upper-level easterlies (also seen in the schematic by Lau *et al.* 1989) tended to vary with the changes in convective activity associated with the MJO. The intensity and areal coverage increased and reached a maximum during the maximum and decreasing convection phases.

The meridional wind composites showed variability mainly in the upper troposphere. Comparison of the two El Niño years and the La Niña year in north-south cross-sections

indicated a phase reversal in the upper-level winds. The warm years had southerly winds north of the equator and northerlies south of the equator at 200 mb, while the cold year had just the opposite. This indicated that the divergent (convergent) pattern associated with the ascending (descending) branch of the mean Hadley circulation and the southward shift of the circulation in 1988-89 was captured in the composite.

In general, there was good agreement between the composites based on the ECMWF and the NMC model analyzed data for both components of the wind discussed above. However, the divergence and vertical motion composites showed some significant differences.

A good comparison of the vertical motion fields between the two models was not possible since ω was available in the NCAR archives of the ECMWF data and not in the NMC data. The vertical motion had to be calculated based on the derived divergence. However, differences seen in the divergence fields indicate how small differences in the analysis of the horizontal winds can be amplified in calculations based on derivatives of these fields.

The horizontal divergence computed from the winds in each model provided evidence of the differences between the two models. Although the maximum upper-level divergence occurred during the maximum convection phase in both models, the magnitude calculated using the NMC data is about half as large as that calculated using the ECMWF data. Both models also showed peaks in the low-level convergence during the increasing and maximum convection phases, indicating that the convergence was important in the initiation and maintenance of convection associated with the MJO. A westward shift of the upper-level divergence associated with the Walker circulation from 170°E in the 1986-87 composite to 145°E in the 1988-89 composite was observed in the east-west vertical cross-sections. The location and westward shift of this large-scale circulation feature was later used to explain some of the zonal variations of atmospheric heating between the El Niño years and the La Niña year.

As was mentioned previously, the vertical motion composite based on the NMC data was very different than the ECMWF composite. The shift of the core of the vertical motion

from just south of the equator in 1986-87 to near 15.0°S in 1988-89 was not evident in the NMC composite. Also evident were differences in the magnitudes of the vertical motion. The ECMWF composite showed the vertical motion to be as much as twice as large as in the NMC composite. Also, the ECMWF composite indicated larger inter-annual modulation of the vertical motion with the warm years being as much as twice as large as the cold years, but in the NMC composite the magnitudes were nearly the same in all three years. The NMC composte is clearly inconsistent with the OLR composite.

The maximum vertical velocity was found to occur during the maximum convection phase of the MJO. The level of maximum vertical velocity was found to be consistent in both composites. During the warm years the peaks were near 300 mb and during the cold year the peak was near 500 mb. This indicated that the convection during the warm years was more vigorous, which is again consistent with the results of Deser and Wallace (1990). Comparison of the two warm years in the pressure versus phase diagrams indicated that the vertical motion profile had a narrow appearance during 1987-88 and was much broader during 1986-87. This suggested that there was much more modulation in the convective activity with the phase of the MJO in 1987-88 than in 1986-87. The core of the vertical motion in the former appeared more vigorous, but confined to the maximum convection phase, while in the latter the core is slightly weaker, but was evident over the increasing and decreasing phases.

The surface pressure anomalies were shown to be consistent in both composites and consistent with the results of Lau and Lau (1986). Near equatorial westerlies (during the decreasing convection phase) were associated with negative pressure anomalies south of the equator and near equatorial easterlies or weaker westerlies (during the increasing convection phase) were associated with positive pressure anomalies south of the equator. The negative pressure anomalies south of the equator were observed to shift farther south with the convection in 1988-89.

The temperature anomalies were weak, but had some consistency with the previous studies of Reed and Recker (1971), Reed *et al.* (1977) and Hendon and Liebmann (1990). Negative temperature anomalies in the low levels found by the previous authors associated

with evaporational cooling in the unsaturated downdrafts were also apparent in the present study. The mid-levels contained a weak warm anomaly due to latent heat release. The upper-levels were found to have negative anomalies during the maximum convection phase (near 100 mb). This is indicative of the cold overshooting tops of the deep convection, as reported by Reed *et al.* (1977).

Reed and Recker (1971) showed a front-to-rear sloping region of positive moisture anomaly in their westward-propagating wave composite. This same front-to-rear sloping region of moisture was shown in the form of positive relative humidity anomalies during the increasing (front), maximum and decreasing (rear) convection phases of the eastward-propagating MJO wave.

The heat and moisture budgets calculated in the present study are consistent with those done by previous authors. The profiles of Q_1 and Q_2 were found to resemble the vertical motion profiles very closely. The maximum heating and drying occurred during the maximum convection phase of the MJO, much like the vertical motion profile. The Q_1 and Q_2 composites during the La Niña year were much weaker than the El Niño years, a trend also observed in the ω field.

The peaks in the Q_1 profile were between 300 mb and 400 mb during the warm years and between 500 mb and 700 mb during the cold year. The convection near Papua New Guinea, however, was shown to have a higher level heating peak (near 400 mb) than the convection over the open ocean to the east (between 500-700 mb) during the La Niña year. The different levels of the heating peaks between the El Niño years and the La Niña year have some significant ramifications to the correct modeling of the MJO wave. As discussed in Chapter 1, the propagation speed of the wave simulated in atmospheric models is sensitive to the level of maximum heating. The wave speed in the model simulations were found to be too fast with heating peaks in the upper troposphere, yet the observations in this and many other studies indicate that the heating peak does occur in the upper troposphere. This suggests that the models used to simulate the MJO may not be accurately representing the oscillation even though the modeled kinematic fields are realistic. The results presented here also suggest that in order to simulate the MJO

correctly, the El Niño-Southern Oscillation (ENSO) cycle must be correctly represented in the model in order to capture subtle, but important, inter-annual variations.

The typical double peak structure in the Q_2 profile was evident in the composite, but the upper-level peak was small. A large peak between 700-850 mb and a secondary peak between 300-400 mb were observed. Yanai *et al.* (1971) showed a peak in Q_1 near 425 mb and two peaks in Q_2, one near 775 mb and another near 525. McBride and Frank (1991) showed Pacific cloud clusters had a peak heating rate between 300-400 mb and a nearly constant drying profile from 800 mb to 400 mb. They also showed the Atlantic cloud clusters had a Q_1 peak near 400 mb and a single peak in Q_2 near 700 mb.

In the Northern Hemisphere, north of 10.0°N, low-level cooling and moistening were observed. Although the exact cause could not be determined from the data, the re-evaporation of cloud drops from trade-wind cumulus was suggested as a possible explanation. Also evident in at the northern latitudes was cooling in the upper-levels. This cooling, which was maximum during the decreasing and minimum convection phases, is believed to be a reflection of the radiational cooling from the tops of cirrus anvils.

As with most studies in the tropics, this study has numerous limitations. The first and most common to most tropical studies is the spatial and temporal resolution of the data. With the exception of the intensive observing periods that take place in most field experiments, most studies suffer from poor data resolution, especially when budgets are attempted.

This study has the additional limitation of being based entirely on model assimilated data. Even though the assimilation systems used in the models have been continuously improved, the amount of data going into the model has remained rather low, especially in the tropical latitudes. The changes in the model assimilation procedure also create limitations themselves. It is difficult to compare one year to another if the model analysis routine has significantly changed. Also, detailed knowledge of the assimilation procedure used is absolutely necessary to compare and evaluate results from different models.

There is also the possibility of aliasing of data between phases of the MJO due to the use of OLR as a composite base and due to the subjective determination of the axes

of maximum and minimum OLR. The results might be more reliable if the OLR data were band-pass filtered to only retain those frequencies near the MJO frequencies before determining the composite days or if a combination of OLR and zonal wind or velocity potential were used as the basis for the composite.

This study was intended to be a starting point or a pilot study for the 1992-93 TOGA COARE field experiment. The data collected during the 4-month experiment is hoped to be of sufficient resolution to allow a much more detailed analysis of the structure of the MJO. The composite scheme employed in this study was used to increase the temporal resolution of the data, but the inferences made in comparing the El Niño years and the La Niña year should be substantiated using a larger data sample. The fact that the MJO is evident in each of the model analyses is a significant result in and of itself. It makes it possible to examine large volumes of model data, which has at least some basis in observations, in order better understand this atmospheric oscillation without using the large amount of resources which are typically necessary for field experiments. A similar composite analysis using many years of data re-analyzed using a constant known assimilation system would allow higher confidence in the results presented within.

Future work should concentrate on the relationships between the three prominent low-frequency oscillations in the tropical atmosphere, namely the MJO, ENSO and the QBO (Quasi-Biennial Oscillation). All three are likely inter-related in some manner that, when finally revealed, will greatly improve long range forecasting in the tropics. In addition, from my own personal experiences in forecasting tropical cyclones the western Pacific and Indian Ocean regions, I believe there are some definite relationships between the phase of the MJO and the formation of tropical cyclones. This relationship likely involves many other aspects of the tropical atmosphere, including monsoon dynamics and cold surges. However, the westerly wind bursts associated with the passage of a MJO are in all likelihood instrumental in injecting the monsoon trough with enough additional vorticity to aid the spin-up of tropical cyclones along its poleward edge.

REFERENCES

Chang, C.-P., and H. Lim, 1988: Kelvin Wave-CISK: A possible mechanism for the 30-50 day oscillations. *J. Atmos. Sci.*, **45**, 1709-1720.

Chen, T.-C., and M.-C. Yen, 1991: A study of the diabatic heating associated with the Madden-Julian Oscillation. *J. Geophys. Res.*, **96**, 13163-13177.

Climate Analysis Center, 1987-91: Climate Diagnostics Bulletin. NOAA/NWS/NMC, Camp Springs, MD.

Deser, C., and J.M. Wallace, 1990: Large scale atmospheric circulation features of warm and cold episodes in the tropical Pacific. *J. Climate*, **3**, 1254-1281.

Dopplick, T.G., 1972: Radiative heating of the global atmosphere. *J. Atmos. Sci.*, **29**, 1278-1294.

Dudhia J., and M.W. Moncrieff, 1987: A numerical simulation of quasi-stationary tropical convective bands. *Quart. J. Roy. Meteorol. Soc.*, **113**, 929-967.

Esbensen, S.K., J.-T. Wang, and E.I. Tollerud, 1988: A composite life cycle of nonsquall mesoscale convective systems over the tropical ocean. Part II: Heat and moisture budgets. *J. Atmos. Sci.*, **45**, 537-548.

Gallus, W.A., Jr., and R.H. Johnson, 1991: Heat and moisture budgets of an intense midlatitude squall line. *J. Atmos. Sci.*, **48**, 122-146.

Gamache, J.F., and R.A. Houze, Jr., 1983: Water budget of a mesoscale convective system in the tropics. *J. Atmos. Sci.*, **40**, 1835-1850.

Graham, N.E. and T.P. Barnett, 1987: Sea surface temperature, surface wind divergence, and convection over tropical oceans. *Science*, **238**, 657-659.

Gray, W.M., 1973: Cumulus convection and larger scale circulations I: Broadscale and mesoscale considerations. *Mon. Wea. Rev.*, **101**, 839-855.

Heddinghaus, T.R., and A.F. Krueger, 1981: Annual and interannual variations in outgoing longwave radiation over the tropics. *Mon. Wea. Rev.*, **109**, 1208-1218.

Hendon, H.H. and B. Liebmann, 1990: The intraseasonal (30-50 day) oscillation of the Australian summer monsoon. *J. Atmos. Sci.*, **47**, 2909-2923.

Houze, R.A., Jr., 1982: Cloud clusters and large-scale vertical vertical motions in the tropics. *J. Meteor. Soc. Japan*, **60**, 396-410.

Jenne, R., 1991: Archived NMC temperature analyses. National Center for Atmospheric Research (NCAR), Scientific Computing Division, Boulder, CO, 80307.

Johnson, R.H., 1982: Vertical motion in the near-equatorial winter monsoon convection. *J. Meteor. Soc. Japan*, **60**, 682-689.

Johnson, R.H., 1984: Partitioning tropical heat and moisture budgets into cumulus and mesoscale components: Implications for cumulus parameterization. *Mon. Wea. Rev.*, **112**, 1590-1601.

Johnson, R.H., 1986: Short-term variations of the tropopause over the winter MONEX area. *J. Atmos. Sci.*, **43**, 1152-1163.

Johnson, R.H., and G.S. Young, 1983: Heat and moisture budgets of tropical mesoscale anvil clouds. *J. Atmos. Sci.*, **40**, 2138-2147.

Joint Typhoon Warning Center (JTWC), 1986-89: Annual tropical cyclone report. U.S. Naval Oceanography Command Center, Joint Typhoon Warning Center, COMNAVMARIANAS Box 17 FPO San Francisco, 96630.

Kasahara, A., A.P. Muzzi, and U.C. Mohanty, 1987: Comparison of global diabatic heating rates from FGGE Level IIIb analyses with satellite radiation imagery data. *Mon. Wea. Rev.*, **115**, 2904-2935.

Khalsa, S.J.S., 1983: The role of sea surface temperature in large-scale air-sea interaction. *Mon. Wea. Rev.*, **111**, 954-966.

Knutson, T.R. and K.M. Weickmann, 1987: 30-60 day atmospheric oscillations: Composite life cycles of convection and circulation anomalies. *Mon. Wea. Rev.*, **115**, 1407-1436.

Lafore, J.-P., J.-L. Redelsperger, and G. Jaubert, 1988: Comparison between a three-dimensional simulation and Doppler radar data of a tropical squall line: Transports of mass, momentum, heat, and moisture. *J. Atmos. Sci.*, **45**, 3483-3500.

Lau, K.-M., and P.H. Chan, 1983: Short-term climate variability and atmospheric teleconnections from satellite-observed outgoing longwave radiation. Part I: Simultaneous relationships. *J. Atmos. Sci.*, **40**, 2735-2750.

Lau, K.-M., and P.H. Chan, 1985: Aspects of the 40-50 day oscillation during the northern winter as inferred from outgoing longwave radiation. *Mon. Wea. Rev.*, **113**, 1889-1909.

Lau, N.-C. and K.-M. Lau, 1986: The structure and propagation of intraseasonal oscillations appearing in a GFDL general circulation model. *J. Atmos. Sci.*, **43**, 2023-2047.

Lau K.-M., and H. Lim, 1984: On the dynamics of equatorial forcing of climate teleconnections. *J. Atmos. Sci.*, **41**, 161-176.

Lau K.-M., and L. Peng, 1987: Origin of low frequency (Intraseasonal) oscillations in the tropical atmosphere. Part I: Basic theory. *J. Atmos. Sci.*, **44**, 950-972.

Lau K.-M., and S. Shen, 1988: On the dynamics of intraseasonal oscillations and ENSO. *J. Atmos. Sci.*, **45**, 1781-1797.

Lau, K.-M., L. Peng, C.-H. Sui, and T. Nakazawa, 1989: Dynamics of super cloud clusters, westerly wind bursts, 30-60 day oscillations and ENSO: An unified view. *J. Meteor. Soc. Japan*, **67**, 205-219.

Liebmann, B., and D.L. Hartmann, 1982: Interannual variations of outgoing IR associated with tropical circulation changes during 1974-78. *J. Atmos. Sci.*, **39**, 1153-1162.

Lowe, P.R. and J.M. Ficke, 1974: The computation of saturation vapor pressure. Environmental Prediction Research Facility Technical Paper No. 4-74, Naval Postgraduate School, Monterey, CA, 24pp.

Luo, H. and M. Yanai, 1984: The large scale circulation and heat sources over the Tibetan Plateau and surrounding areas during the early summer of 1979. Part II: Heat and moisture budgets. *Mon. Wea. Rev.*, **112**, 966-989.

Madden, R.A., 1986: Seasonal variations of the 40-50 day oscillation in the tropics. *J. Atmos. Sci.*, **43**, 3138-3158.

Madden, R.A., and P.R. Julian, 1971: Detection of a 40-50 day oscillation in the zonal wind in the tropical Pacific. *J. Atmos. Sci.*, **28**, 702-708.

Madden, R.A., and P.R. Julian, 1972: Description of global-scale circulation cells in the tropics with a 40-50 day period. *J. Atmos. Sci.*, **29**, 1109-1123.

McBride, J.L., and W.M. Frank, 1991: Vertical profiles of cumulonimbus heating and drying in the tropics. *Preprints, 19th Conference on Hurricanes and Tropical Meteorology*, Miami, Florida, Amer. Meteor. Soc., 220-225.

Neelin, J.D., I.M. Held, and K.H. Cook, 1987: Evaporation-wind feedback and low-frequency variability in the tropical atmosphere. *J. Atmos. Sci.*, **44**, 2341-2348.

Nitta, T., S.K. Esbensen, 1974: Heat and moisture budget analyses using BOMEX data. *Mon. Wea. Rev.*, **102**, 17-28.

Numaguti, A., and Y.-Y. Hayashi, 1991: Behavior of cumulus activity and the structure of circulations in an "Aqua Planet" model. Part II: Eastward moving planetary scale structure and the Intertropical Convergence Zone. *J. Meteor. Soc. Japan*, **69**, 563-579.

Reed, R.J, and E.E. Recker 1971: Structure and properties of synoptic- scale wave disturbances in the equatorial western Pacific. *J. Atmos. Sci.*, **28**, 1117-1133.

Reed, R.J, D.C. Norquist, and E.E. Recker 1977: Structure and properties of African wave disturbances as observed during Phase III of Gate. *Mon. Wea. Rev.*, **105**, 317-333.

Sui, C.-H., and K.-M. Lau, 1989: Origin of low-frequency (Intraseasonal) oscillations in the tropical atmosphere. Part II: Structure and propagation of mobile wave CISK modes and their modifications by lower boundary forcings. *J. Atmos. Sci.*, **46**, 37-56.

Takayabu, Y.N., and M. Murakami, 1991: The structure of super cloud clusters observed in 1-20 June 1986 and their relationship to easterly waves. *J. Meteor. Soc. Japan*, **69**, 105-125.

Tiedtke, M., W.A. Heckley, and J. Slingo, 1988: Tropical forecasting at ECMWF: The influence of physical parameterization on the mean structure of forecasts and analysis. *Quart. J. Roy. Meteorol. Soc.*, **114**, 639-664.

Trenberth, K.E. and J.G. Olson, 1988: ECMWF global analysis 1979-1986: Circulation statistics and data evaluation. NCAR Technical Note, Boulder, CO, NCAR TN-300 + STR, 94 pp.

Vincent, D.G., K.H. North, R.A. Velasco, and P.G. Ramsey, 1991: Precipitation rates in the tropics based on the Q_1 -budget method: 1 June 1984-31 May 1987. *J. Climate*, **4**, 1070-1086.

Wang, B., 1988: Dynamics of tropical low-frequency waves: An analysis of the moist Kelvin Wave. *J. Atmos. Sci.*, **45**, 2051-2065.

Weickmann, K.M., and S.J.S. Khalsa, 1990: The shift of convection from the Indian Ocean to the western Pacific Ocean during the 30-60 day oscillation. *Mon. Wea. Rev.*, **118**, 964-978.

World Meteorological Organization (WMO), 1990: Scientific plan for the TOGA Coupled Ocean-Atmosphere Response Experiment (COARE). WMO/TD No. 64 Addendum. World Meteorological Organization, Geneva, Switzerland, 112pp.

Yanai, M., S.K. Esbensen, and J.-H. Chu, 1973: Determination of bulk properties of tropical cloud clusters from large-scale heat and moisture budgets. *J. Atmos. Sci.*, **30**, 611-627.

Zhang, C., 1991: Empirical relationships between OLR and SST over the tropical Pacific Ocean. *Preprints, 19th Conference on Hurricanes and Tropical Meteorology*, Miami, Florida, Amer. Meteor. Soc., 343-348.

Appendix A

COMPOSITE DAYS

As mentioned in Chapter 3, the composite is based on data from the beginning of November to the end of February for 1986-87, 1987-88 and 1988-89. Tables A.1-A.3 list the Julian days used to construct the composite at each longitude for each convective phase of the MJO.

Table A.1: Julian days used in the MJO composite for 1986-87.

Longitude	Maximum Convection	Decreasing Convection	Minimum Convection	Increasing Convection
140.0E	309-319 336-343 027-045	320-325 344-356 046-059	326-330 357-006	305-308 331-335 007-026
142.5E	313-320 337-344 028-046	321-326 345-357 047-059	327-331 358-006	305-308 332-336 007-027
145.0E	313-321 338-344 028-047	322-327 345-358 048-059	328-332 359-007	305-309 333-337 008-027
147.5E	313-322 338-345 029-047	323-328 346-358 048-059	329-332 359-008	305-310 333-337 009-028
150.0E	313-322 339-346 030-048	323-328 347-359 049-059	329-333 360-008	305-311 334-338 009-029
152.5E	313-323 339-346 031-049	324-328 347-359 050-059	329-334 360-009	305-312 335-338 010-030
155.0E	313-323 340-347 032-049	324-329 348-359 050-059	330-334 360-009	305-312 335-339 010-031
157.5E	314-324 340-347 032-049	325-329 348-360 050-059	330-335 361-010	305-313 336-339 011-031
160.0E	314-324 341-348 033-050	325-329 349-359 051-059	330-336 360-010	305-313 337-340 011-032

Table A.1 (cont): Julian days used in the MJO composite for 1986-87.

Longitude	Maximum Convection	Decreasing Convection	Minimum Convection	Increasing Convection
162.5E	315-325 341-348 034-051	326-330 349-360 052-059	331-336 361-011	305-314 337-340 012-033
165.0E	315-325 342-349 035-051	326-330 350-360 052-059	331-337 361-011	305-314 338-341 012-034
167.5E	316-326 342-349 035-052	327-331 350-360 053-059	332-337 361-012	305-315 338-341 013-034
170.0E	317-327 343-350 036-053	328-331 351-361 054-059	332-338 362-012	305-316 339-342 013-035
172.5E	318-328 343-350 037-053	329-332 351-361 054-059	333-338 362-013	305-317 339-342 013-036
175.0E	318-328 344-351 037-054	329-332 352-362 055-059	333-339 363-013	305-317 340-343 014-036
177.5E	319-329 344-351 037-054	330-333 352-362 055-059	334-340 363-014	305-318 341-343 015-036
180.0E	319-329 344-352 038-055	330-334 353-362 056-059	335-340 363-015	305-318 341-343 016-037

*Note: Due to truncation of data by NMC, the period 2-8 November of 1986 was omitted from the NMC composite for that year.

Table A.2: Julian days used in the MJO composite for 1987-88.

Longitude	Maximum Convection	Decreasing Convection	Minimum Convection	Increasing Convection
140.0E	312-319 345-356 035-047	320-324 357-006 048-060	325-332 007-020	305-311 333-344 021-034
142.5E	313-320 346-357 036-047	321-324 358-006 048-060	325-333 007-020	305-312 334-345 021-035
145.0E	314-320 346-358 037-047	321-325 359-007 048-060	326-334 008-022	305-313 335-345 023-036
147.5E	314-320 347-359 038-050	321-326 360-009 051-060	327-334 010-023	305-313 335-346 024-037
150.0E	315-321 348-360 038-051	322-326 361-010 052-060	327-335 011-023	305-314 336-347 024-037
152.5E	315-321 349-360 039-052	322-327 361-010 053-060	328-335 011-024	305-314 336-348 025-038
155.0E	315-322 349-361 040-053	323-327 362-011 054-060	328-336 012-025	305-314 337-348 026-039
157.5E	315-322 350-362 040-053	323-328 363-011 054-060	329-336 012-025	305-314 337-349 026-039
160.0E	316-322 350-362 041-054	323-328 363-012 055-060	329-337 013-026	305-315 338-349 027-040

Table A.2 (cont): Julian days used in the MJO composite for 1987-88.

Longitude	Maximum Convection	Decreasing Convection	Minimum Convection	Increasing Convection
162.5E	317-323 351-363 042-055	324-328 364-013 056-060	329-337 014-027	305-316 338-350 028-041
165.0E	317-323 351-364 042-055	324-329 365-013 056-060	330-338 014-027	305-316 339-350 028-041
167.5E	317-324 352-365 043-056	325-330 001-014 057-060	305 331-338 015-028	306-316 339-351 029-042
170.0E	317-324 353-001 044-057	325-330 002-014 058-060	305 331-339 015-029	306-316 340-352 030-043
172.7E	318-324 354-002 044-057	325-330 003-015 058-060	305-306 331-339 016-029	307-317 340-353 030-043
175.0E	318-325 355-003 045-058	326-331 004-015 059-060	305-306 332-340 016-030	307-317 341-354 031-044
177.5E	318-325 355-003 046-059	326-332 004-016 060	305-306 333-340 017-031	307-317 341-354 032-045
180.0E	319-326 356-004 047-060	327-332 005-017	305-307 333-341 018-031	308-318 342-355 032-046

Table A.3: Julian days used in the MJO composite for 1988-89.

Longitude	Maximum Convection	Decreasing Convection	Minimum Convection	Increasing Convection
140.0E	338-352 023-032 054-059	353-360 033-037	306-318 361-007 038-044	319-337 008-022 045-053
142.5E	339-353 024-033 054-059	354-360 034-038	306-319 361-007 039-045	320-338 008-023 046-053
145.0E	339-354 024-033 055-059	355-361 034-039	306-320 362-008 040-045	321-338 009-023 046-054
147.5E	339-354 025-034 056-059	306 355-362 035-039	307-320 363-009 040-046	321-338 010-024 047-055
150.0E	341-355 026-035 056-059	306 356-363 036-040	307-321 364-010 041-047	322-340 011-025 048-055
152.5E	342-356 026-035 057-059	306 357-364 036-040	307-322 365-011 041-047	323-341 012-025 048-056
155.0E	343-356 027-036 058-059	306-307 357-364 037-041	308-322 365-011 042-047	323-342 012-026 048-057
157.5E	343-357 028-036 058-059	306-308 358-001 037-041	309-323 002-012 042-048	324-342 013-027 049-057
160.0E	344-358 028-037 059	306-308 359-002 038-042	309-324 002-013 043-049	325-343 014-027 050-058

Table A.3 (cont): Julian days used in the MJO composite for 1988-89.

Longitude	Maximum Convection	Decreasing Convection	Minimum Convection	Increasing Convection
162.5E	345-359 029-037	306-308 360-003 038-042	309-324 004-014 043-049	325-344 015-028 050-059
165.0E	346-360 030-038	306-309 361-003 039-043	310-325 004-015 044-050	326-345 016-029 051-059
167.5E	347-360 030-039	306-310 361-004 040-043	311-326 005-015 044-051	327-346 016-029 052-059
170.0E	347-361 031-039	306-310 362-005 040-044	311-326 006-016 045-051	327-346 017-030 052-059
172.7E	348-362 032-040	306-311 363-005 041-045	312-327 006-017 046-052	328-347 018-031 053-059
175.0E	349-363 032-040	306-311 364-006 041-045	312-328 007-017 046-052	329-348 018-031 053-059
177.5E	350-364 033-041	306-312 365-007 042-046	313-328 008-018 047-053	329-349 019-032 054-059
180.0E	351-364 034-041	306-312 365-007 042-046	313-329 008-019 047-053	330-350 020-033 054-059